The Enhancement of Nonlinear Ultrasonic Testing to Detect Micro-structural Defects in Metals

by

Amir Mostavi
B.S. (Sharif University of Technology) 2010
M.S. (Sharif University of Technology) 2012

Thesis submitted in partial fulfillment of the requirements
for the degree of Doctor of Philosophy in Civil Engineering
in the Graduate College of the
University of Illinois at Chicago, 2018

Chicago, Illinois

Defense Committee:
Dr. Didem Ozevin, Chair and Advisor
Dr. Sheng-Wei Chi
Dr. Eduard Karpov
Dr. J. Ernesto Indacochea
Dr. Reza Shahbazian-Yassar, Mechanical & Industrial Engineering

This thesis is dedicated to,

my dearest and wonderful parents,

and my beloved, beautiful and brilliant wife, Minoo,

I'm blessed to have them in my life.

ACKNOWLEDGMENT

These years of graduate study at University of Illinois at Chicago have been a period of extensive learning for me, both academically and personally. I would like to acknowledge all the individual who trained me, supported me, and cheered me along the way. First and foremost, I would like to express my deepest appreciation to my advisor, Professor Didem Ozevin, for always being supportive and providing highly motivative atmosphere during my research at university of Illinois at Chicago. I thank her for not only being a great teacher and mentor for me, but also providing the opportunity to explore new ideas and grow as an independent researcher. I also would like to express my sincere gratitude to all members of my thesis committee, Professors J.Ernesto Indacochea, Sheng-Wei Chi, Eduard Karpov and Reza Shahbazian-Yassar for reviewing my work and giving me helpful advice. My appreciation also extends to my labmates and collaborators, Neda, Hossain, Lu, Hanieh, Zeynab, Onur, Gorkem, Negar and Niloofar, for providing a friendly work environment, and to the department's wonderful staff, Pam, Sara, Dansel, and James. I would like to thank my family for their love and support throughout all my life. Thanks to my wonderful dearest parents, Shahnaz and Alireza, whose love and guidance are with me in whatever I pursue. Thanks to my beloved, wonderful siblings, Omid, Ehsan, Atefeh and Ali for providing me through moral and emotional support. You guys are always there for me. Finally, there are my friends, Neda, Hossain, Hooman, Apameh, Amirhassan, Sanaz, Behnam, Zohreh, Majid and Maryam. You guys are fantastic friends, my extended family. This dissertation would not have been possible, without their endless support, warm love and continued patience. Finally and most importantly,

ACKNOWLEDGMENT (Continued)

I thank my precious Minoo, my soulmate and best friend. Thanks for supporting, encouraging and having faith in me at all times. I feel blessed to have you in my life.

CONTRIBUTION OF AUTHORS

This thesis includes seven chapters. Chapter 1 introduces the problem statement and motivations, the research objectives and summary of approach, contributions, and summary of the research. In Chapter 2, the relevant background literatures are presented that includes the general understandings of the non-destructive evaluation (NDE) methods, nonlinear ultrasonic testing, signal processsing methods, nonlinear wave propagation in fluids, immersion nonlinear ultrasonic testing and phononic crystals. The literature research presented in this chapter was partially published in the Journal of the International Measurement Confederation (IMEKO) with the title of "Wavelet Based Harmonics Decomposition of Ultrasonic Signal in Assessment of Plastic Strain in Aluminum" in collaboration with Negar Kamali, Niloofar Tehrani, and Professors Didem Ozevin, Sheng-Wei Chi, Ernesto Indacochea [1], at the journal of Applied Physics Letter with the title of "The Integration of Superlattices and Immersion Nonlinear Ultrasonics to Enhance Damage Detection Threshold" in collaboration with Minoo Kabir, and Professor Didem Ozevin [2], in the proceeding of the IWSHM conference, Structural Health Monitoring 2017 with the title of "Enhancing the Robustness of Nonlinear Ultrasonic Testing by Implementing 1D Phononic Crystals" in collaboration with Minoo Kabir, and Professor Didem Ozevin [3], and in AIP Conference Proceedings with the title of "The Application of Water Coupled Nonlinear Ultrasonics to Quantify the Dislocation Density in Aluminum 1100" in collaboration with Negar Kamali, Niloofar Tehrani, and Professors Didem Ozevin, Sheng-Wei Chi, Ernesto Indacochea [4]. In Chapter 3, wavelet based harmonic decomposition method is introduced and experimental studies are presented. The content presented in this chapter was partially published in the Measurement Journal with the title of "Wavelet Based Harm-

onics Decomposition of Ultrasonic Signal in Assessment of Plastic Strain in Aluminum" in collaboration with Negar Kamali, Niloofar Tehrani, and Professors Didem Ozevin, Sheng-Wei Chi, Ernesto Indacochea [1]. Kamali performed the theoretical studies, Tehrani prepared the experimental specimens and Mostavi performed the nonlinear ultrasonic testing experiments and analyzed the data. Ozevin, Chi and Indacochea supervised and reviewed the experiments and the results. In chapter 4, the enhancement of damage detection through the integration of superlattices and immersion nonlinear ultrasonic testing is described, which includes numerical studies on the design of the superlattices structure and the experimental studies on the validation of the enhancement of damage detection. The content presented in this chapter is partially published at the journal of Applied Physics Letter with the title of "The Integration of Superlattices and Immersion Nonlinear Ultrasonics to Enhance Damage Detection Threshold" in collaboration with Minoo Kabir, and Professor Didem Ozevin [2], and in the proceeding of the IWSHM conference, Structural Health Monitoring 2017 with the title of "Enhancing the Robustness of Nonlinear Ultrasonic Testing by Implementing 1D Phononic Crystals" in collaboration with Minoo Kabir, and Professor Didem Ozevin [3]. Kabir performed the numerical simulations to design the superlattices structure and Mostavi prepared the immersion nonlinear ultrasonic testing experiments, prepared superlattices and analyzed the data, the experiments are preformed by Ozevin, Mostavi and Kabir, and Ozevin reviewed the results. Chapter 5 presents the application of wavelet based harmonic decomposition method to analyze the nonlinear ultrasonic testing data to detect creep damage in stainless steel 410. This chapter will be partially published in a journal with the title of "Assessing Creep Damage in

CONTRIBUTION OF AUTHORS(continued)

410 Stainless Steel using Acoustic Micro Imaging" in collaboration with Niloofar Tehrani, Negar kamali and Professors Didem Ozevin, Sheng-Wei Chi, J. Ernesto Indacochea. Tehrani performed the creep specimens and literature studies. Mostavi performed the nonlinear ultrasonic testing, analyzed the data and performed literature review. Kamali, Ozevin, Chi and Indacochea supervised and reviewed the experiments and the results. Chapter 6 presents the immersion nonlinear ultrasonic testing integrated with superlattices to detect creep damage in stainless steel 410. The content presented in this chapter will be partially submitted to a journal with the title of "Assessing Creep Damage in Stainless Steel 410 using Integrated Immersion Nonlinear Ultrasonic Testing and Acoustic Metamaterials" in collaboration with Minoo Kabir, and Professor Didem Ozevin. Kabir performed the numerical simulations to design the superlattices structure and Mostavi prepared the immersion nonlinear ultrasonic testing experiments, prepared superlattices and analyzed the data, the experiments are preformed by Ozevin, Mostavi and Kabir, and Ozevin reviewed the results. The conclusions and future work are summarized in Chapter 7.

TABLE OF CONTENTS

CHAPTER			PAGE
1	**INTRODUCTION**		1
	1.1	Problem Statement and Motivation	1
	1.2	Research Objective and Summary of Approach	4
	1.3	Contribution to Knowledge	6
	1.4	Organization of Dissertation	8
2	**BACKGROUND LITERATURE**		10
	2.1	Introduction	10
	2.2	Nonlinear Ultrasonic Testing (NLUT)	11
	2.2.1	Limitations of NLUT using Higher Harmonics	14
	2.3	Signal Processing Methods for Signal Decomposition	15
	2.3.1	Fast Fourier Transform (FFT)	15
	2.3.2	Wavelet Transform (WT)	17
	2.4	Second Harmonic Generation (SHG) Method using Immersion NLUT	20
	2.4.1	Nonlinear Acoustics in Fluid	20
	2.4.2	Ultrasonic Wave Distortion in Fluid	21
	2.4.3	The Contribution of Solid-Fluid Interface in the Measured Nonlinearity	24
	2.5	Introduction to Phononic Crystals (PCs)	25
	2.5.1	One-Dimensional Mono-Atomic PCs	27
	2.5.2	One-Dimensional Bi-Atomic PCs	30
3	**WAVELET-BASED HARMONIC DECOMPOSITION OF NONLINEAR ULTRASONIC SIGNAL IN ASSESSMENT OF PLASTIC STRAIN IN ALUMINUM**		32
	3.1	Introduction	32
	3.2	Wavelet-based Harmonic Decomposition Method	32
	3.3	Materials Preparation	33
	3.4	Contact NLUT Method	36
	3.5	Experimental Results Using FFT	38
	3.6	Experimental Results Using WT	40
	3.7	Summary	47
4	**THE INTEGRATION OF SUPERLATTICES AND IMMERSION NLUT TO ENHANCE DAMAGE DETECTION THRESHOLD**		49
	4.1	Introduction	49
	4.2	Technical Approach	50

TABLE OF CONTENTS (Continued)

CHAPTER **PAGE**

4.3	Numerical Results	51
4.4	Experimental Study	52
4.4.1	Solid-Fluid SLs Fabrication	54
4.4.2	Ultrasonic Measurement Procedure	55
4.5	Results	58
4.5.1	Immersion NLUT Without the Presence of SLs	60
4.5.2	Immersion NLUT With the Presence of SLs	61
4.5.3	The Influence of the Propagation Distance in the Immersion NLUT	63
4.5.4	Third Harmonic Generation NLUT	64
4.6	Solid-Solid SLs for the Contact NLUT	64
4.6.1	Numerical Results	64
4.6.2	Experimental Results	66
4.7	Summary	67
5	**ASSESSING CREEP DAMAGE OF STAINLESS STEEL 410 USING NLUT AND WAVELET TRANSFORMATION**	71
5.1	Introduction	71
5.2	Creep Damage	71
5.3	Experimental Procedure	72
5.3.1	Materials Preparation	72
5.3.2	Contact Nonlinear Ultrasonic Testing (NLUT)	73
5.4	NLUT Results	74
5.5	Summary	77
6	**INTEGRATING SUPERLATTICES AND IMMERSION NLUT TO ASSESS CREEP DAMAGE OF STAINLESS STEEL 410**	78
6.1	Introduction	78
6.2	Technical Approach	78
6.3	Experimental Setup	79
6.4	Third Harmonic Non-linearity Parameter with the Immersion NLUT and SLs	83
6.5	Summary	85
7	**CONCLUSIONS AND FUTURE WORK**	87
7.1	Conclusions	87
7.2	Future Work	90
	APPENDICES	91
	Appendix A	92
	CITED LITERATURE	97

LIST OF TABLES

TABLE		PAGE
I	NOMINAL CHEMICAL COMPOSITION OF ALUMINUM 1100	35
II	ACOUSTIC NON-LINEARITY PARAMETER OBTAINED BY FFT . . .	42
III	BINARY MATERIALS CONSIDERED IN NUMERICAL STUDIES . . .	53

LIST OF FIGURES

FIGURE		PAGE
1	The research framework.	7
2	Complex Morlet with central frequency of 1.5 Hz and bandwidth of 1 Hz, (a) time domain, (b) frequency domain.	19
3	Wave distortion due to the propagation of finite-amplitude monochromatic wave in fluid.	22
4	The variation of dimensionless Fourier coefficient as a function of σ.	23
5	Schematics of (a) 1D mono-atomic PCs and (b) its dispersion curve.	28
6	Schematics of (a) 1D bi-atomic PCs and (b) its dispersion curve.	31
7	Schematic to obtain the acoustic non-linearity parameter β using WT.	34
8	Tensile test sample dimensions (All dimensions are in mm).	35
9	Ultrasonic testing of aluminum specimens: (a) experimental setup, (b) schematic diagram, (c) ultrasonic transmitter and receiver in through-transmission mode, and (d) transducer calibration curves.	37
10	Typical time-domain waveforms and their frequency spectra for (a) pristine specimen, (b) 2% strain specimen, and (c) 4% strain specimen.	39
11	The variations in the acoustic non-linearity parameter corresponding to time-domain windows calculated by FFT: (a) 0-15μs, (b) 0-9 μs, (c) 1.2-7.0μs and (d) 2.0-5.5μs.	41
12	Fundamental and second harmonic waveforms extracted from the spectrograms corresponding to samples: (a) pristine, (b) 2% strained, (c) 3% strained, and (d) 4% strained.	43
13	Stress-strain curve and normalized non-linearity-strain curve using the time-invariant approach on two-scale plot.	44

LIST OF FIGURES (Continued)

FIGURE **PAGE**

14 (a) Time-history waveform of the first harmonic, (b) time-history waveform of the second harmonic, and (c) change in acoustic non-linearity parameter with time (for pristine specimen). 45

15 Change in acoustic non-linearity parameter within time for different strain levels. 46

16 Stress-strain curve and normalized non-linearity-strain curve using the time-dependent approach on two-scale plot. 47

17 The approach to integrate the SLs with the immersion NLUT (a) NLUT setup with the presence of SLs, (b) the designed band gap tuned to the second harmonic frequency. 51

18 (a) Numerical model, and (b) transmission loss through SLs (100 μm glass-100 μm water). 53

19 The displacement field through the designed SLs at two different frequencies (a) 2.25 MHz, and (b) 4.5 MHz. 54

20 Testing the band gap formation of the designed SLs (a) the fabricated SLs made of glass and water, (b) the immersion NLUT setup. 56

21 Frequency spectra of immersion NLUT for two cases: (i) with the SLs and (ii) without the SLs (there is no specimen in the path of transmitter and receiver). . 57

22 Immersion NLUT setup, (a) schematic diagram of immersion NLUT without the presence of SLs, (b) schematic diagram of immersion NLUT with the presence of SLs. 58

23 Immersion NLUT without the presence of SLs, (a) the time-domain signal, (b) frequency spectrum obtained by applying FFT on the selected 15 cycles of the time-domain signal of pristine specimen. 59

24 Immersion NLUT with the presence of SLs, (a) the time-domain signal, (b) frequency spectrum obtained by applying FFT on the selected 15 cycles of the time domain of pristine specimen. 60

25 Normalized β (solid black line) and absolute β (dashed gray line) versus plastic strain resulted from immersion NLUT without the presence of SLs. 61

26 Normalized β (solid black line) and absolute β (dashed gray line) versus plastic strain resulted from immersion NLUT with the presence of SLs. 62

LIST OF FIGURES (Continued)

FIGURE		PAGE
27	Measured non-linearity versus propagation distance (a) without the SLs, and (b) with the SLs for the 2% strained specimen.	63
28	Schematic diagram of the contact NLUT setup integrated with the solid-solid SLs.	65
29	(a) Numerical model, and (b) transmission loss through SLs (254 μm steel-200 μm glass).	66
30	The pressure field through the designed SLs at two different frequencies (a) 2 MHz, and (b) 4 MHz.	67
31	The frequency spectra of the received signals for two cases, (i) with and (ii) without SLs.	68
32	Contact NLUT, (a) and (b) the spectrograms of the received signals for the cases without and with the presence of SLs, respectively, (c) and (d) the harmonic waveforms extracted using WT, respectively.	69
33	Tensile test sample dimensions (All dimensions are in mm.)	73
34	NLUT experiment, (a) experimental setup, (b) schematic of experimental setup, and (c) transducer calibration curves.	75
35	Typical received signal for pristine specimen of stainless steel 410 (a) received time-domain signal, (b) frequency spectra of the received signal, (c) the spectogram of the received signal, and (d) the extracted fundamental and second harmonic waveforms from the wavelet spectrum and the corresponding non-linearity parameter calculated over time.	76
36	The change in β with, (a) creep damage, and (b) thermal aging.	77
37	Proposed approach to block the third harmonic signal (a) the immersion NLUT setup with the presence of SLs, (b) the designed band gap tuned to the second and third harmonic frequencies.	80
38	Testing the band gap formation of the designed SLs (a) the fabricated SLs made of glass and water, (b) the immersion NLUT setup, (c) schematic diagram of experimental setup to test the SLs, (d) the calibration curves of ultrasonic transducers, and (e) frequency spectra of ultrasonic signals for two cases as without and with the SLs.	81

LIST OF FIGURES (Continued)

FIGURE		PAGE
39	Immersion NLUT setup using stainless steel specimens, (a) schematic diagram of immersion NLUT without the presence of SLs, and (b) schematic diagram of immersion NLUT with the presence of SLs.	82
40	Immersion NLUT without the presence of SLs, (a) time-domain signal, (b) frequency spectrum using the first 10 cycles of time-domain signal.	84
41	Immersion NLUT with the presence of SLs, (a) time-domain signal, (b) frequency spectrum using the first 10 cycles of time-domain signal.	84
42	Normalized γ versus creep strain resulted from (a) the immersion NLUT without the presence of SLs, and (b) the immersion NLUT with the presence of SLs.	85

LIST OF ABBREVIATIONS

BS	Bragg's Scattering
FFT	Fast Fourier Transform
LR	Local Resonance
NDE	Nondestructive Evaluation
NDT	Nondestructive Testing
NLUT	Nonlinear Ultrasonic Testing
PCs	Phononic Crystals
SHG	Second Harmonic Generation
SHM	Structural Health Monitoring
SLs	Superlattices
STFT	Short Time Fourier Transform
UT	Ultrasonic Testing
WT	Wavelet Transform

SUMMARY

Over the last decades, nondestructive evaluation (NDE) of materials has been implemented to assess the structural integrity by detecting structural flaws, such as fatigue crack, creep, corrosion, and thermal aging. Different NDE methods are developed and employed, including electromagnetics, eddy currents, acoustic emission and ultrasonics. Ultrasonic testing (UT) is a well-established NDE method that measures materials state by monitoring the propagation of high frequency elastic waves within materials. UT can be categorized as linear and nonlinear methods. The linear UT detects flaws by measuring wave velocity, attenuation, time of flight reflection from flaws or linear resonance frequency. Although it is successfully applied in detecting defects on the order of wavelength, the sensitivity of this method is limited to the wavelength of ultrasonic signal. On the other hand, nonlinear UT (NLUT) is sensitive to the microscopic imperfections in sub-wavelength that nucleate in the early stages of damage. One of the well-known NLUT methods is called second harmonic generation (SHG), which is based on the distortion of a single frequency wave confronting the micro-structural features as it passes through the material. This distortion arises from the deviation from Hooke's law in a nonlinear medium that generates higher frequency components of the fundamental frequency. The amplitudes of the fundamental and second harmonics are used to calculate the acoustic non-linearity parameter (β) and the amplitudes of the fundamental and third harmonics are used to calculate the third order acoustic non-linearity parameter (γ). The correlation between the acoustic non-linearity parameter and the extent of micro-structural features in materials has been reported in literature; however, the major challenges of this method are high sensitivity of harmonic amplitudes to the signal processing method and the experimental variables,

such as coupling condition and instrumental non-linearities (e.g. arbitrary function generator and amplifiers can introduce significant non-linearity), which introduce significant variability in the reported non-linearity parameters representing different defects. The objective of this research is to minimize the variability of non-linearity parameter in relation to damage by introducing wavelet-based signal decomposition approach, and blocking the non-linearity in medium and instruments by phononic crystals (PCs). The research has two major components: (i) understanding the major drawback of the most prevalent signal processing method and formulating a more robust harmonic decomposition method, and evaluating the proposed method in the NLUT experiments to detect plastic strain and creep damage; (ii) blocking the non-linearity generated in instrument and couplant (water for the case of immersed NLUT) by implementing one-dimensional PCs, known as superlattices (SLs). It is demonstrated that the wavelet-based signal decomposition reduces the variability of harmonic amplitudes as compared to Fourier transform-based signal decomposition. SLs are numerically modeled to block higher harmonics selected in this research, and tested experimentally. It is shown that non-linearity in water and electronics in the transmission side of data acquisition equipment can be blocked while the NLUT method can be used with immersion method with the reduced coupling effect. The NLUT method integrated with SLs is demonstrated on detecting plastic deformation in aluminum with the second harmonic approach and creep damage in steel with the third harmonic approach.

CHAPTER 1

INTRODUCTION

1.1 Problem Statement and Motivation

Ultrasonic Testing (UT) is a well-established nondestructive evaluation (NDE) method of materials and structures. The method can detect the presence of flaws in materials by studying the interaction of high frequency ultrasonic waves with microstructure and defects. The method has been developed in many applications to detect the presence of various defects (e.g., crack, corrosion, delamination) in materials [5; 6; 7]. The requirement that the wavelength of ultrasonic signal should be smaller than the size of defects when the linear UT is implemented limits the capability of assessing materials state involving micro-structural defects, such as early stages of fatigue and creep damage. On the other hand, the nonlinear characteristics of wave motion have been utilized to investigate micro-structural defects [8; 9; 10; 11]. These methods commonly rely on observing small changes of elastic wave motion in frequency and/or time domains. The materials non-linearity can be measured by two means: stress-dependent ultrasonic wave velocity known as acoustoelasticity [12; 13; 14] and the detection of higher harmonics [15; 16; 17; 18]. Nonlinear ultrasonic testing (NLUT) method is able to detect the micro-structural features (e.g. dislocation density and porosity) in the order of magnitude smaller than ultrasonic wavelength [19]. The acoustoelastic effect is negligibly small when the stress level is far below the yield point, which is beyond the scope of this research. When a single-frequency elastic wave propagates in a material, the interaction of single-frequency wave mode with micro-structural

defects generates higher frequency components known as higher harmonics. The excitation frequency is referred in literature as the fundamental wave frequency and the higher harmonics are integer multiples of the excitation frequency.

The most common NLUT method is called second harmonic generation (SHG) method. This method is based on measuring the acoustic non-linearity parameter, β, which is proportional to the ratio of the second harmonic amplitude A_2 to the square of the first harmonic (fundamental frequency) amplitude A_1, $(\frac{A_2}{A_1^2})$ [1; 19; 20]. To date, there are several applications of NLUT to assess micro-structural changes in metallic alloys, such as fatigue damage [21; 22], dislocation density [23; 24], creep damage [25; 26; 27], radiation damage [18], thermal aging [28; 29], and cold work [30]. Various wave types can be utilized for detecting micro-structural damage using nonlinear ultrasonics such as longitudinal waves [27; 31; 32], Rayleigh waves [18; 33; 34], or Lamb waves [22]. Matlack et al. [35] have presented a comprehensive review of the SHG method for detecting micro-structural damage.

The SHG method has received significant interests recently, as the reliability and integrity of structural components become increasingly important, and the recent developments in the accuracy of ultrasonic data acquisition systems make high precision measurements possible. However, while β is sensitive to material micro-structural features, consequently, the error tolerance in the NLUT method, from both experimental variables (i.e., couplant material and thickness, amount of force to couple sensors with structure) and signal processing methods, is more stringent than that the linear UT method [36].

The most common harmonic decomposition method is to transform time-domain signal into frequency domain using fast Fourier transform (FFT), and read the amplitude of each frequency from the frequency spectrum [25; 33; 37; 38]. The major drawbacks of this approach are that temporal infor-

mation is not preserved and the transformation is ineffective in dealing with truncated signals or ones with discontinuity. Pruell et al. [22] applied the short time Fourier transform (STFT) to obtain time-frequency images. However, STFT has a fixed window size, and it cannot yield good resolution based on time and frequency simultaneously. Kim and Kim [37] compared STFT and wavelet transformation (WT) and discovered that the WT is a promising method to analyze the acoustic signals. In general, the acoustic non-linearity parameter β rises with an increase in the density of microscopic heterogeneities, e.g., dislocation density, precipitates, or porosity. However, significant variations in the reported data and high errors in repeated measurements show the inevitability of more robust signal processing tools to decompose harmonic frequencies. This research presents a wavelet-based signal decomposition aiming to more accurate extraction of frequency components in the NLUT method with minimum variance.

Immersion UT reduces the influences of couplant and pressure applied to transducers to harmonic amplitudes with comparatively low acoustic attenuation [39; 4; 40]. However, when a period of finite amplitude sinusoidal wave propagates in water, high pressure zone (the crests of the wave) travels faster than low pressure zone (the troughs of the wave). This phenomenon leads to wave distortion and transfer of energy to higher harmonics [41; 42; 43]. Consequently, water generates high non-linearity that can mask the weak non-linearity in solid. This fact adversely affects the applicability of immersion NLUT [44]. While eliminating the system non-linearity in contact NLUT has been studied through non-collinear and collinear wave mixing [45; 46], an approach to prevent the system non-linearity in immersion NLUT has not been investigated yet. This research aims to enhance immersion NLUT by means of removing the non-linearity generated in water and instruments. The non-linearity blocking

is achieved by implementing phononic crystals (PCs). PCs or acoustic metamaterials are a class of metamaterials that provide unnatural features to manipulate the propagation of elastic waves [47; 48]. PCs are developed to control the elastic waves in solid inspired by the concept of photonic crystals that control electromagnetic waves [49]. Both of phononic and photonic crystals are based on the idea that periodic structures can affect the wave propagation and generate unnatural features, such as band gap formation. As a result of the band gap, certain frequencies are blocked while others are allowed to propagate (pass band). This feature comes from different acoustic properties of layers and the periodic placement of layers compared to bulk materials [50]. The dispersion behavior of PCs can be tuned to exhibit band gaps that restrict the propagation of particular frequency and wave mode [51]. In literature, PCs have been studied in different applications, such as wave guiding [52], filtering [53] and rectifying [54] the acoustic waves. The periodic structure of PCs can be arranged in one, two or three dimensions. The one-dimensional PCs are called superlattices (SLs). The SLs structure is composed of two or more periodically repeated layers, which are placed along the SLs growth direction. Each unit cell of SLs can be made of solid-solid layers or solid-fluid layers [50]. In literature, the solid-fluid SLs composed of limited number of periodic cells are shown experimentally and numerically to exhibit large band gaps [55; 56].

1.2 Research Objective and Summary of Approach

The objective of this research is to enhance damage detection using NLUT by addressing two major challenges introduced in section 1.1. The challenges are aimed to be overcome by attaining a robust signal decomposition method, and generating an strategy to mitigate the NLUT experimental variables including inconsistent coupling condition and instrumental non-linearity. The components of the

research to achieve the research objective are presented in Figure 1. The research has two major components: (a) the enhancement of contact NLUT through wavelet-based signal decomposition method and (b) the enhancement of coupling condition in NLUT through the integration of immersed NLUT with SLs.

(a) In NLUT method signal processing is a major process of damage detection. A wavelet-based signal decomposition method is introduced to better extract higher harmonics from time-history signals and thus more accurately obtain the acoustic non-linearity parameter. WT uses functions that are localized in both real and Fourier spaces, called mother wavelets. In higher-frequency components, the window size becomes smaller to maintain higher-frequency resolution, while in signals with lower frequency higher frequency resolution is obtained by a larger window size. By using wavelet harmonic decomposition method, spectral amplitudes over time is obtained for the fundamental and higher harmonics frequencies. In this study, two wavelet-based algorithms are introduced to analyze the ultrasonic waveforms: time-dependent and time-invariant. In the time-dependent algorithm, β varies with each discrete point along the time history signal, while in the time-invariant algorithm, the maximum amplitudes of fundamental and second harmonic waves, within a period of time, are selected for calculating a constant β value for each time history signal. Both of the proposed methods employ complex Morlet mother wavelet function. The algorithms are implemented to determine the variation of the acoustic non-linearity parameter due to different levels of plastic deformation and creep damage. The traditional fast Fourier transform (FFT) is also used to acquire the acoustic non-linearity parameter for comparison. The NLUT experiment in this part is implemented in contact mode and light lubrication oil is used as the couplant between the transducers and the specimens.

(b) Coupling condition is a major source of error in NLUT. In order to provide a consistent coupling force and minimize the coupling error due to surface condition of the specimens, immersed NLUT is applied in this study. To eliminate the non-linearity generated in water and instruments in the excitation side, it is proposed to integrate immersed NLUT with SLs. The SLs structure is designed to provide a band gap range that includes the second and third harmonic frequencies used in this study, and placed right before the solid medium facing to the transmitter. The SLs made of binary layers of solid-solid and solid-fluid are numerically modeled using COMSOL Multiphysics to study the wave transmission loss, employing the pressure acoustics module. The performance of the designed SLs to enhance the immersed NLUT is experimentally demonstrated on two sets of specimens with different levels of plastic deformation and creep damage.

1.3 Contribution to Knowledge

The major contributions of this research to the knowledge are the followings:

- The accuracy of harmonic decomposition of nonlinear wave signal due to plastic deformation and creep damage is improved by applying the wavelet-based algorithms. Good correlation between the increase of β and the increase in plastic deformation or creep damage is obtained using the contact NLUT method. The developed signal processing algorithm enhances the minimum detectable micro-structural changes in materials using nonlinear ultrasonics.
- For the first time in literature, the integration of SLs into the immersion NLUT is demonstrated in this research. SLs are numerically designed to remove the non-linearity generated in water and instruments. The results reveal that the SLs with a band gap tuned to higher harmonic frequencies and a pass band that includes the fundamental harmonic frequency enhances the damage

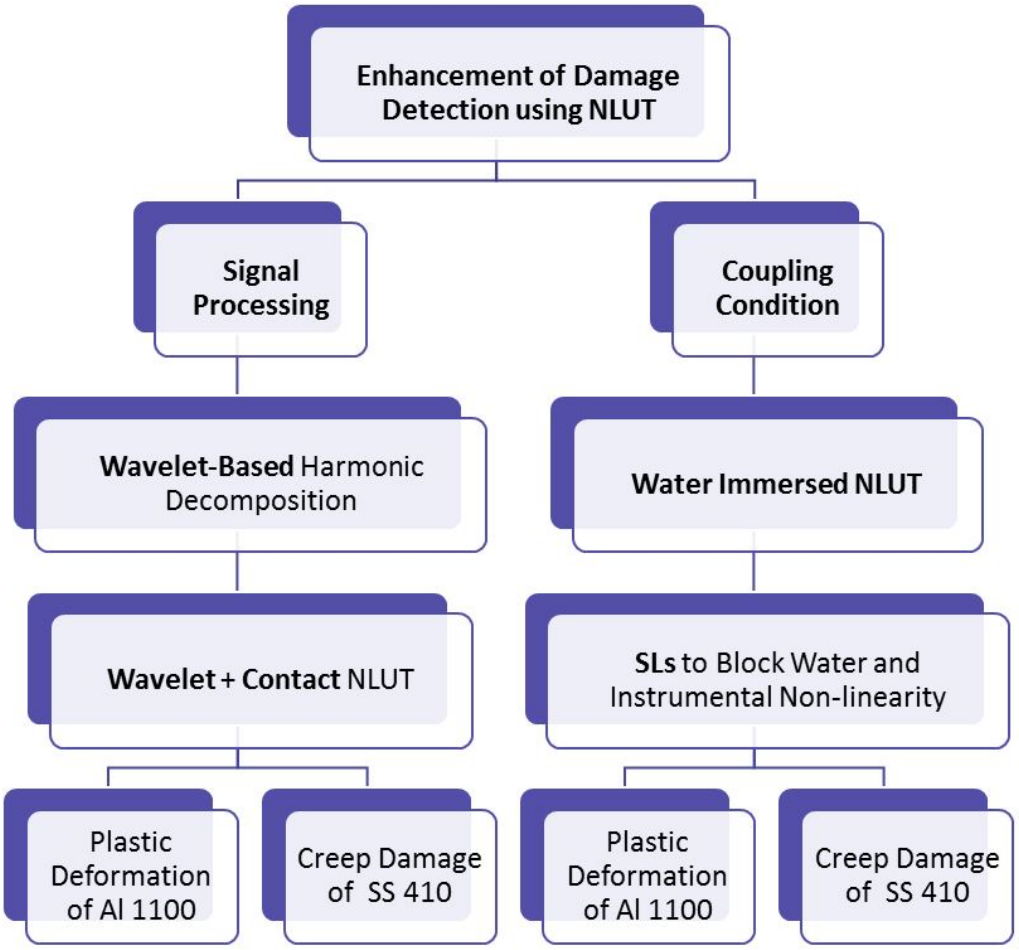

Figure 1. The research framework.

detection sensitivity of immersion NLUT as compared to the current practice. The approach reduces the errors introduced by couplant and instruments and enhances the minimum detectable micro-structural changes in solids.

1.4 Organization of Dissertation

Following this introductory chapter, the remainder of this thesis is organized as follows:

Chapter 2 presents the background literature related to this research. The chapter begins with the introduction to the linear and nonlinear ultrasonic testing, higher harmonic generation method, and their advantages and limitations. Then, the nonlinear wave propagation equations and the generation of higher harmonics are presented. The chapter continues with presenting the signal processing methods implemented to perform the harmonic decomposition in NLUT method. Next, the immersion NLUT and the non-linearity generated in water are discussed, and finally phononic crystals and acoustic metamaterials are introduced. Chapter 3 presents the formulation of the proposed SHG method based on the wavelet-based harmonic decomposition method. The approach is experimentally applied to detect different levels of plastic deformation in aluminum 1100 specimens. In chapter 4, the enhancement of immersion NLUT by exploiting superlattices (SLs) is presented. The wave propagation through the SLs is numerically studied to tailor the periodic geometry and tune the band gap to the second and third harmonic frequency. The desired SLs are fabricated and the band gap formation is validated through an immersion NLUT experimental setup. The improvement in the sensitivity of the NLUT is demonstrated through detecting the plastic strain in aluminum 1100 specimens. In chapter 5, the developed wavelet-based SHG method is applied to study the micro-structural changes in metals due to creep damage. The changes in β for different levels of creep and thermal damages in stainless steel 410 are measured using

the contact NLUT. In chapter 6, the integration of the immersed NLUT and SLs using the third harmonic generation method is employed to detect the creep damage in stainless steel 410 specimens. The results of the immersed NLUT in two cases, (i) without the presence of SLs, and (ii) with the presence of SLs are reported. Finally, in chapter 7, the major conclusions and future work of this research are presented.

CHAPTER 2

BACKGROUND LITERATURE

The content presented in this chapter is partially published at the Journal of the International Measurement Confederation (IMEKO) with the title of "Wavelet Based Harmonics Decomposition of Ultrasonic Signal in Assessment of Plastic Strain in Aluminum" in collaboration with Negar Kamali, Niloofar Tehrani, and Professors Didem Ozevin, Sheng-Wei Chi, Ernesto Indacochea [1], at the journal of Applied Physics Letter with the title of "The Integration of Superlattices and Immersion Nonlinear Ultrasonics to Enhance Damage Detection Threshold" in collaboration with Minoo Kabir, and Professor Didem Ozevin [2], in the proceeding of the IWSHM conference, Structural Health Monitoring 2017 with the title of "Enhancing the Robustness of Nonlinear Ultrasonic Testing by Implementing 1D Phononic Crystals" in collaboration with Minoo Kabir, and Professor Didem Ozevin [3], and in AIP Conference Proceedings with the title of "The Application of Water Coupled Nonlinear Ultrasonics to Quantify the Dislocation Density in Aluminum 1100" in collaboration with Negar Kamali, Niloofar Tehrani, and Professors Didem Ozevin, Sheng-Wei Chi, Ernesto Indacochea [4].

2.1 Introduction

The aim of this chapter is to present and outline of the linear and nonlinear ultrasonic testing, higher harmonic generation method, and their advantages and limitations. The chapter continues with studying two major challenges of NLUT method, (i) signal processing and (ii) coupling condition. The signal processing methods implemented to perform the harmonic decomposition are introduced. The immer-

sion NLUT and the non-linearity generated in water are discussed, and finally phononic crystals (PCs) are introduced.

2.2 Nonlinear Ultrasonic Testing (NLUT)

Structures are exposed to different types of loads (e.g., dead, live, wind, thermal) which may lead to structural defects, such as fatigue crack [33; 57], creep [25], corrosion [58] and thermal aging [28]. The defects at critical size influence the structural integrity and may lead to an unexpected failure. It is important to detect them before they reach to critical stage by nondestructive evaluation (NDE) methods. In the last decade, diferrent NDE methods are developed and implemented to detect the presence of defects, including electromagnetics, eddy currents, acoustic emission and ultrasonics [59; 60; 61].

Ultrasonic Testing (UT) is an active NDE method that is based on detecting the properties of propagating waves in materials generated by a transmitting transducer. UT can be categorized as linear and nonlinear methods [22; 7]. The linear UT detects flaws by measuring wave velocity, time of flight reflection from defects, attenuation or linear resonance frequency [33; 62], and has been applied for damage assessment of structures, such as pipelines, railroads and aircraft components [63; 64].

While the linear UT method has been successfully developed in many applications to detect the presence of various flaws (e.g., crack, corrosion, delamination) in materials [5; 6], it faces a major limitation that the wavelength of ultrasonic signal should be smaller than the size of defects. On the other hand, on account of the advancement of UT instrumentation and the theory of nonlinear wave propagation, the nonlinear characteristics of wave motion has been utilized to investigate micro-structural defects [8; 9; 10]. These methods commonly rely on observing small changes of the elastic wave motion in frequency and/or time domains. The nonlinear ultrasonic testing (NLUT) method is able to detect the

microstructural features, (e.g., dislocation density, porosity), in the order of magnitude smaller than the ultrasonic wavelength [8; 9; 10].

The materials non-linearity can be measured by different NLUT methods. The stress-dependent ultrasonic wave speed known as acoustoelasticity is based on the fact that ultrasonic velocity is stress-dependent [65]. Nonlinear elastic wave spectroscopy (NEWS) method uses the nonlinear hysteretic nature of materials such as concrete and rock. This method is implemented in two modes. The first mode measures the shifts in the resonance frequency due to the change in the excitation amplitude, known as nonlinear resonant ultrasound spectroscopy (NRUS). Second, the nonlinear wave modulation spectroscopy (NWMS) method mixes a very low frequency and high frequency ultrasonic waves, and measures the modulation of frequencies [66; 67; 68; 69]. To detect surface defects in geophysics applications, nonlinear time reversal is applied [70]. Higher harmonic generation method is based on the generation of higher harmonics of the excitation frequency propagating in a nonlinear medium due to micro-structural defects. This method is shown to be sensitive to defects in their early stages before the nucleation of macroscopic damage [35]. In this research, higher harmonics-based NLUT is studied.

The higher harmonics NLUT method is based on the theory that, when a single-frequency (i.e., the excitation frequency) elastic wave propagates in a material, the interaction of single-frequency wave with micro-structural defects distorts the wave and generates higher-frequency components of the excitation frequency, called higher harmonics. This distortion arises from the deviation from Hooke's law in a nonlinear medium that generates higher frequency components [71]. The amplitudes of the fundamental and higher harmonics are used to calculate the acoustic non-linearity parameters [72]. The excitation frequency is referred in the literature as the fundamental wave frequency and the higher harmonics are

integer multiples of the excitation frequency. The wave motion in solids is governed by the following equation:

$$\frac{\rho Dv}{Dt} = \Delta.\sigma \tag{2.1}$$

where ρ is the material density, v is the particle velocity, D denotes the material time derivative, and the body force is neglected. σ is the Cauchy stress tensor and can be obtained from the strain energy density function. Considering the longitudinal wave, u, with a sinusoidal excitation $u(0,t) = u_0 sin(\omega t)$, the solution of Equation 2.1 is given as follows [73]:

$$u(x,t) = u_0 sin\omega(t - \frac{x}{c_l}) + \frac{\beta'}{4}(\frac{\omega}{c_l})^2 u_0^2 x cos2\omega(t - \frac{x}{c_l}) + \frac{\beta'^2}{8}(\frac{\omega}{c_l})^4 u_0^3 x^2 sin3\omega(t - \frac{x}{c_l}) + ... \tag{2.2}$$

where c_l is the propagation speed of longitudinal wave.

A subset of higher harmonic methods is the second harmonic generation (SHG) method which measures the acoustic non-linearity parameter, β. β is calculated based on the ratio of the second harmonic amplitude to the square of the fundamental harmonic amplitude [30; 71; 74]. In Equation 2.2 let A_1 and A_2 be the fundamental and second harmonic amplitudes of the ultrasonic signal while converted to the frequency domain. β can be quantified by Equation 2.3:

$$\beta \equiv \frac{A_2}{A_1^2} = \beta' \frac{xk^2}{4} \tag{2.3}$$

where $k = \frac{\omega}{c_l}$ is the wave number of the fundamental wave and x is the propagation distance [19; 30].

Recently, the generation of third harmonics is reported in literature to characterize the defects in materials [75; 76]. Narayana et al. [77] compared the second and third harmonic generations to detect creep damage in pure copper specimens and reported that third harmonic generation is more sensitive to detect the creep damage. Third harmonic generation method is based on the measurement of fundamental and third harmonic amplitudes of the ultrasonic wave to calculate the third order non-linearity parameter γ as presented in Equation 2.4 [78].

$$\gamma = \frac{6A_3}{xk^3A_1^3} \equiv \frac{A_3}{A_1^3} \tag{2.4}$$

where γ is the third harmonic non-linearity parameter, A_1 and A_3 are the fundamental and third harmonic amplitudes of the recieved signal, respectively, k is the wave number of the fundamental wave and x is the propagation distance [78].

2.2.1 Limitations of NLUT using Higher Harmonics

Second and third harmonic-based NLUT methods have been studied to investigate the micro-structural defects in materials. However, as the methods depend on the measurement of ultrasonic amplitudes, error due to measurements and signal processing is higher than that the linear UT [79; 80]. The measured non-linearity is originated from two different sources: (i) materials related non-linearity due to the micro-structural changes in solid, and (ii) measurement related non-linearity, which originates from experimental variables (for example, measurement instruments such as amplifiers, transducers, and the arbitrary function generator (AFG) can introduces non-linearities). The materials related non-linearities can be orders of magnitude smaller than the measurement related non-linearities, which may hinder the correlation between the non-linearity parameters and defects [79].

Liu et al. [79] studied the key experimental variables that affected the nonlinear ultrasonic testing such as coupling conditions, instrument non-linearities, transducer natural filter effect, transducer location and measurement angle, signal processing and windowing type. They showed that relative transducer position, coupling condition and signal processing are the major variables affecting the nonlinear ultrasonic testing [79]. Despite these limitations, the sensitivity of nonlinear harmonic generation to the micro-structural changes in materials has motivated the researchers to study further enhancement of NLUT. The enhancement of contact and immersion NLUT methods depends on two variables: (i) signal decomposition method to determine the amplitudes of fundamental and higher harmonic frequencies, and (ii) the influence of coupling condition between transducers and specimen.

2.3 Signal Processing Methods for Signal Decomposition

In this section, the basic theories and equations of commonly used signal processing methods for the ultrasonic signal decomposition are reviewed to illustrate their advantages and disadvantages in the extraction of higher harmonic amplitudes.

2.3.1 Fast Fourier Transform (FFT)

FFT is the most commonly used signal processing method to find the frequency content of transient signals based on the Fourier series expansion. The Fourier series of a time-dependent signal $h(t)$ within the limit of $-T < t < T$ is [81]:

$$h(t) = \sum_{n=-\infty}^{\infty} c_n e^{\frac{i\pi n}{T}t} \tag{2.5}$$

$$c_n = \frac{1}{2T}\int_{-T}^{T} h(t)e^{\frac{-i\pi n}{T}t}dt \tag{2.6}$$

where c_n corresponds to the n^{th} coefficient in the Fourier series. To process a signal with finite discrete values, discrete Fourier transform (DFT) is used. In DFT, the sequence h_n with N values is transformed to the frequency domain as [81]:

$$H_k = \sum_{n=0}^{N-1} h_n e^{\frac{-i2\pi nk}{N}}, \qquad k = 0,....,N-1 \tag{2.7}$$

where k is the wave number and H_k is the corresponding sequence in the frequency domain. Due to the large computational cost of calculating DFT for large N, this method is seldom used. Instead, by rearranging some multiplications and sums, a simple yet effective algorithm called FFT, which decreases the computational cost by reducing N, the number of points needed for computation from $2N^2$ to $2\log N$. If frequency is constant in time, FFT works effectively [82]. However, in nonlinear ultrasonic testing, the objective is to find the complex non-stationary higher-order harmonic signals, which potentially poses a challenge for FFT. Moreover, some inherent characteristics of FFT affect the accuracy of signal harmonic decomposition. FFT uses global basis functions, and any perturbations in the transient signal in the time domain can dramatically affect the frequency spectrum [83]. Therefore, FFT is less accurate to handle local discontinuity in the time-varying signal with transient properties [84]. To solve this problem, Dennis Gabor introduced the STFT method to embed the temporal information into the frequency-domain analysis [85]. In this method a fixed length analysis window is introduced that slides through the time axis and computes the time-localized Fourier transform [86]. While the STFT

approach is introduced to overcome the limitation of FFT that the temporal information is excluded, in this method, an implicit assumption is that the signal within the processing frame is repetitive and that the signal can only be sampled for a limited time [87]. In STFT, the time resolution can be improved by decreasing the window size to calculate FFT, but the frequency resolution is reduced when the FFT window has limited data points [88]; thus STFT cannot provide good resolution in time and frequency simultaneously [84; 86; 89]. In conclusion, FFT is ineffective to decompose non-stationary transient signal accurately, and it is important to apply a more robust signal decomposition approach to calculate the acoustic non-linearity parameter.

2.3.2 Wavelet Transform (WT)

In contrast to FFT, WT uses functions that are localized in both real and Fourier spaces, called wavelets [90]. By reconstructing signals into the mother wavelets, $\psi(t)$, frequency components with the window of each wavelet can be identified. As discussed before, STFT requires a constant window length (called window size), which slides through the time axis to calculate the FFT in each window and to add the temporal information of the signal into FFT [86]. Unlike the STFT method, the window size in WT is not constant, and it is a function of frequency. In higher-frequency components, the window size becomes smaller to maintain higher frequency resolution while in signals with lower frequency, higher frequency resolution is obtained by a larger window size [89; 91]. WT has been successfully applied in obtaining time-frequency images in both linear and nonlinear systems and the other applications in signal/image processing and damage detection [90; 92; 93; 94; 95; 96].

The fundamental equation of wavelet transform can be expressed as [81]:

$$W_n(s,\tau) = \int_{-\infty}^{\infty} h(t)\,\psi^*_{s,\tau} dt \tag{2.8}$$

where $h(t)$ is the time-domain signal, $(*)$ denotes the complex conjugate, and $\psi_{s,\tau}$ is called the daughter wavelet and can be characterized with the dilation and translation parameters, s and τ, respectively, as:

$$\psi_{s,\tau}(t) = \frac{1}{\sqrt{s}}\psi(\frac{t-\tau}{s}) \tag{2.9}$$

The dilation and translation parameters, s and τ, vary continuously to represent different times in the time-domain signal and different contractions and dilations of the mother wavelet. The wavelet function should have zero mean and be localized in both time and frequency [97]. Additionally, the mother wavelets $\psi(t)$ must satisfy the following admissibility conditions:

$$\int_{-\infty}^{\infty} \frac{|\hat{\psi}(\omega)|^2}{|\omega|} d\omega < \infty, \qquad \hat{\psi}(\omega) = \int \psi(t) e^{-i\omega t} dt. \tag{2.10}$$

Among many wavelets, the Morlet wavelet have the best temporal and spatial resolutions [96]. A wavelet function can be either real or complex. A complex wavelet is advantageous to represent oscillatory waves as it preserves the information for both amplitude and phase [98]. In this study, the complex Morlet wavelet obtained by the product of a complex exponential, and a Gaussian function is selected as the mother wavelet. The exponential decay in complex Morlet results in very precise time localization. This wavelet provides the best resolution in time and frequency; therefore, it is the most suitable wavelet

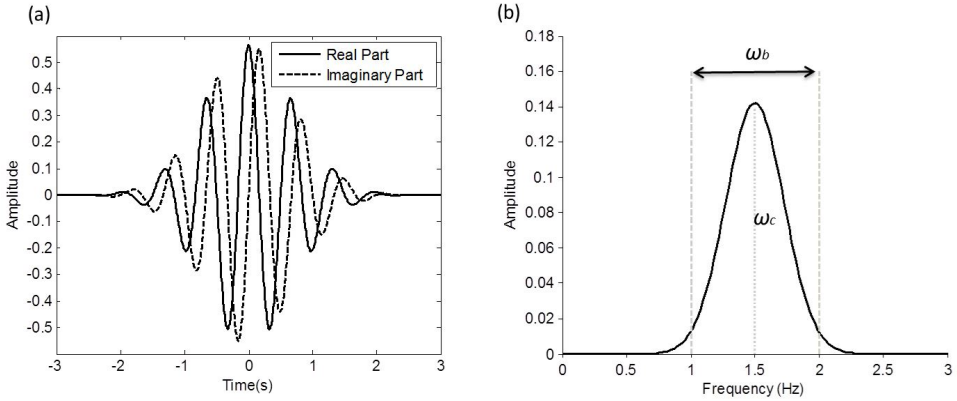

Figure 2. Complex Morlet with central frequency of 1.5 Hz and bandwidth of 1 Hz, (a) time domain, (b) frequency domain.

for spectrogram analysis [99; 100]. The complex Morlet wavelet has the following forms in the time and frequency domains [101]:

$$\psi_M(t) = \frac{1}{\sqrt{\pi\omega_b}} e^{i2\pi\omega_c t} e^{-\frac{t^2}{\omega_b}} \tag{2.11}$$

$$\psi_M(\omega) = e^{\pi^2\omega_b(\omega-\omega_c)^2} \tag{2.12}$$

where ω_b and ω_c are the parameters controlling the frequency bandwidth and the central frequency, respectively. Figure 2 shows the complex Morlet wavelet with the central frequency of 1.5 Hz and bandwidth of 1 Hz.

2.4 Second Harmonic Generation (SHG) Method using Immersion NLUT

The ultrasonic wave in the immersion NLUT propagates through water, solid and water to reach to the receiving transducer. The wave confronts two solid-fluid interfaces through its propagation path. The surfaces reflect and transmit a portion of both fundamental and higher harmonic waves. It is important to understand the contributions of each propagating medium as well as the influence of solid-fluid interfaces to the measured non-linearity. In this section, the non-linearity generated in water is described and then the influence of solid-fluid interfaces to SHG is discussed.

2.4.1 Nonlinear Acoustics in Fluid

To explain the propagation of high intensity sound in air, Nonlinear acoustics was first introduced by Euler (1766). The studies by J.M. Burgers in nonlinear acoustics led to one of the most important equations in the field of nonlinear acoustics in viscous fluids and in thermo-viscous gases [102]. Bjørnø [41] developed the nonlinear wave propagation equations in fluids based on the equations of continuity, motion, energy and state. Solving these equations and simplifying the solution result in three dimensional nonlinear acoustics wave equation called Kuznetsov's equation as shown in Equation 2.13.

$$\frac{\partial^2\Phi}{\partial^2 t} - c_0^2\Delta\Phi = \frac{\partial}{\partial t}[(\nabla\Phi)^2 + \frac{1}{2c_0^2}(\gamma-1)(\frac{\partial\Phi}{\partial t})^2 + \frac{b}{\rho_0}\Delta\Phi], \tag{2.13}$$

where b is fluid dissipation constant caused by viscosity and thermal conductivity and defined as:

$$b = \kappa(\frac{1}{c_v} - \frac{1}{c_p}) + \frac{4}{3}\eta + \xi \tag{2.14}$$

where Φ is the velocity potential which is introduced as $p = \rho_f \frac{\partial \Phi}{\partial t}$, and p is acoustic pressure, κ is heat conduction number, η and ξ are viscosity coefficients, c_p and c_v are "capacities per unit mass of the fluid of constant pressure and volume respectively, ρ is density and T is temperature. The number $\gamma - 1$ in the coefficient of the second term of right-hand side of Kuznetsov's equation (Equation 2.13) is called the parameter of non-linearity of fluid" [102]. Some of the most important wave equations in nonlinear acoustics are derived out of Kuznetsov's equations, such as the "Burgers' equation describing plane waves in homogeneous space, the generalized Burgers' equations describing cylindrical and spherical waves in homogeneous space and the Khoklov-Zabolotskaya-Kuznetsov (KZK) equation describing the propagation of sound beams" [102; 103].

2.4.2 Ultrasonic Wave Distortion in Fluid

When a finite-amplitude ultrasonic signal propagates in a fluid, it is exposed to two different effects influencing the time domain signal. First, dissipation which is caused by heat conductivity and viscosity and second, medium non-linearity due to wave distortion, which leads to the generation of higher harmonics of the fundamental frequency. Figure 3 shows the distortion of a sinusoidal wave through the space during its propagation in fluid. σ is a dimensionless distance parameter describing relative distance between ultrasonic source and measurement point. $\sigma = 1$ is the distance that the wave is distorted enough to form the first vertical tangent. The distance x, where $\sigma = \frac{x}{\ell} = 1$, is called discontinuity distance. The discontinuity distance is calculated in Equation 2.15.

$$\ell = ((\frac{B}{2A} + 1)kM)^{-1} \tag{2.15}$$

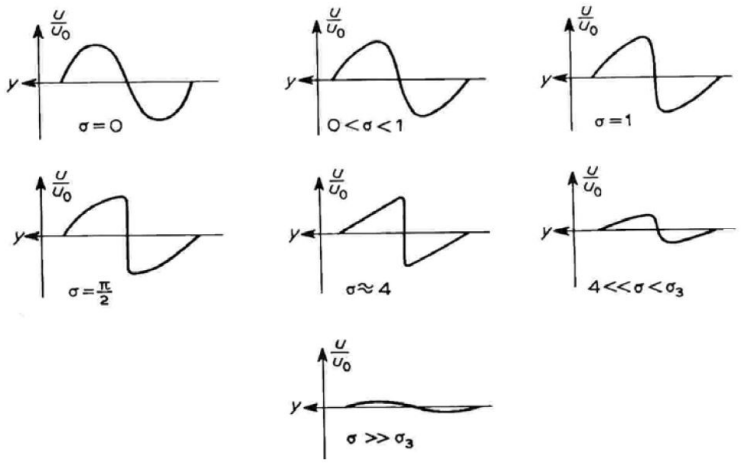

Figure 3. Wave distortion due to the propagation of finite-amplitude monochromatic wave in fluid. [41, p. 9]

where $M = \frac{u}{c_0}$ is acoustic Mach number (u is particle velocity, and c_0 is linear speed of sound), k is wavenumber and $\frac{B}{A}$ is called the second-order non-linearity parameter that quantifies the fluid acoustic non-linearity. [41].

In the range of $0 \leq \sigma \leq 1$, the dissipation is small and the dominent effect is the fluid acoustic non-linearity which leads to an increasing distortion in the sinusoidal wave and steepens the wave resulting in shock formation [41]. The distortion in time-domain signal shown in Figure 3 is represented in frequency domain by the formation of higher harmonics of the fundamental frequency. In Figure 4, the second and third harmonics along the propagation distance are shown. Figure 4 dipicts a typical variation of dimensionless amplitude (Fourier coefficient) as a function of σ for the fundamental frequency wave B_1 and second and third harmonic frequencies B_2 and B_3, respectively. Equations 140 and 105

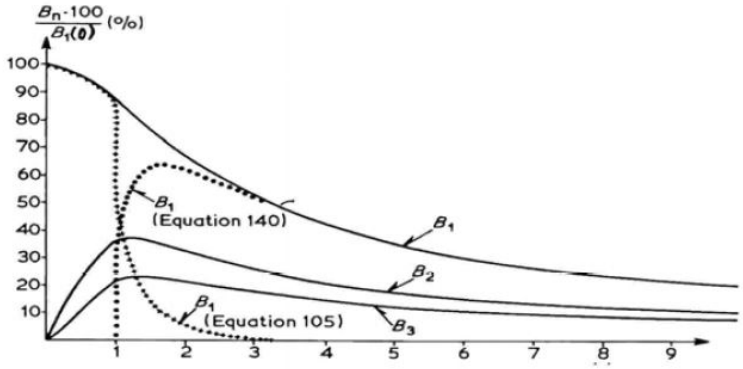

Figure 4. The variation of dimensionless Fourier coefficient as a function of σ. [41, p. 11]

refer to the Fubini and Fay solutions, respectively [41]. While the amplitude B_1 reduces continuously as the wave propagates through fluid, which is caused by the dissipation and energy transformation to higher harmonics, the amplitudes of higher harmonics show an increasing trend up to $\sigma = 1$, then a decreasing trend due to dissipation.

The exact solution of Kuznetsov's equation (Equation 2.13) in the pre-shock regime is given by the Fubini solution and in the post-shock regime is given by the Fay solution [104]. The Fubini solution is given by:

$$p(x,t) = p_0 \sum_{n=1}^{\infty} \frac{2}{n\bar{x}} J_n(n\bar{x}) sin(n\omega\tau) \tag{2.16}$$

where $J_n(x)$ is the Bessel function of order n, and $\bar{x} = \frac{x}{\ell}$ and $\tau = t - \frac{x}{c_0}$. The Fay solution is:

$$p(x,t) = p_0 \frac{2}{\Gamma} \sum_{n=1}^{\infty} \frac{sin(n\omega\tau)}{sinh(n(1+\ell)\Gamma)} \tag{2.17}$$

where Γ is the ratio of the absorption length to the shock formation distance [104]. Equation 2.16 and Equation 2.17 are used to calculate the second harmonics generated in water as the ultrasound wave propagates through water before reaching to the solid interface.

2.4.3 The Contribution of Solid-Fluid Interface in the Measured Non-linearity

Landsberger et al. [44] theoretically investigated the second harmonic generation due to the propagation of wave through the immersed solid, and compared that with the second harmonic generated in the surrounding fluid considering the reflection and transmission at the interfaces. Assuming that the ultrasonic wave propagation is normal to the solid-fluid interface, they theoretically calculated the ratio of the second harmonic amplitude generated in solid to the amplitude of the second harmonic generated in fluid as shown in Equation 2.18. In this formulation, they ignored the absorption in the fluid and the non-linearity generated in fluid on the back surface of solid. The second assumption is reasonable as the fundamental wave gets weaker due to the absorption in solid and the reflections at interface, and also the receiver can be placed very close to the back surface of the solid.

$$\frac{|P_{2t}^s|}{|P_{2t}^f|} = \frac{2A_s}{(1+Z_s/Z_f)} (\frac{h}{d_i})(\frac{\beta_s}{\beta_f})(\frac{C_f}{C_s})^2 \tag{2.18}$$

where P_{2t}^s and P_{2t}^f are the transmitted waves through solid due to the incident wave generated in solid and in fluid, respectively. Z_f and Z_s are the specific impedances of fluid and solid, respectively, d_i is

distance from the transmitter to the first interface with solid, h is solid thickness, β_f and β_s are non-linearity parameters in fluid and solid, respectively. C_f and C_s are longitudinal ultrasonic wave velocity in fluid and solid, respectively and A_s is an absorption parameter that is calculated by Equation 2.19.

$$A_s = \frac{e^{(\alpha_2^s - 2\alpha_1^s)h} - 1}{(\alpha_2^s - 2\alpha_1^s)h} \tag{2.19}$$

where α_1^s and α_2^s are absorption coefficients at the fundamental and second harmonic frequencies, respectively. The absorption parameter is approximately equal to one if either $\alpha_{1,2}^s \cong 0$ or $\alpha_2^s \cong 2\alpha_1^s$. In Equation 2.18, the incident wave is assumed as normal to the solid-fluid interface and the receiver is assumed to be placed very close to the second interface of solid. Landsberger et al. [44] calculated the ratio for an aluminum specimen and showed that the second harmonic generated in a 60 mm thick aluminum plate placed 100 mm away from the transmitter is only 4% of what is generated in the surrounding water. This implies that the contribution of the non-linearity of aluminum is negligible, compared to the non-linearity generated in fluid. This hinders the detection of micro-structural changes in materials using the immersion NLUT. However, major advantage of immersion NLUT is consistent coupling facilitating the comprehensive volume scanning, which motivates this research to investigate an approach based on phononic crystals to block the non-linearity in fluid.

2.5 Introduction to Phononic Crystals (PCs)

Phonon is a unit of vibrational energy in which a lattice of atoms uniformly oscillates at a single frequency within a crystal. Due to the bonds between atoms, the displacement of one atom leads to vibration of next atom and results in the propagation of the elastic waves [105]. Simply, one may consider a mechanical wave made of particles, known as phonons [106]. The idea of controlling the dispersion

relation for phonons has been studied by many researchers, by knowing the range of band gaps in which vibration or phonons are restricted [51]. PCs are developed to control the elastic waves in solids inspired by the concept of photonic crystals that control electromagnetic waves in air [49]. Both of phononic and photonic crystals are based on the idea that periodic structures can affect the wave propagation and generate unnatural features such as band gap formation. PCs, also known as acoustic metamaterials, are artificial composite, man-made periodic systems creating new responses through physical constraints in the constituent materials [50; 107]. The superior property of the acoustic metamaterial is attributed to its engineered geometry and artificially induced inhomogeneity [108]. The periodicity or the lattice constant, and composite behavior of resonating unit cells control the scattering of elastic waves, as a consequence, the wave properties. The reflections can be destructive or constructive based on the periodic geometry and the wave frequency. The destructive reflection attenuates the propagating wave and formes the band gap in PCs [49; 50; 109]. By tailoring the band structure, these materials can exhibit band gaps that attenuate particular frequencies and wave modes while passes other frequencies [51]. The band gap of the metamaterial can be controlled by the contrast of elastic constants, the filling fraction and the lattice (i.e., periodicity) of the constructed element, and the thickness of the base plate [110; 111]. The band gap formation offers many applications such as wave field focusing [112; 113; 114], wave filtering [2; 115], and acoustic rectification [116]. In structural applications, the global periodicity is considered to reduce structural vibrations from earthquakes [117; 118; 119], and noise reduction in residential structures [120].

The band gap forms through two different mechanisms, known as Bragg's scattering and local resonance. The Bragg's band gap is formed by destructive interface of waves through the periodic media

[50; 3]. The wavelength associated with the Bragg type is in the same order as the periodicity of the structure. In contrast, the local resonant type exhibits band gaps at wavelengths much larger than their lattice size, which makes this type preferable for low frequency applications [121]. The band gap results from the local resonators in the medium, such as stubs that are periodically placed on the surface of a plate [122].

The periodic structure can be arranged in one, two or three dimensions. The one-dimensional periodic phononic crystals (PCs) are called superlattices (SLs). The SLs structure is composed of two or more periodically repeated layers which are placed along the SLs growth direction. Each unit cell of SLs can be made of solid-solid or solid-fluid layers [50].

2.5.1 One-Dimensional Mono-Atomic PCs

The basic concept of wave propagation through a periodic structure is theoretically studied by Hussein et al. [123], and briefly described in this section. The discussion starts from the case of 1D mono-atomic crystals and is followed by the case of 1D bi-atomic crystals. First, consider a one-dimensional periodic system in the form of a spring-mass chain as shown in Figure 5(a). The sequence of masses, m, are connected by linear springs, α, at distance a.

In the absence of an external load, the wave equation of motion for the n^{th} mass is presented by Equation 2.20 [50]:

$$m\frac{d^2u_n}{dt^2} = \alpha(u_{n+1} - u_n) - \alpha(u_n - u_{n-1}) \tag{2.20}$$

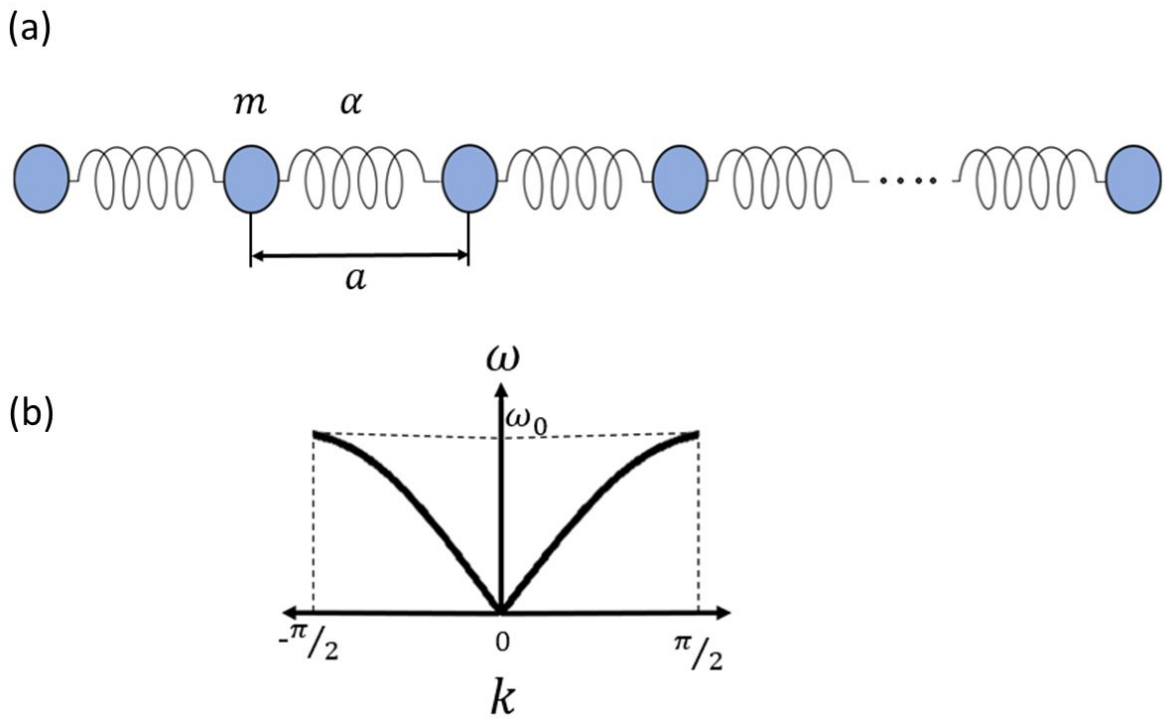

Figure 5. Schematics of (a) 1D mono-atomic PCs and (b) its dispersion curve.

where u_n is the displacement of mass number n in reference to the rest position. The solution of the equation of motion can be found in the form of a harmonic plane wave as presented in Equation 2.21 [50]:

$$u_n = Ae^{ikna-i\omega t} \tag{2.21}$$

where k is the wave number and ω is the angular frequency of the wave. The spatial part of the solution, as presented in Equation 2.22, represents the Bloch-Floquet theorem, which describes the plane wave propagation in a periodic medium.

$$\hat{u}_n = Ae^{ikna} \tag{2.22}$$

The imaginary component in this expression designates the spatial decay as the wave propagates through the lattice. After substituting the spatial solution in the wave equation of motion and finding the nontrivial solutions, one can find the dispersion relation for the 1D lattice as:

$$\omega(k) = \omega_0 |sink\frac{a}{2}| \tag{2.23}$$

The dispersion relation for propagating wave in a 1D mono-atomic crystal is illustrated in Figure 5(b), where $\omega_0 = 2\sqrt{\frac{\alpha}{m}}$ is the highest angular frequency. Equation 2.23 is considered in the symmetric period of $k = [-\frac{\pi}{a}, +\frac{\pi}{a}]$ which is called the first Brillouin zone of the 1D PCs [50].

2.5.2 One-Dimensional Bi-Atomic PCs

The bi-atomic crystals consist of two different masses, m_1 and m_2 in a lattice that are connected by spring α, as shown in Figure 6(a). In this case, there are two equations of motion for two adjacent masses (with displacements u and v) inside a lattice, in the absence of an external load expressed as [124]:

$$\begin{aligned} m_1 \frac{d^2 u_n}{dt^2} &= \alpha(v_n + v_{n-1} - 2u_n) \\ m_2 \frac{d^2 v_n}{dt^2} &= \alpha(u_{n+1} + u_n - 2v_n) \end{aligned} \tag{2.24}$$

The solution of periodic system with the elementary cell size as D is defined as [124]:

$$\begin{aligned} u_n &= U e^{nkD-\omega t} \\ v_n &= V e^{nkD-\omega t} \end{aligned} \tag{2.25}$$

The dispersion equation that shows the relationship between ω and k is obtained by substituting Equation 2.25 into Equation 2.24 as [124]:

$$\omega^2 = \alpha \frac{m_1 + m_2 \pm \sqrt{(m_1 + m_2)^2 - 2m_1 m_2 (1 - cos(kD))}}{m_1 m_2} \tag{2.26}$$

The corresponding dispersion diagram obtained from Equation 2.26 is shown in Figure 6(b). The dispersion relation has two branches: (i) optical branch that corresponds to the "$+$" part of Equation 2.26 and (ii) acoustic branch that corresponds to the "$-$" part of Equation 2.26. In a non-

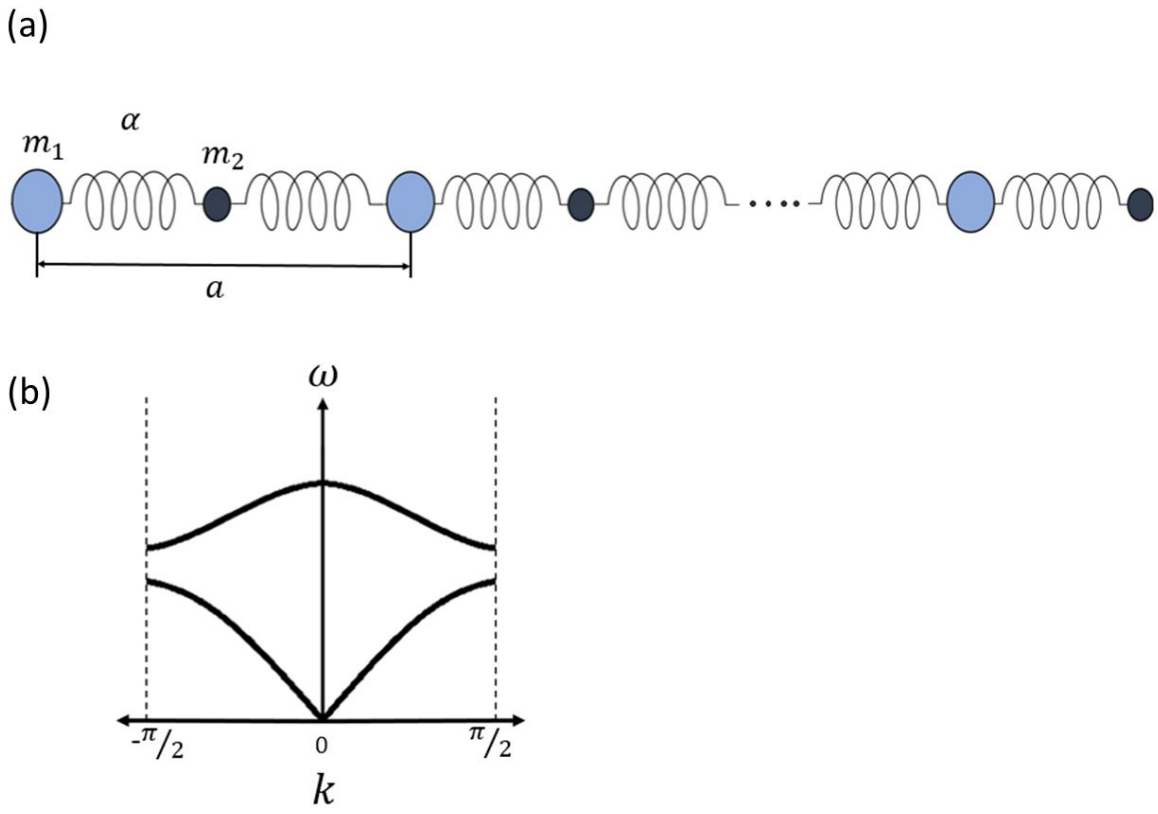

Figure 6. Schematics of (a) 1D bi-atomic PCs and (b) its dispersion curve. [124]

homogeneous 1D bi-atomic crystals ($m_1 \neq m_2$) there is a separation between the two branches which is called band gap.

CHAPTER 3

WAVELET-BASED HARMONIC DECOMPOSITION OF NONLINEAR ULTRASONIC SIGNAL IN ASSESSMENT OF PLASTIC STRAIN IN ALUMINUM

This chapter is partially published at Measurement Journal with the title of "Wavelet Based Harmonics Decomposition of Ultrasonic Signal in Assessment of Plastic Strain in Aluminum" in collaboration with Negar Kamali, Niloofar Tehrani, and Professors Didem Ozevin, Sheng-Wei Chi, Ernesto Indacochea [1].

3.1 Introduction

This chapter presents the wavelet-based signal decomposition approach to determine the amplitudes of fundamental frequency and its harmonics. The approach is experimentally demonstrated on aluminum 1100 samples with different levels of plastic deformation, and compared with the conventional Fourier transform-based approach. The NLUT is employed in contact mode using lubricant oil as the coupling between the specimen and transducers.

3.2 Wavelet-based Harmonic Decomposition Method

Figure 7 shows the schematic of the proposed method to extract the amplitudes of the first and second harmonic frequencies. A typical received time-domain signal obtained from a pristine specimen is shown in Figure 7(a). The Fourier spectrum of the received signal shows that the fundamental frequency is 2.014 MHz and the second harmonic frequency is 4.028 MHz. The time-frequency spectrogram is then obtained with the selected mother wavelet (complex-Morlet mother wavelet function with the cen-

tral frequency of 1.5 Hz and bandwidth of 1 Hz) (Figure 7(b)). The fundamental and second harmonic frequencies are marked in the wavelet spectrogram using red dashed lines. The amplitudes of the fundamental and second harmonics with respect to time, $A_1(t_i)$ and $A_2(t_i)$, respectively, related to the red lines and extracted from the wavelet spectrogram, are shown in Figure 7(c). Here the subscript i denotes the i^{th} data point. In this study, unless otherwise indicated, the time history signals consist of 2048 discrete points. Using the time histories of the fundamental and second harmonics, the acoustic non-linearity parameter is obtained by two different schemes: (i)time-invariant: $\beta(t_i) = \frac{max|A_2(t_i)|}{max|A_1^2(t_i)|}$ and (ii) time-dependent: $\beta(t_i) = \frac{A_2(t_i)}{A_1^2(t_i)}$.

In the time-invariant approach, the peak amplitudes of the fundamental and second harmonics are identified from their time history signals, while in the time-dependent approach the acoustic non-linearity parameter is calculated over time and averaged in the stable time interval.

3.3 Materials Preparation

Aluminum 1100 is used in this investigation with a chemical composition shown in Table I. Nine tensile specimens are machined from a 6.3 mm (0.25 in.) thick cold rolled plate according to ASTM standard E8 to the dimensions shown in Figure 8. All samples are stress relieved at 250 °C for 15 minutes prior to tensile testing. An MTS tensile machine, model 1125 is used for the tensile tests using a strain rate of 2.54 mm/min. The samples are plastically deformed between 0.5% and 4% at 0.5% strain increments to produce different uniform plastic strains through the strain gauge to avoid non-uniform plastic deformation.

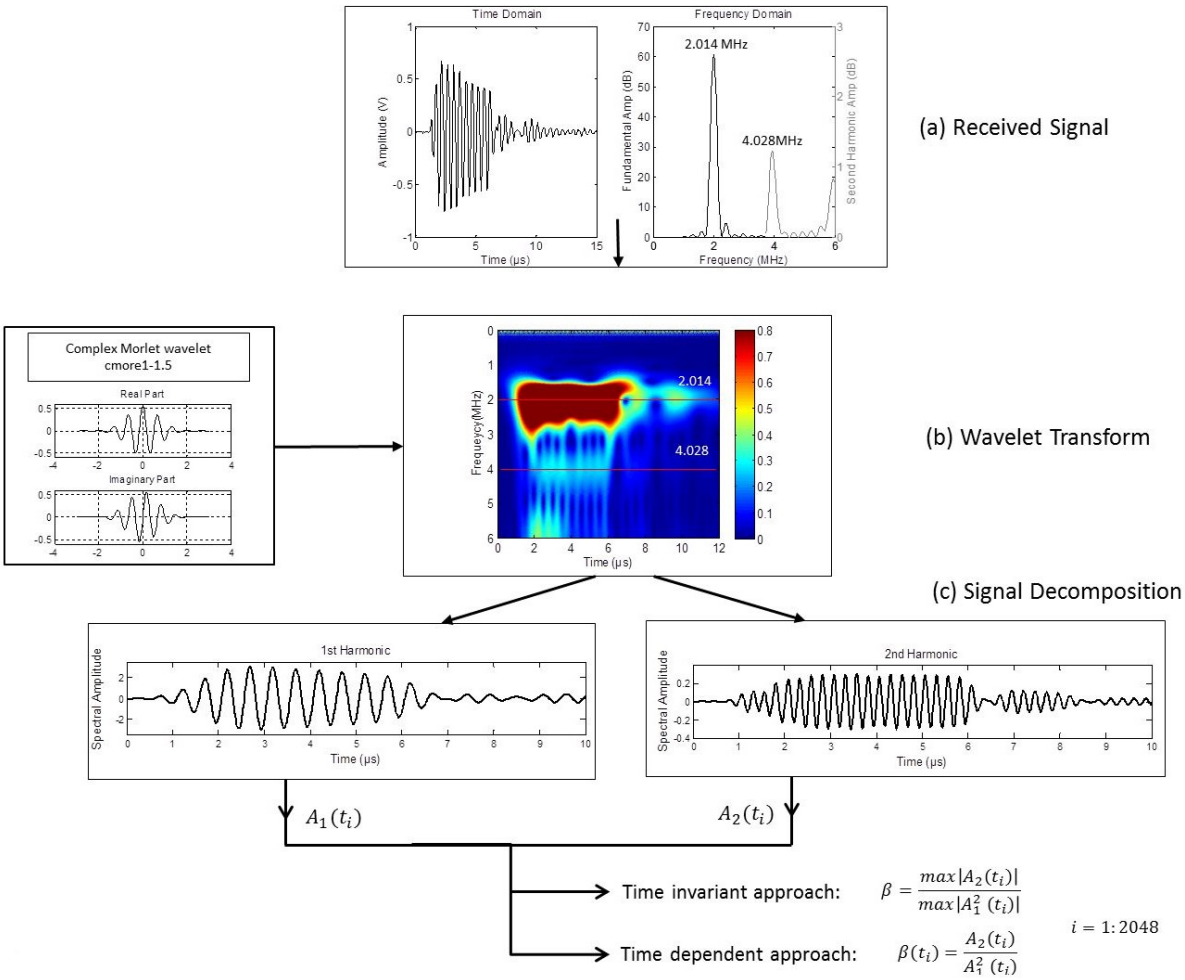

Figure 7. Schematic to obtain the acoustic non-linearity parameter β using WT.

TABLE I

NOMINAL CHEMICAL COMPOSITION OF ALUMINUM 1100

Aluminum 1100	Al	Cu	Mn	P	Si + Fe	Zn	Others
Weight%	99 min	0.05-0.2	0.05 max	0-0.03	0.95 max	0.1 max	0.15 total

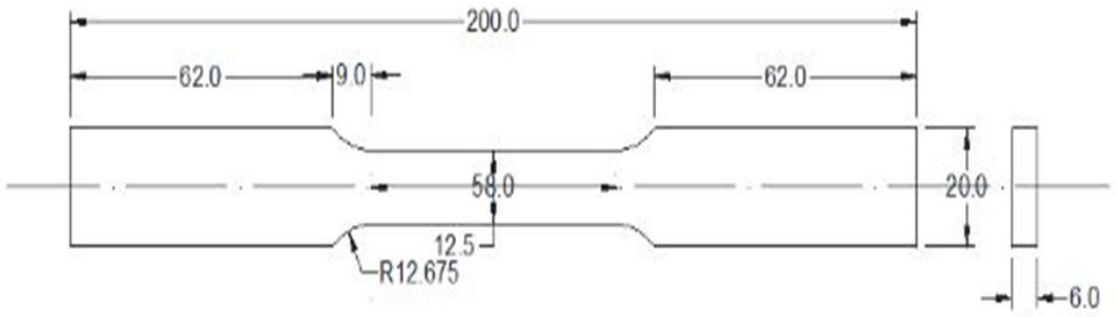

Figure 8. Tensile test sample dimensions (All dimensions are in mm).

3.4 Contact NLUT Method

There are two modes of ultrasonic testing: through-transmission and pulse-echo. Separate transducers are needed for transmitting a signal to a structure and receiving the propagating waves in the structure for the through-transmission mode. The transmitting transducer is placed on one side of the structure, and the receiving transducer is placed on the opposite side of the structure. For the pulse-echo mode, the same transducer is used as both transmitter and receiver. As nonlinear ultrasonic method is based on detecting higher-harmonic signals, the through-transmission mode should be selected for tuning the receiving transducer to the higher harmonics of the transmitting transducer (Figure 9(a) and (b)). The schematic ultrasonic testing setup in through-transmission mode is shown in Figure 9(b). In order to provide a consistent coupling force and minimize the coupling error as discussed by Liu et al. [36] a weighted grip (24.5 N) is used to hold the transducers aligned to each other (Figure 9(c)). Light lubrication oil is used as the couplant between the transducers and the test specimens. The experiments are repeated three times with recoupling the ultrasonic transducers between each measurement to check the repeatability. The transmitting and receiving transducers used in this study are piezoelectric transducers manufactured by Olympus and have effective diameter of 0.95 cm (0.375 inch) with the central frequencies of 2.25 MHz (transmitter) and 5 MHz (receiver), and the calibration curves shown in Figure 9(d).

The major inputs to the data acquisition of NLUT operating in through-transmission mode are input voltage, excitation frequency, and cycles in harmonic loading. In this study, the input signal is a 10-cycle 100-volt tone burst at 2.25 MHz, which is generated by the Pocket UT system manufactured by MISTRAS Inc. The time-history signal of the 5 MHz receiver is recorded using the same UT system

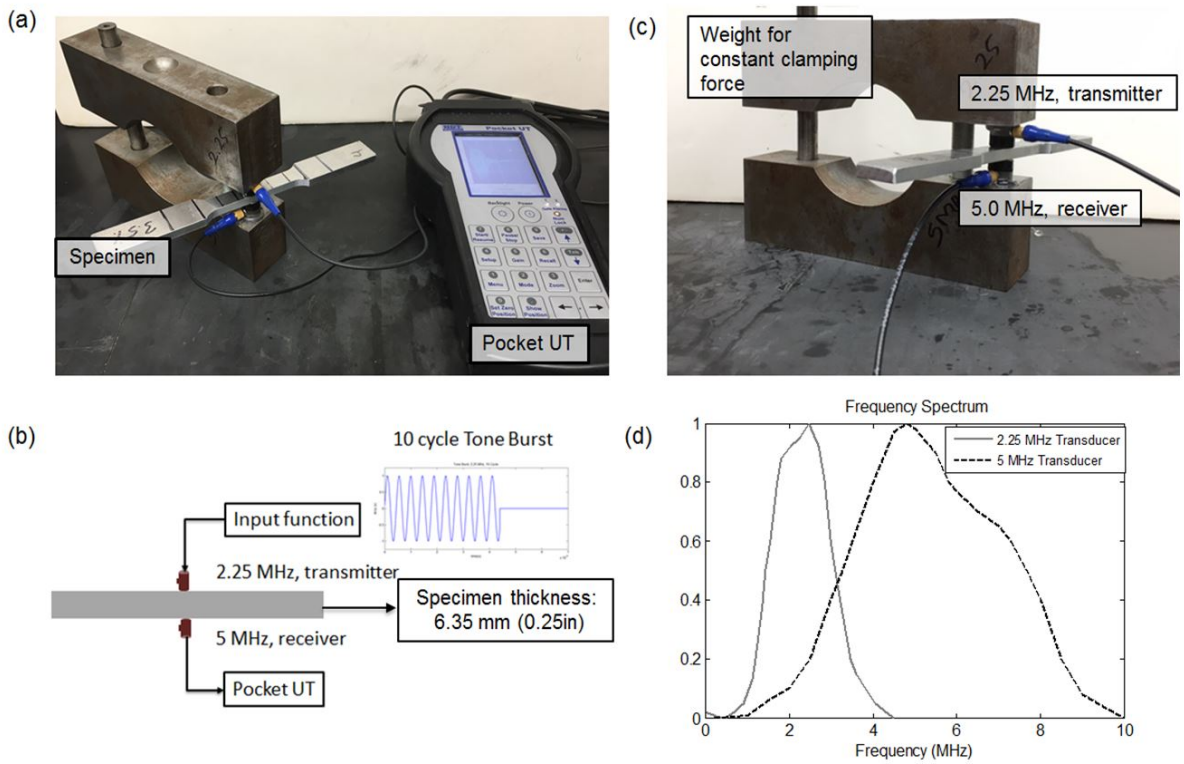

Figure 9. Ultrasonic testing of aluminum specimens: (a) experimental setup, (b) schematic diagram, (c) ultrasonic transmitter and receiver in through-transmission mode, and (d) transducer calibration curves.

with the sampling frequency of 100 MHz and a band-pass filter of 1 MHz-20 MHz. To improve the signal to noise ratio (SNR), twenty signals are averaged. The signal processing is performed using MATLAB software. It is important to note that the specimen thickness is smaller than the spatial length of 10-cycle tone burst signal, which causes the interference of incident and reflected waves. However, as the experimental conditions are preserved for testing each sample, the change in the acoustic non-linearity parameter is correlated with the presence of plastic deformation.

3.5 Experimental Results Using FFT

Once the aluminum specimens are loaded up to different strain levels and released with different permanent plastic strains, they are tested using longitudinal ultrasonic waves in a through-transmission mode to correlate the plastic deformation with the acoustic non-linearity parameter. An example of time-domain and frequency-domain signals is shown in Figure 10. The waveform is obtained from the pristine, 2% strained, and 4% strained samples and the frequency domain obtained by applying FFT. The amplitude of the second harmonic signal (1.5 dB) near 4 MHz is significantly lower than the amplitude of the first harmonic signal (65 dB) near 2 MHz.

When FFT is applied to perform the harmonic separation, it is observed that the amplitudes of harmonic frequencies highly depend on the window selected in the time domain. Figure 11 shows the normalized acoustic non-linearity parameter calculated using the A1 and A2 amplitudes obtained by conducting FFT by selecting different time windows. The gray dashed lines show the window selected to compute the Fourier transform. As the ultrasonic non-linearity due to plastic deformation is weak, the slight changes in the amplitudes of harmonic frequencies significantly affect the result. As shown in Figure 11, when the window is selected as (a) 0-15 μs, the acoustic non-linearity parameter increases

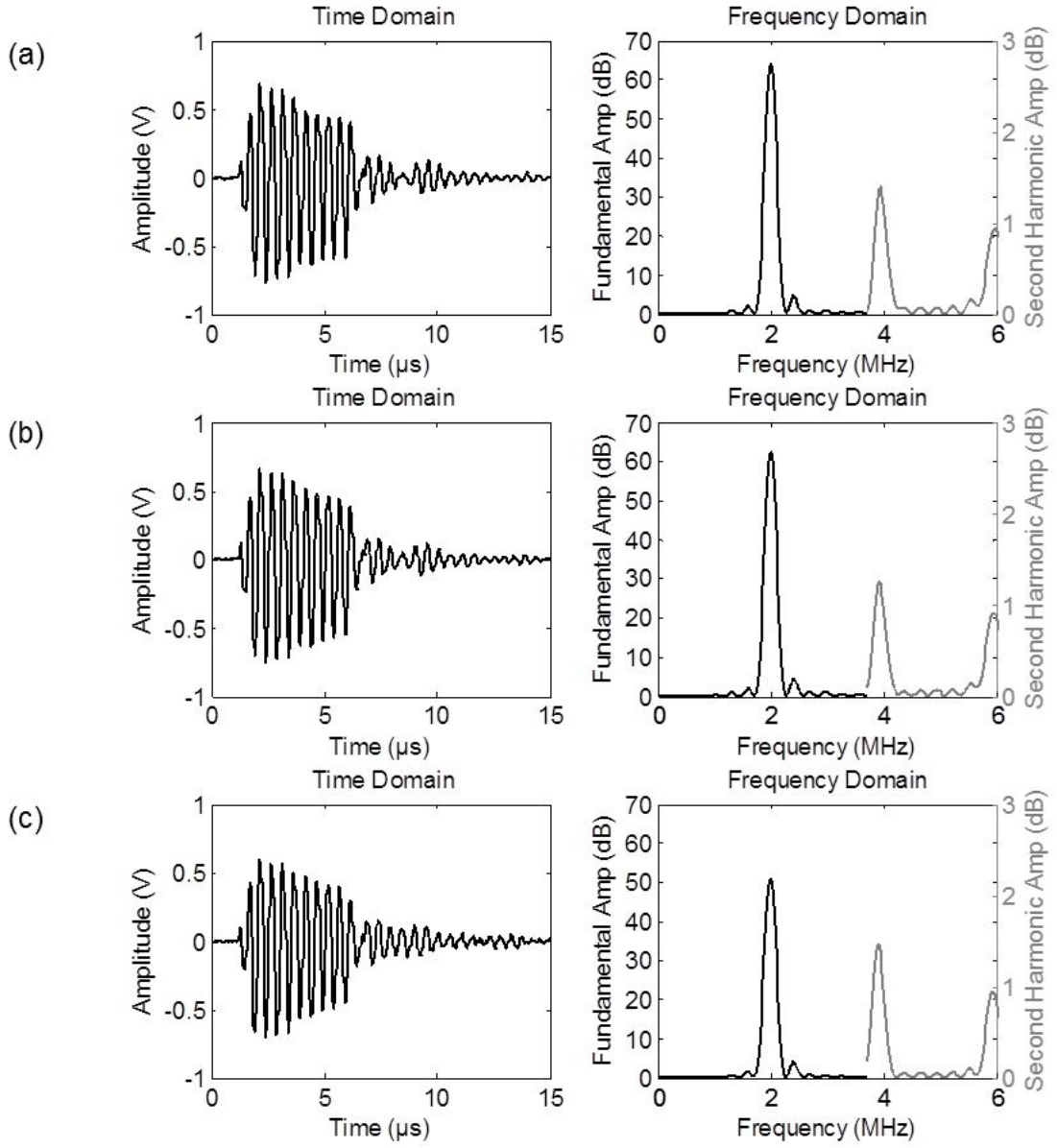

Figure 10. Typical time-domain waveforms and their frequency spectra for (a) pristine specimen, (b) 2% strain specimen, and (c) 4% strain specimen.

with the increase of plastic strain. However, when the window is changed to (b) 0-9μs, (c) 1.2-7.0μs, or 2.0-5.5 μs, the correlation between the acoustic non-linearity parameter and the plastic strain does not exist.

Table II shows the values of the acoustic non-linearity parameter obtained by different time windows. The last row in Table II shows the maximum percentile variation of the calculated non-linearities for each specimen compared to the mean value of the calculated non-linearities of that specimen. For the same data set, the acoustic non-linearity parameter can change more than 100% by varying the time window. Therefore, identifying the acoustic non-linearity parameter by FFT introduces significant error in the measurement. Therefore, identifying the acoustic non-linearity parameter by FFT introduces significant error in the measurement.

3.6 Experimental Results Using WT

Figure 12 shows the time histories of wavelet coefficients for the first and second harmonic frequencies for four different plastic strains. The second harmonic amplitude is almost one order of magnitude smaller than the fundamental amplitude. Figure 13 shows the stress-strain curve for the aluminum 1100 specimen together with the normalized acoustic non-linearity parameter of each sample calculated using time-invariant approach. As the thickness changes in different plastic strain levels, the thickness of each sample is measured and taken into the account to calculate acoustic non-linearity parameter. These parameters are plotted as a function of strain as shown in Figure 13. It is observed that the acoustic non-linearity parameters exhibit stationary behavior up to 1% strain. A rapid increase in the acoustic non-linearity parameter occurs between 1% strain and 3.5% strain, but then saturation in the acoustic

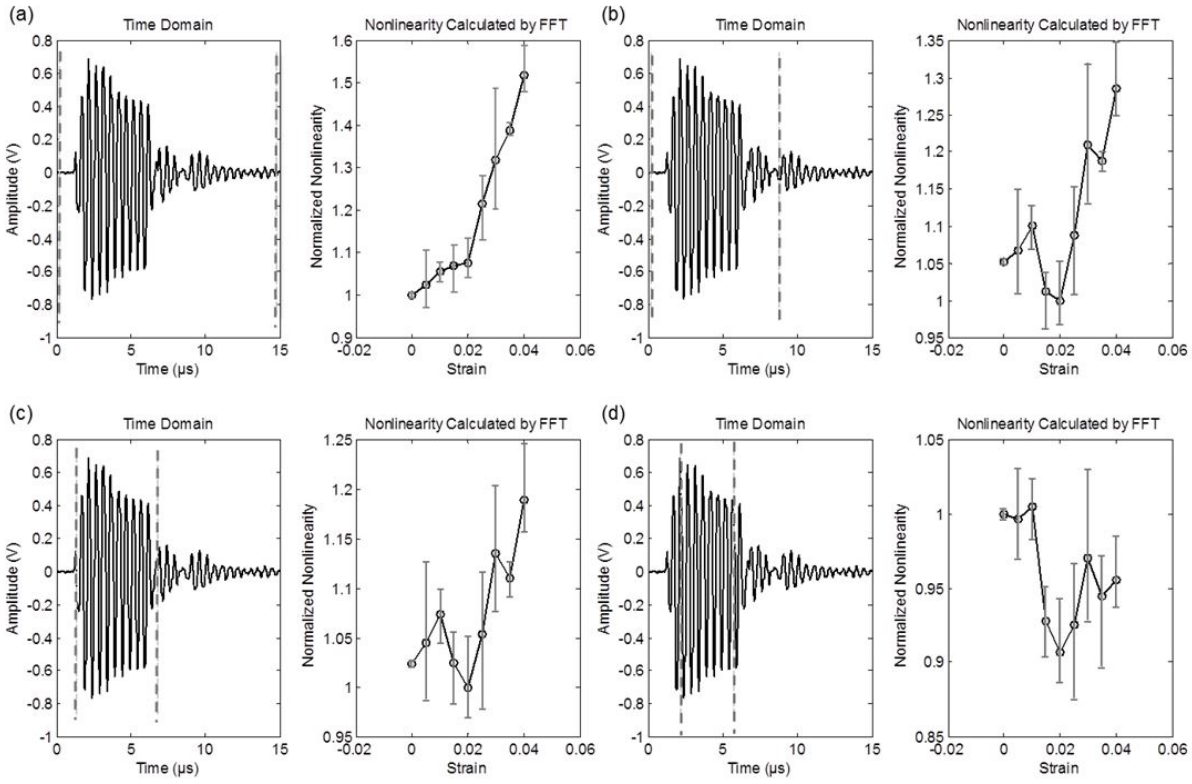

Figure 11. The variations in the acoustic non-linearity parameter corresponding to time-domain windows calculated by FFT: (a) 0-15μs, (b) 0-9 μs, (c) 1.2-7.0μs and (d) 2.0-5.5μs.

TABLE II

ACOUSTIC NON-LINEARITY PARAMETER OBTAINED BY FFT

Start Time(μs)	Finish Time(μs)	Acoustic Nonlinearity Parameter				
		Pristine	0.01	0.02	0.03	0.04
0	15	0.272	0.287	0.293	0.359	0.414
0	9	0.147	0.154	0.140	0.169	0.180
1	8	0.106	0.111	0.104	0.124	0.132
1.5	7.5	0.092	0.095	0.088	0.102	0.111
2	7	0.091	0.091	0.084	0.091	0.090
2.5	6.5	0.088	0.089	0.083	0.091	0.092
3	6	0.114	0.116	0.104	0.115	0.117
	%change	109.193	113.293	128.937	139.126	155.042

non-linearity parameter ensues near 3.5% strain, which is close to the necking point. The ultrasonic measurement is repeated three times for each sample.

The second approach to identify the acoustic non-linearity parameter using the time histories of wavelet coefficients for the first and second harmonics is based on obtaining the wave envelopes at each frequency, and calculating acoustic non-linearity parameter to the entire time-history data as shown in Figure 14 for the pristine specimen. While the peak amplitudes of each frequency component do not occur at the same time, the acoustic non-linearity parameter shows a constant regime within the time interval 2.0 - 5.5 μs. The same approach is repeated for the rest of the specimens that underwent different levels of plastic strain as shown in Figure 15. In general, the time-dependent acoustic non-

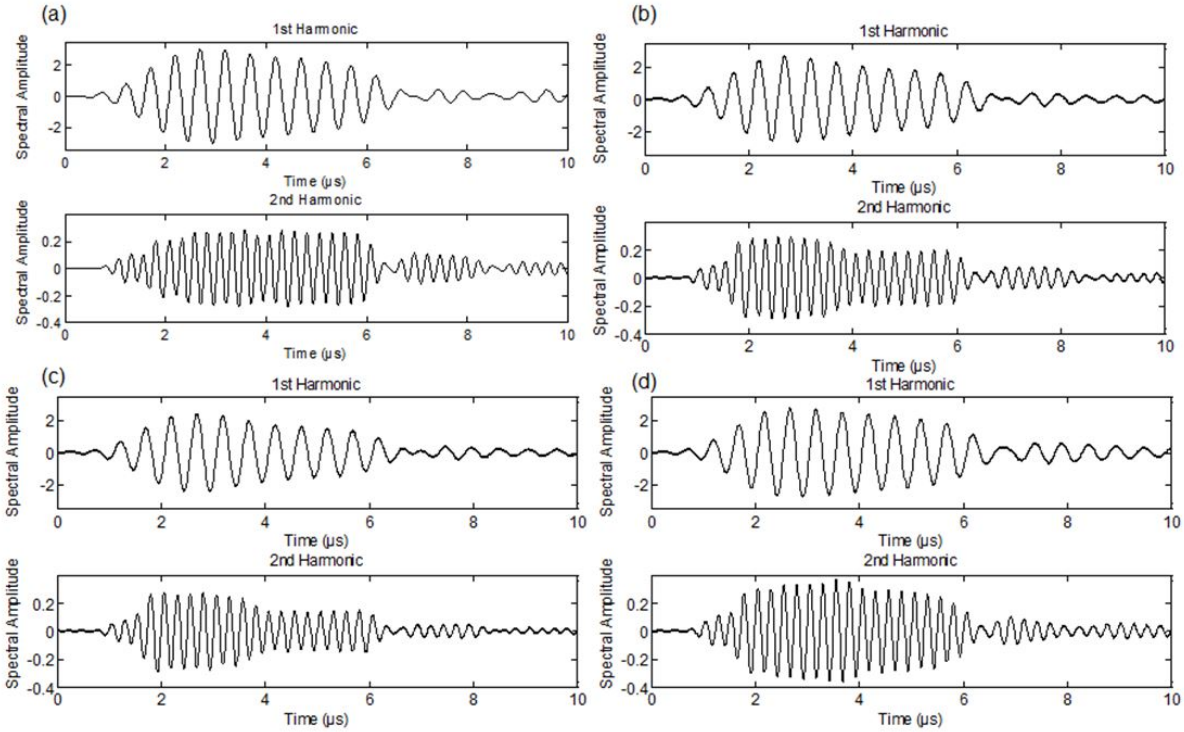

Figure 12. Fundamental and second harmonic waveforms extracted from the spectrograms corresponding to samples: (a) pristine, (b) 2% strained, (c) 3% strained, and (d) 4% strained.

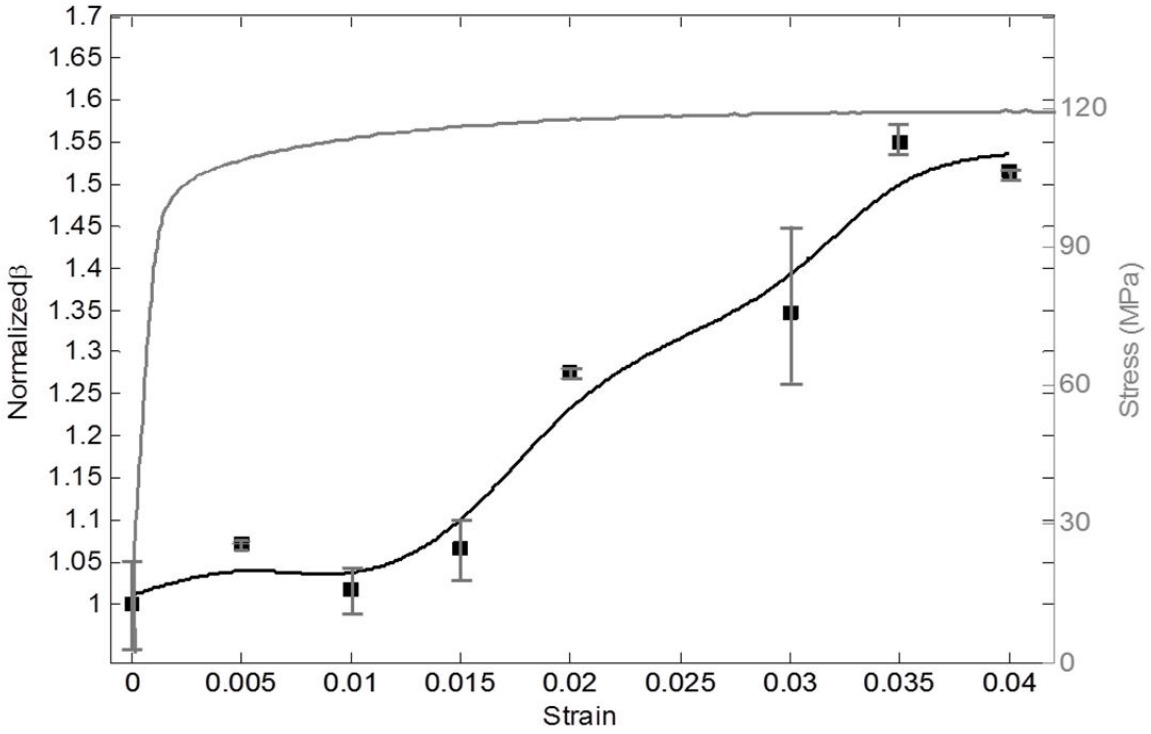

Figure 13. Stress-strain curve and normalized non-linearity-strain curve using the time-invariant approach on two-scale plot.

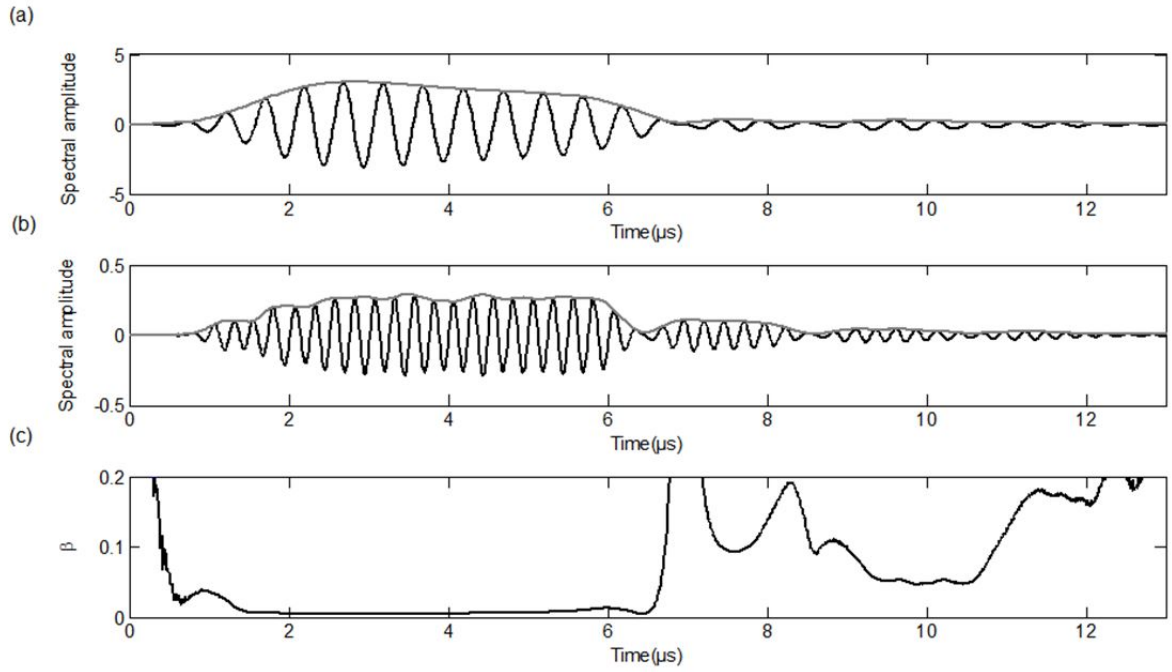

Figure 14. (a) Time-history waveform of the first harmonic, (b) time-history waveform of the second harmonic, and (c) change in acoustic non-linearity parameter with time (for pristine specimen).

linearity parameter increases with the increase of plastic strain while some fluctuations are observed in the data set.

All the acoustic non-linearity parameters are averaged in the time interval of 2.6 -3.6 μs and plotted as a function of the amount of strain as presented in Figure 16, along with the stress-strain curve for a pristine aluminum 1100 sample. The results of both wavelet-based algorithms, time-invariant and time-dependent, link the acoustic non-linearity parameter and plastic strain in the material. The acoustic non-

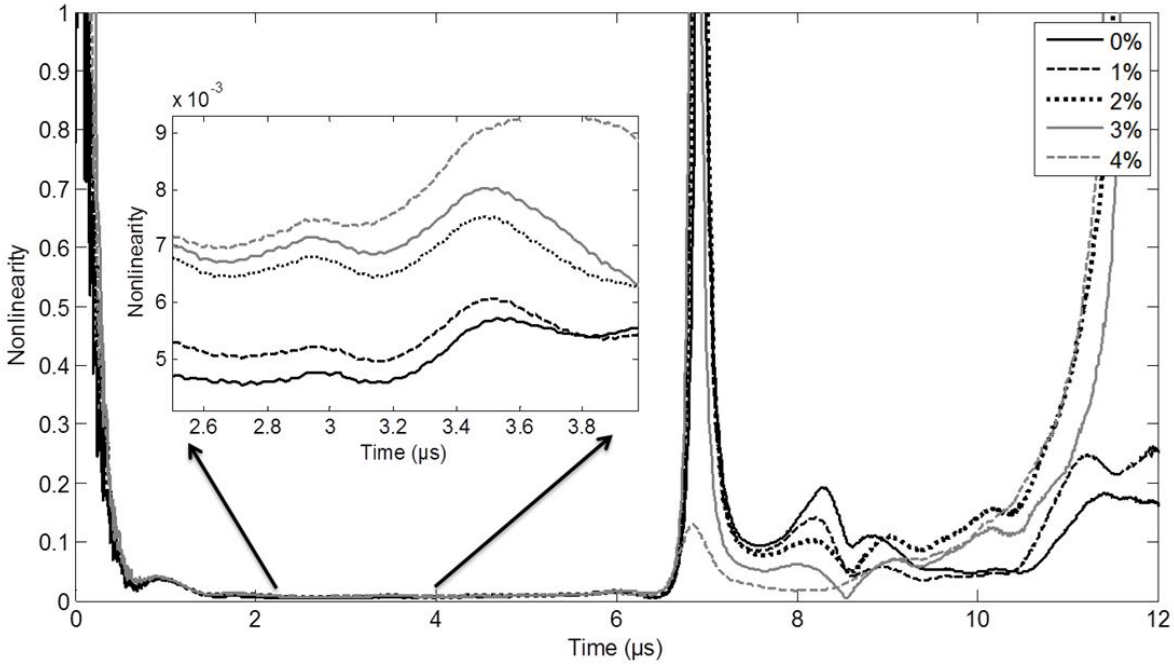

Figure 15. Change in acoustic non-linearity parameter within time for different strain levels.

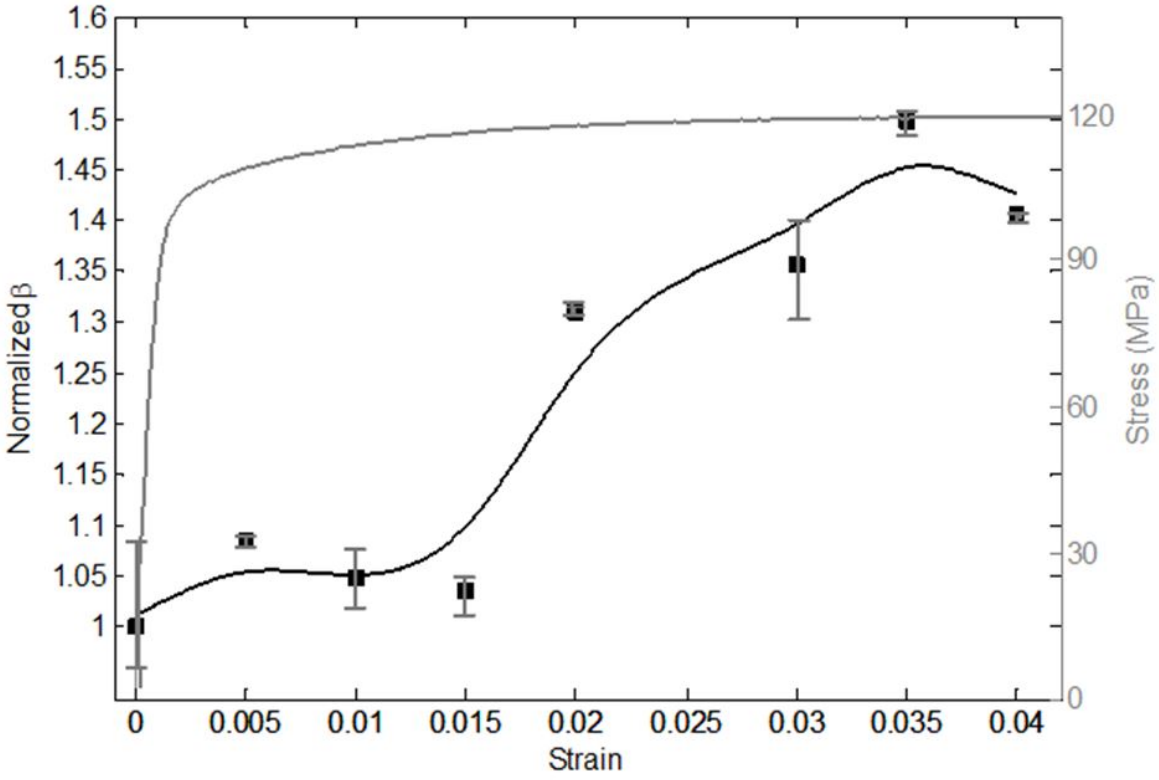

Figure 16. Stress-strain curve and normalized non-linearity-strain curve using the time-dependent approach on two-scale plot.

linearity parameter increases by 55% in the time-invariant algorithm, and 45% in the time-dependent algorithm.

3.7 Summary

The measurement of β using the most common signal processing method, FFT, shows significant variation depending on the selection of different time windows of the ultrasonic waveform. It is shown

that the measured β can change more than 100% by varying the time window. Therefore, identifying β by FFT can introduce significant error in the measurement. Two wavelet-based algorithms are introduced to obtain β: time-dependent and time-invariant. The developed wavelet based schemes are employed to investigate the change of acoustic non-linearity parameter β caused by plastic deformation for validation. The accuracy of harmonic decomposition of nonlinear wave signal due to plastic deformation is improved by applying the wavelet-based algorithm. Although a good correlation with the reduced error between β and plastic deformation is obtained in both wavelet-based algorithms, the time-dependent algorithm is employed in the next chapter as it provides more data points.

CHAPTER 4

THE INTEGRATION OF SUPERLATTICES AND IMMERSION NLUT TO ENHANCE DAMAGE DETECTION THRESHOLD

The content presented in this chapter is partially published at the journal of Applied Physics Letter with the title of "The Integration of Superlattices and Immersion Nonlinear Ultrasonics to Enhance Damage Detection Threshold" in collaboration with Minoo Kabir, and Professor Didem Ozevin [2], and in the proceeding of the IWSHM conference, Structural Health Monitoring 2017 with the title of "Enhancing the Robustness of Nonlinear Ultrasonic Testing by Implementing 1D Phononic Crystals" in collaboration with Minoo Kabir, and Professor Didem Ozevin [3].

4.1 Introduction

While chapter 3 studies the improvement of contact NLUT through applying wavelet-based signal processing method, this chapter presents the enhancement of immersion NLUT by exploiting superlattices (SLs). SLs are proposed to remove the non-linearity arisen from water and experimental instruments. The chapter begins with introducing to the technical approach. Then, the wave propagation through the SLs is numerically studied to tailor the periodic geometry, and tune the band gap to the second harmonic frequency. The chapter continues with experimentally studying the band gap formation in SLs through the immersion NLUT setup. The improvement in the sensitivity of the NLUT is demonstrated through detecting the micro-structural changes associated with plastic deformation in aluminum 1100 specimens. Subsequently, a solid-solid SLs are introduced with the purpose of removing the instru-

ment non-linearity in the contact NLUT. The solid-solid SLs are numerically designed and the band gap formation is experimentally demonstrated.

4.2 Technical Approach

As discussed above, the SHG method is based on the measurement of fundamental and second harmonic amplitudes of the ultrasonic wave to calculate the acoustic non-linearity parameter β. Non-linearity is generated in every stage of the NLUT experiment. For instance, function generator and amplifiers can induce large non-linearities [79]. Additionally, in the case of immersion NLUT, water also introduces high non-linearity to the measured signal, which obscures the weak non-linearity in solids [41; 44]. To remove the ambient non-linearity generated in the immersion NLUT, SLs are integrated with the measurement system. SLs are designed to provide a band gap range that includes the second harmonic frequency (4.5 MHz) while passing the fundamental frequency (2.25 MHz) as used in the NLUT in this specific research. Figure 17(a) shows the immersion NLUT setup. The transducers are immersed into the water tank. The central frequencies of transmitter and receiver are 2.25 and 5 MHz, respectively. The solid medium (the same specimens as Chapter 3) is placed in the ultrasonic propagation path, and the SLs are placed right before the solid medium facing to the transmitter. Figure 17(b) shows the frequency domain of a typical received signal with the black line, and the desired band gap, presented by a transmission loss, with a blue shade. A_2 is placed in the band gap frequency range. As a result of this, SLs can remove the second harmonic frequency generated by water and instruments in the transmitting side.

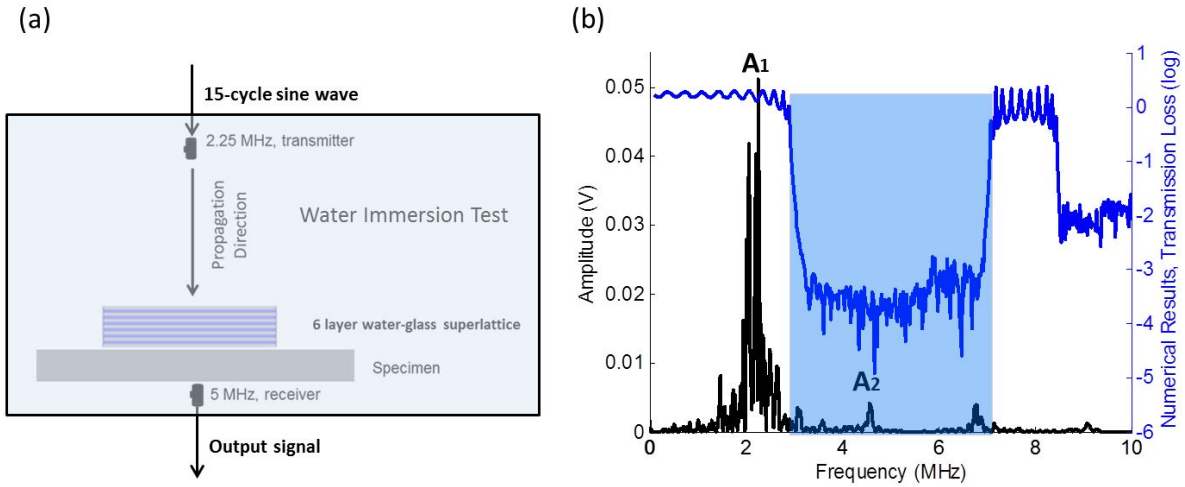

Figure 17. The approach to integrate the SLs with the immersion NLUT (a) NLUT setup with the presence of SLs, (b) the designed band gap tuned to the second harmonic frequency.

4.3 Numerical Results

Numerical simulation of the SLs structure is performed to study the wave transmission loss. The SLs structure made of binary layers of solid-fluid is numerically modeled using COMSOL Multiphysics. The structure is modeled using solid mechanics module, and a frequency domain study is implemented in the frequency range of 100 kHz to 10 MHz. The numerical model of the solid-fluid SLs is shown in Figure 18(a). A unit boundary load is applied on the left layer for excitation and the displacement is measured on the right layer. The ratio of the average boundary displacement on the received and transmitted sides of the SLs is then calculated as the transmission loss through the periodic layers. The perfectly match layers (PML) are introduced to prevent the boundary reflections. Free triangular

elements are used to mesh this model. In general, denser mesh provides more accurate results in the numerical simulations; however, it makes the computation more expensive in terms of time and computer resources. In order to achieve acceptable accuracy as well as high efficiency, the mesh resolution is kept at least 20 elements in one wavelength of the second harmonic frequency [125; 126; 127]. In this research, receiver and transmitter frequencies provide responses as 2.25 MHz and 4.5 MHz, respectively. Therefore, the SLs are tuned to a pass band including 2.25 MHz and a band gap consisting of 4.5 MHz. Binary composite structures made of different solid materials and water as presented in Table III are numerically studied [56]. It is observed that layer thickness (lattice size) and materials properties can affect the position and width of the band gap frequency. After trying different geometries and materials, the final geometry is selected as periodic layers of 100 μm water and 100 μm glass. Figure 18(b) shows the numerical result of the through transmission study for the designed SLs. The dark shade shows the band gap range, and it contains 4.5 MHz while 2.25 MHz is in the pass band range. Figure 19 shows the displacement field at the fundamental and second harmonic frequencies through the simulated SLs (2.25 MHZ and 4.5 MHz, respectively). The 4.5 MHz signal cannot propagate through an array of 100 μm thick glass and 100 μm thick water while 2.25 MHz signal propagates through the designed SLs.

4.4 Experimental Study

In this section, the acoustic non-linearity parameters measured using two different immersion NLUT setups ((i) without the SLs and (ii) with the SLs) are presented. The SLs fabrication, ultrasonic measurement procedure and experimental setup are discussed. The specimens used in this study are the same as the specimens used in section 3.3.

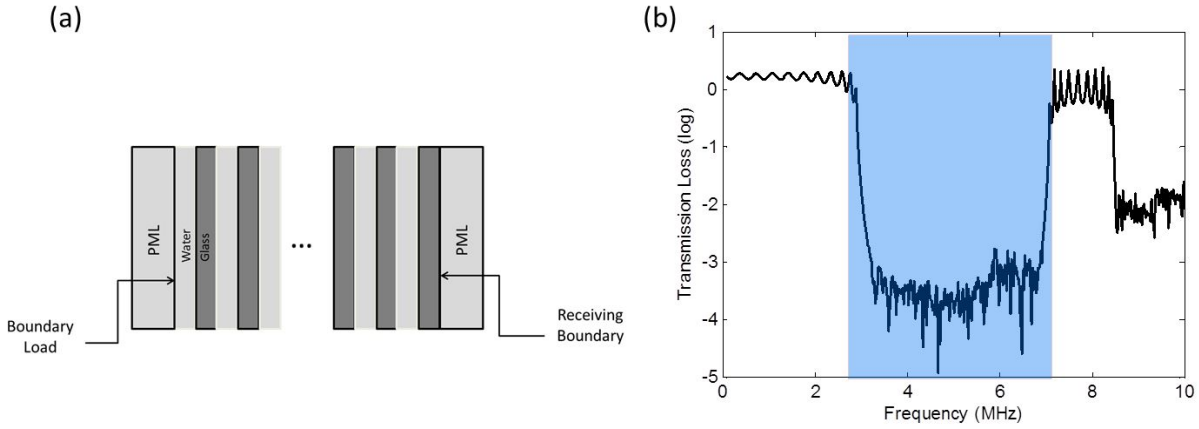

Figure 18. (a) Numerical model, and (b) transmission loss through SLs (100 μm glass-100 μm water).

TABLE III

BINARY MATERIALS CONSIDERED IN NUMERICAL STUDIES

Material	Density (Kg/m^3)	Young's Modulus (GPa)	Longitudinal Velocity (m/s)
Water	1000	2.2	1500
Glass	2210	60	4500
Aluminum 1100	2720	72	6320
Low Carbon Steel	7850	200	5850

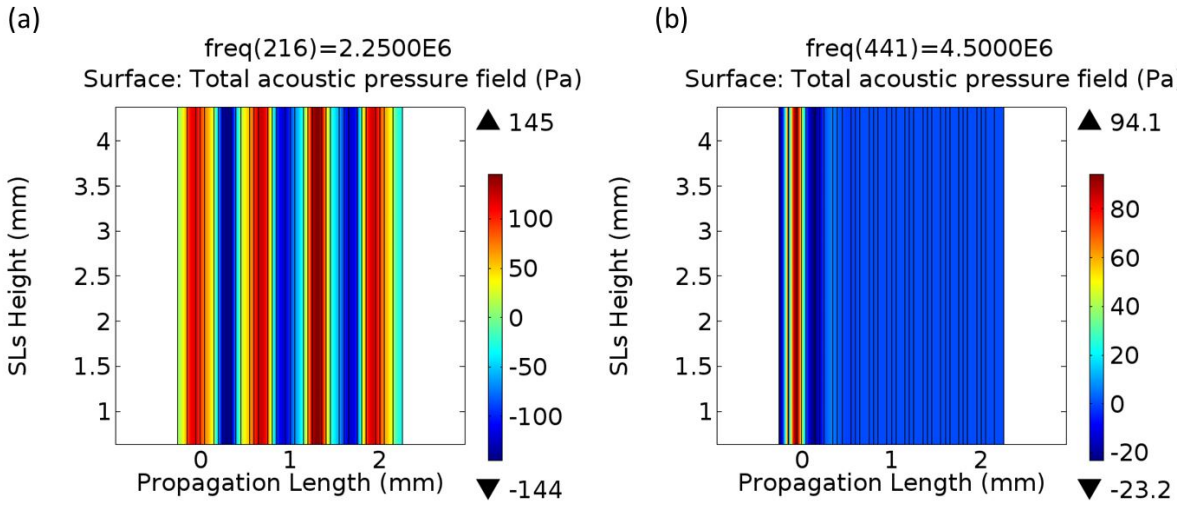

Figure 19. The displacement field through the designed SLs at two different frequencies (a) 2.25 MHz, and (b) 4.5 MHz.

4.4.1 Solid-Fluid SLs Fabrication

Based on the numerical study, the desired SLs have periodic layers of 100 μm glass and 100 μm water. The SLs geometry made of six layers of water and glass is prepared in laboratory, as shown in Figure 20(a). To evaluate the band gap formation, the SLs is tested in the immersion NLUT setup. Figure 20(b) shows the experimental setup of the immersion NLUT. The transducers implemented to transmit and receive the longitudinal ultrasonic waves are commercial piezoelectric transducers with the effective diameter of 6.35 mm (0.25 in) manufactured by Olympus. The SLs is placed near the receiving transducer of 5 MHz while the transmitting transducer is tuned to 2.25 MHz. Tablet UT device manufactured by Mistras Group Inc. is used to generate the 15-cycle tone burst input signal

at the frequency of 2.25 MHz and amplitude of 100 V. The recieved signal is recorded by the same Tablet UT device at the sampling rate of 100 MHz. A band pass filter of 0.5-20 MHz is then applied to the received signal and 200 received signals are averaged to improve signal to noise ratio [128]. The frequency response is calculated using MATLAB software by applying the FFT. The frequency spectra of the two cases ((i) without and (ii) with the SLs) are shown in Figure 21. It can be seen that 2.25 MHz is completely passed through the SLs, and the 4.5 MHz is blocked when SLs is placed near the receiving transducer.

4.4.2 Ultrasonic Measurement Procedure

As compared to the experiments discussed in section 4.4.1, aluminum samples with different plastic strains are placed between transmitter and receiver. The experiments are repeated without the SLs and with the SLs when they are placed right before the specimen, facing the transmitting transducer (Figure 22(a) and (b)). The presence of solid medium in the wave propagation path decreases the transmitted wave energy. Therefore, the amplitude of input signal is increased to 400 V to improve signal to noise ratio.

A typical measured time-domain signal for the pristine specimen without the presence of SLs is presented in Figure 23(a). The first 15 cycles of the signal is selected to perform the FFT. Figure 23(b) shows the Fourier spectrum of the selected 15 cycles of the received signal. The fundamental and second harmonic amplitudes are plotted in two different scales. Figure 24 shows a typical time-domain signal and its frequency spectrum for the pristine specimen with the presence of SLs. The ratio of the second harmonic amplitude to the square of fundamental harmonic amplitude $(\frac{A_2}{A_1^2})$ results in the acoustic non-linearity parameter β. The second harmonic amplitude measured for the pristine specimen

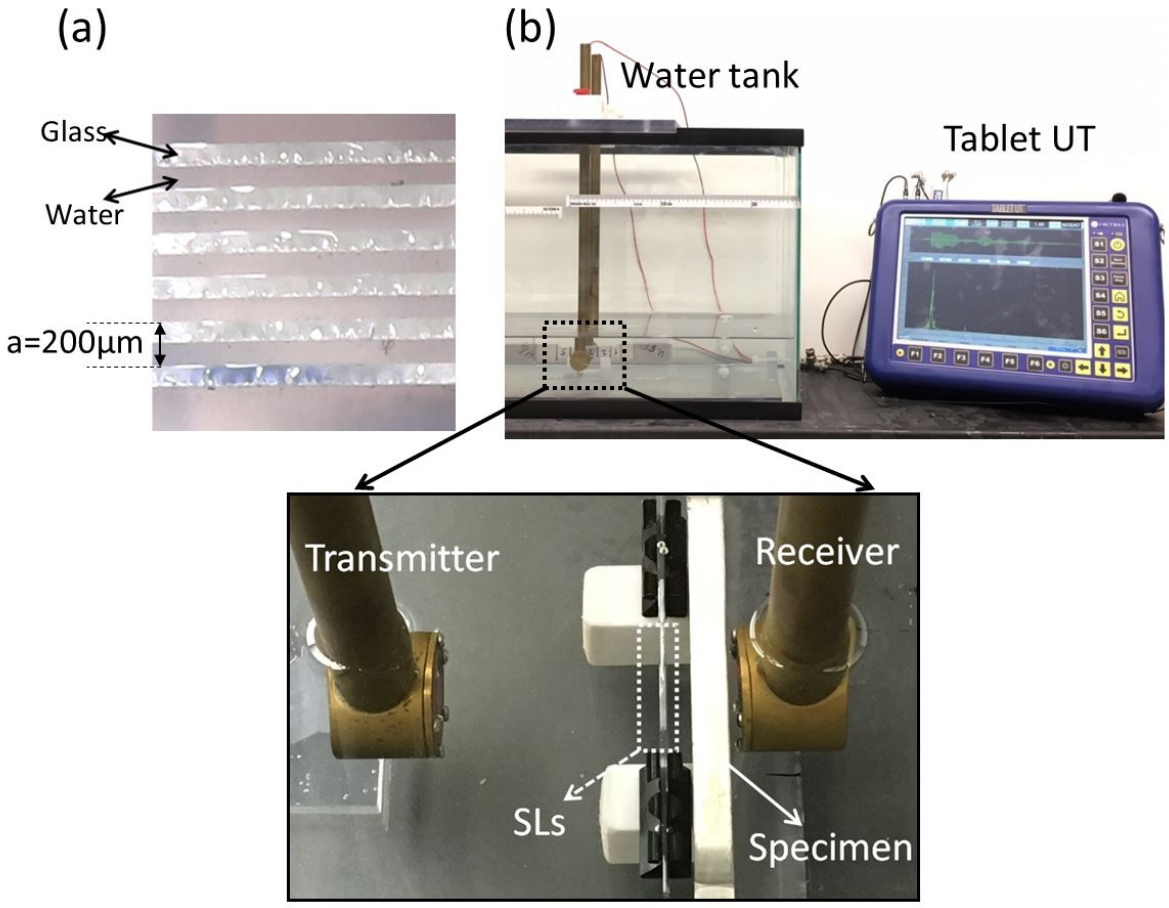

Figure 20. Testing the band gap formation of the designed SLs (a) the fabricated SLs made of glass and water, (b) the immersion NLUT setup.

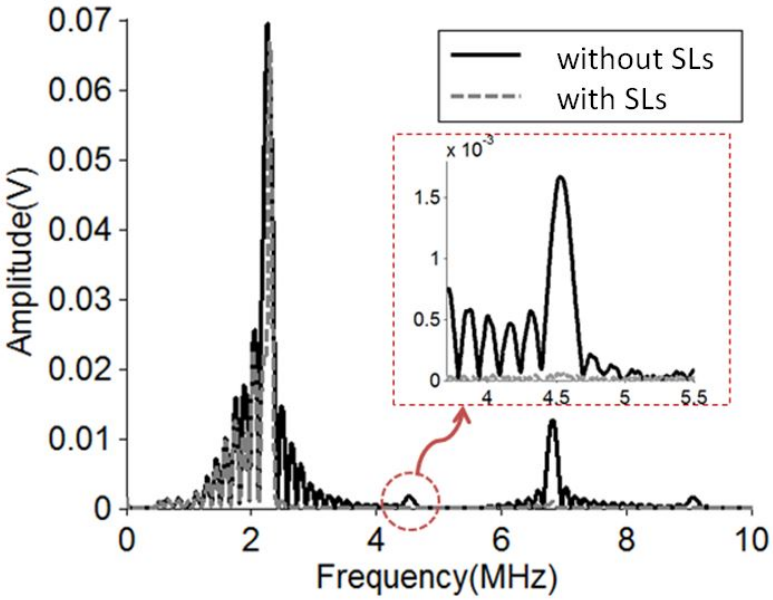

Figure 21. Frequency spectra of immersion NLUT for two cases: (i) with the SLs and (ii) without the SLs (there is no specimen in the path of transmitter and receiver).

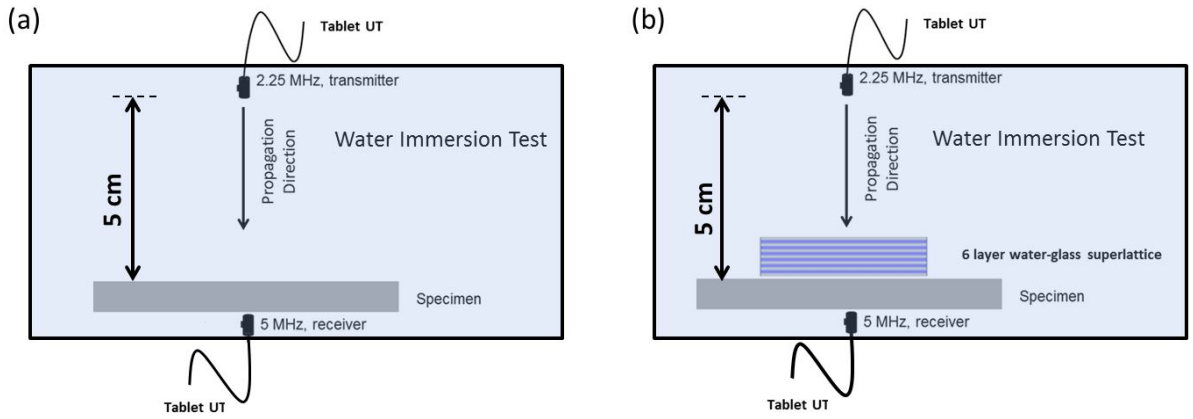

Figure 22. Immersion NLUT setup, (a) schematic diagram of immersion NLUT without the presence of SLs, (b) schematic diagram of immersion NLUT with the presence of SLs.

with the presence of the SLs is 24 times lower than the second harmonic amplitude measured for the same specimen without the presence of SLs as the second harmonic generated in water is blocked by the SLs.

4.5 Results

This section presents the measured β using the immersion NLUT with the specimens between transmitter and receiver for two cases: (i) without the presence of SLs and (ii) with the presence of SLs. The effectiveness of the SLs to detect only non-linearity in solid is further unveiled through the measurement of β for the pristine specimen by changing the transmitter position with respect to receiver.

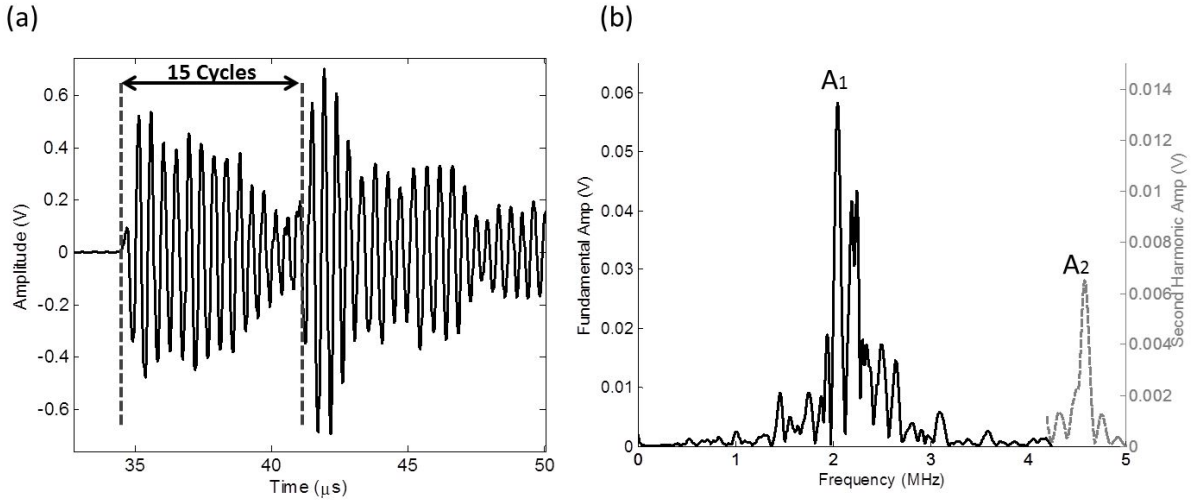

Figure 23. Immersion NLUT without the presence of SLs, (a) the time-domain signal, (b) frequency spectrum obtained by applying FFT on the selected 15 cycles of the time-domain signal of pristine specimen.

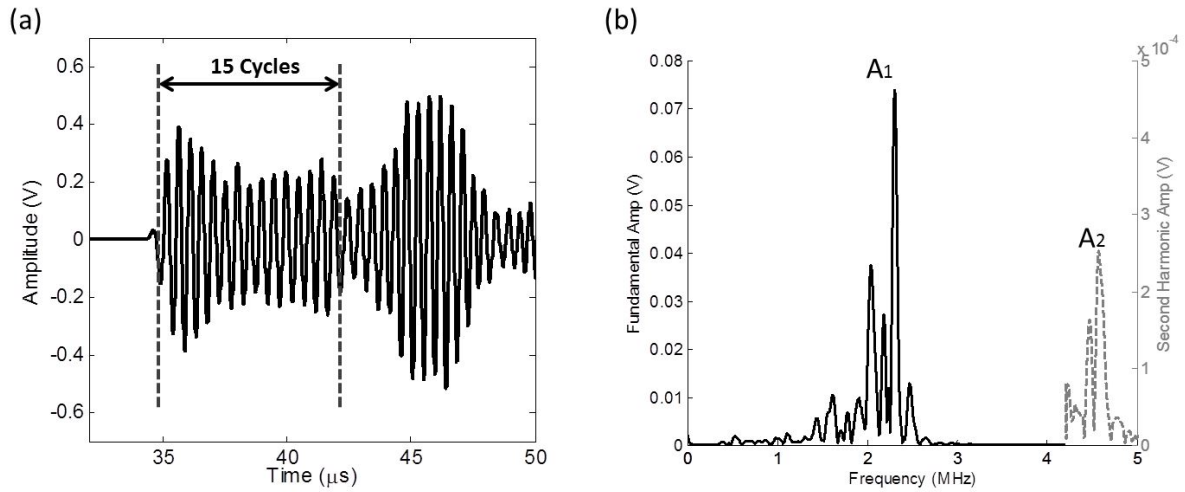

Figure 24. Immersion NLUT with the presence of SLs, (a) the time-domain signal, (b) frequency spectrum obtained by applying FFT on the selected 15 cycles of the time domain of pristine specimen.

4.5.1 Immersion NLUT Without the Presence of SLs

Figure 25 shows the results of immersion NLUT without the presence of SLs using the specimens subjected to different plastic strains. The left vertical axis presents the value of $\frac{A_2}{{A_1}^2}$ normalized by the average $\frac{A_2}{{A_1}^2}$ of the pristine specimen and the right vertical axis presents the measured value of $\frac{A_2}{{A_1}^2}$. The measurement is repeated three times for each specimen. In Figure 25, each red square represents the mean values of the three measurements, and the corresponding error bar represents the range of variation in the measured values. Spline curve is fitted to the mean values to show the trend of $\frac{A_2}{{A_1}^2}$. Spline curve applies piecewise-polynomial interpolation that lowers the interpolation error [129]. In general, the

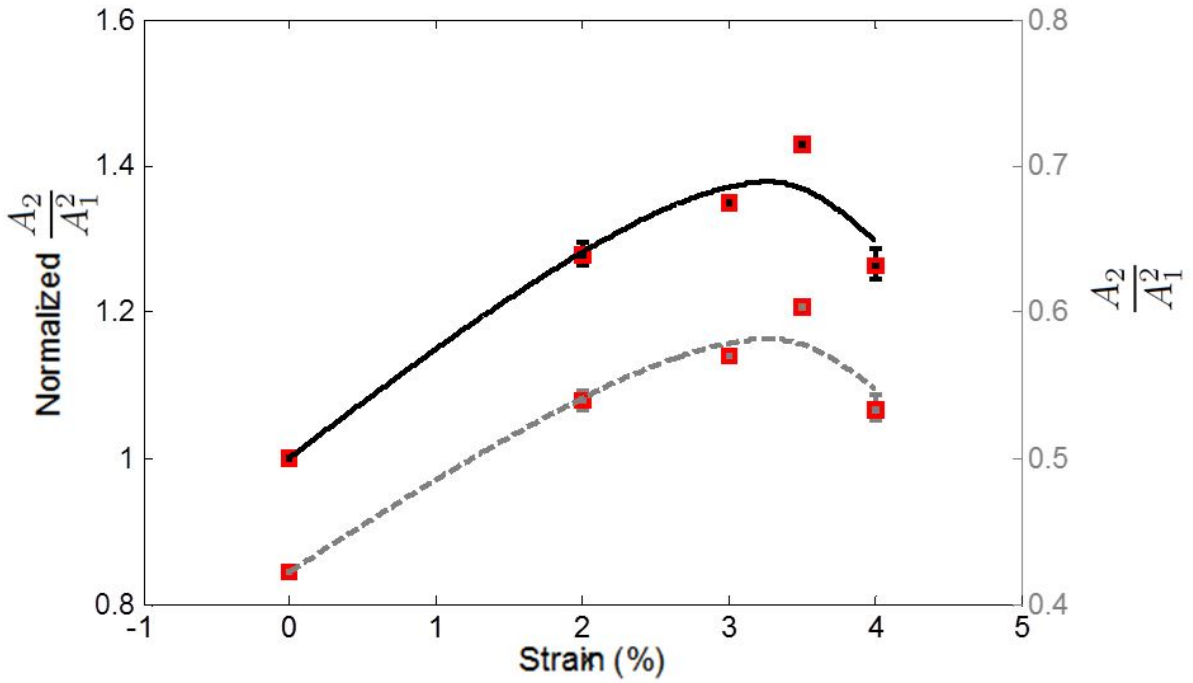

Figure 25. Normalized β (solid black line) and absolute β (dashed gray line) versus plastic strain resulted from immersion NLUT without the presence of SLs.

results show an increasing trend in value of $\frac{A_2}{{A_1}^2}$ by increasing the plastic deformation. The value of $\frac{A_2}{{A_1}^2}$ increases by 42% from 2% to 3.5% plastic strain, and there is a small drop from 3.5 to 4%.

4.5.2 Immersion NLUT With the Presence of SLs

Figure 26 shows the results of immersion NLUT with the presence of SLs placed near the specimen facing the transmitter. The left vertical axis presents the value of $\frac{A_2}{{A_1}^2}$ normalized by the average $\frac{A_2}{{A_1}^2}$ of the pristine specimen and the right vertical axis presents the measured $\frac{A_2}{{A_1}^2}$. Similar to the experiments

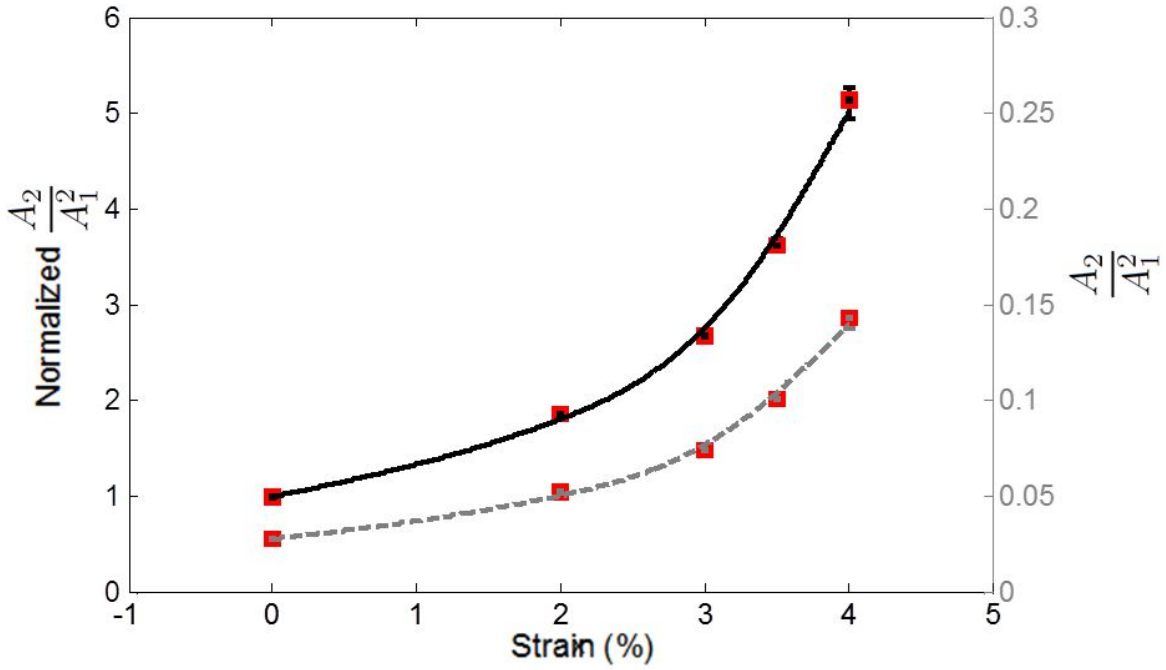

Figure 26. Normalized β (solid black line) and absolute β (dashed gray line) versus plastic strain resulted from immersion NLUT with the presence of SLs.

without SLs, measurement is repeated three times for each specimen and the average value is plotted as the red square, and the variation is presented by the error bars. The value of $\frac{A_2}{{A_1}^2}$ increases by 420% from the pristine specimen to 4% plastic strain. The measured $\frac{A_2}{{A_1}^2}$ decreases as compared to the case of without the presence of SLs as the influence of water non-linearity is blocked. However, the relative change in $\frac{A_2}{{A_1}^2}$ increases higher with the increase of plastic deformation. Additionally, error in measurement is reduced by implementing the SLs into immersion NLUT experiments.

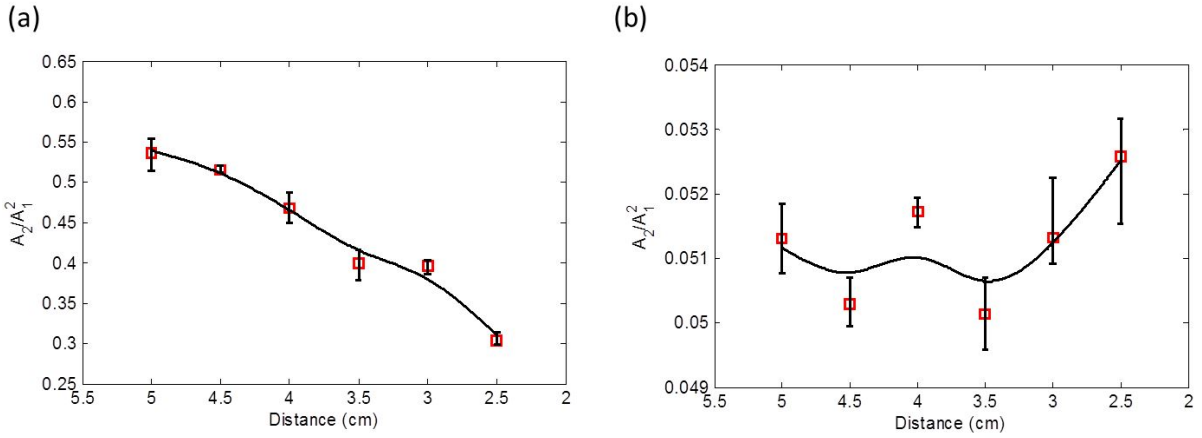

Figure 27. Measured non-linearity versus propagation distance (a) without the SLs, and (b) with the SLs for the 2% strained specimen.

4.5.3 The Influence of the Propagation Distance in the Immersion NLUT

To demonstrate the effectiveness of the SLs, the immersion NLUT is repeated by keeping everything constant and changing the wave propagation path by moving the transmitting transducer. These tests is performed for two cases, first without the presence of SLs, and second time with the presence of SLs. The 2% strained specimen is used in this test and the first propagation distance is set to be the same as the distance used in section 4.4.2, and it is incrementally decreased by 0.5 cm. Figure 27 shows the changes in the measured non-linearity while the propagation distance is changing. The results show that, in the case of without SLs (Figure 27(a)), decreasing the propagation distance from 5 cm to 2.5 cm decreases the measured non-linearity by 43%, while the measured non-linearity in the case of with the SLs (Figure 27(b)) is almost unchanged with the propagation distance change.

4.5.4 Third Harmonic Generation NLUT

The integration of SLs with the immersion NLUT using the third harmonic non-linearity parameter γ is applied to assess the plastic strains of aluminum 1100 specimens. γ for different specimens is measured for two cases: (i) without the SLs and (ii) with the SLs. No correlation is found between γ and the level of plastic strain in aluminum 1100 specimens when the immersion NLUT is employed with the SLs.

4.6 Solid-Solid SLs for the Contact NLUT

While sections 4.2-4.4.2 study the enhancement of immersion NLUT by exploiting solid-fluid SLs, this section presents a method to improve the contact NLUT by applying solid-solid SLs. By placing the SLs between the transmitter and the specimen, it is considered that the non-linearity generated in the transmission side of the experimental setup would decrease. Figure 28 shows the schematic diagram of the test setup. The SLs structure is placed between transmitter and specimen, and the receiving transducer is placed at the other surface of the specimen normal to the transmitting transducer.

4.6.1 Numerical Results

Similar to the immersion NLUT, the SLs structure is designed to provide a band gap range tuned to the second harmonic frequency using solid-solid layers. The range and width of the band gap depend on materials properties and geometric dimensions of the periodic structure. Numerical studies are conducted to find the proper geometries and materials. Here, one-dimensional PCs are simulated in COMSOL Multiphysics software to study the transmission loss of the propagating wave through the PCs. For the contact NLUT, the periodic layers are made of glass and steel, and the effects of different material properties and lattice sizes are studied. The final geometry is made of periodic layers of 254

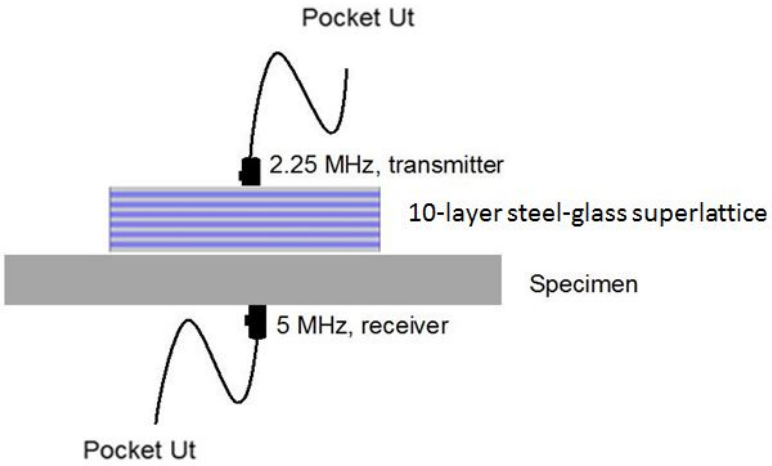

Figure 28. Schematic diagram of the contact NLUT setup integrated with the solid-solid SLs.

(μm) steel and 200 (μm) glass to generate a band gap including 4 MHz. Figure 29 shows the numerical result of through transmission study of the designed SLs. The blue shade indicates the band gap range, which includes the required 4 MHz frequency. The design allows complete passage of 2 MHz, which is the fundamental ultrasonic frequency utilized in this research. Figure 30 shows the pressure field at the fundamental and second harmonic frequencies through the simulated SLs. 4 MHz signal dissipates through an array of 200 μm thick glass and 254 μm thick steel while 2 MHz signal propagates through the designed SLs.

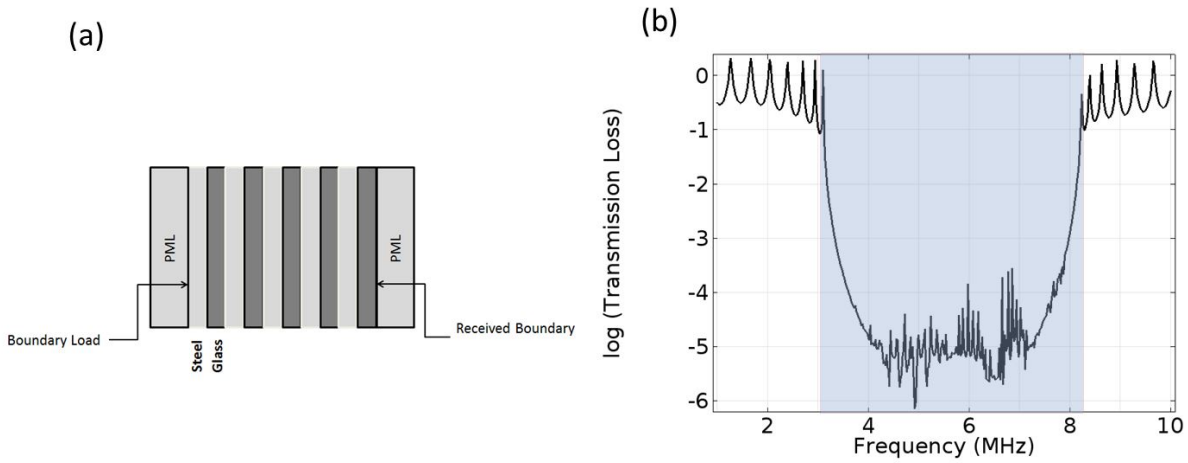

Figure 29. (a) Numerical model, and (b) transmission loss through SLs (254 μm steel-200 μm glass).

4.6.2 Experimental Results

The same contact NLUT setup as presented in Chapter 3 is employed in this study. Ten periodic layer SLs consisting of 254 (μm) steel and 200 (μm) glass are fabricated in laboratory. Light lubricant oil is applied between the surfaces as couplant. To evaluate the band gap formation, the NLUT experiment is implemented without the presence of SLs and with the presence of SLs. Figure 31 shows the frequency spectra of the received signals for two experiments. Figure 32 shows the WT results of the contact NLUT experiments. The fundamental and second harmonic frequencies are indicated by two red lines on the spectrograms. The spectral amplitudes over time, related to the red lines, are shown in Figure 32 (c) and (d). The presence of SLs allows the passage of 2 MHz, which is the fundamental frequency, while it blocks the majority of 4 MHz.

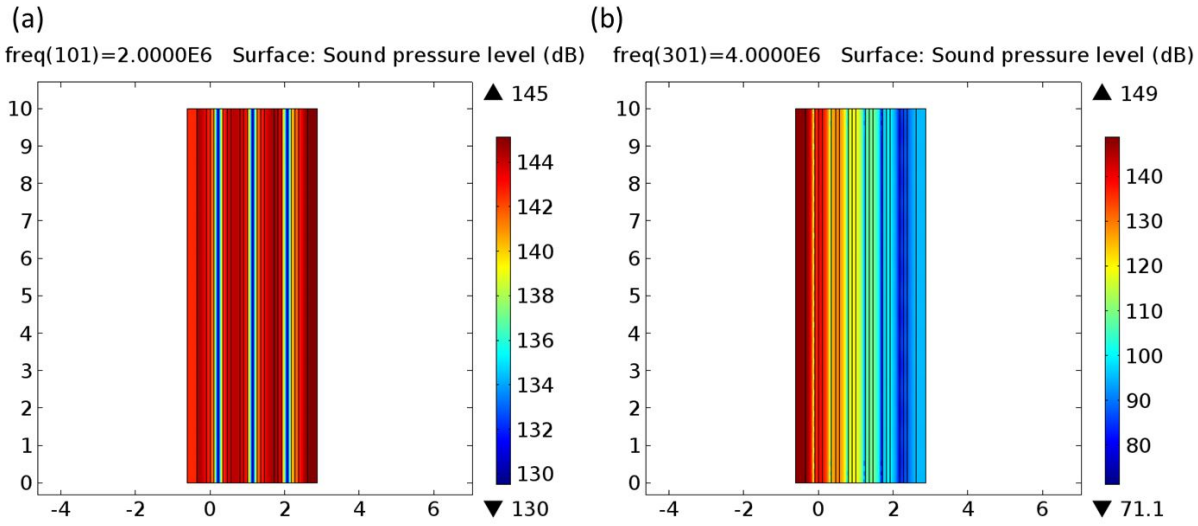

Figure 30. The pressure field through the designed SLs at two different frequencies (a) 2 MHz, and (b) 4 MHz.

4.7 Summary

The integration of SLs into the immersion NLUT is studied to remove the non-linearity generated in water. The numerical results show that the SLs consisting of periodic layers of 100 μm thick water and 100 μm thick glass can block 4.5 MHz while it allows 2.25 MHz to pass. We observed experimentally that integrating the SLs into the immersion NLUT on plastically strained aluminum specimens can enhance the sensitivity of damage detection by about 9 times (from 45% change in the case of without the presence of SLs to 420% in the case of with the presence of SLs). Implementing SLs in the immersion NLUT overcomes the influence of strong non-linearity generated in water. The results reveal

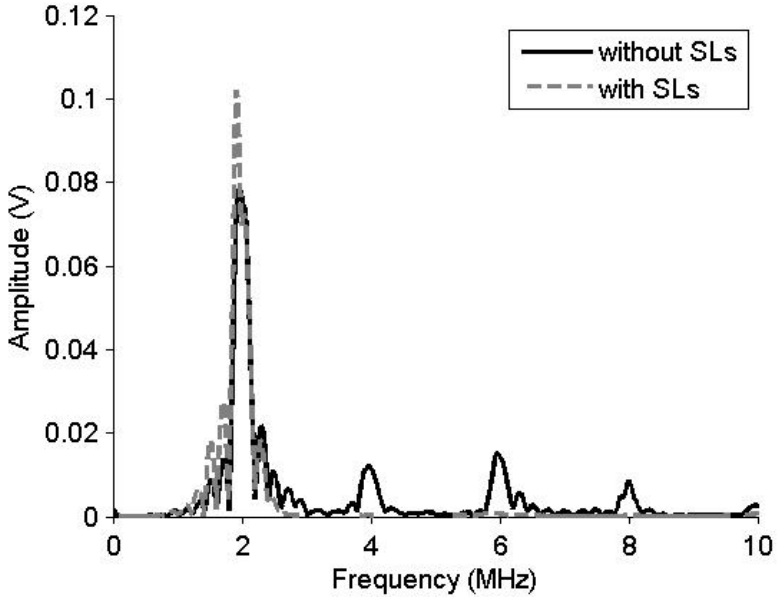

Figure 31. The frequency spectra of the received signals for two cases, (i) with and (ii) without SLs.

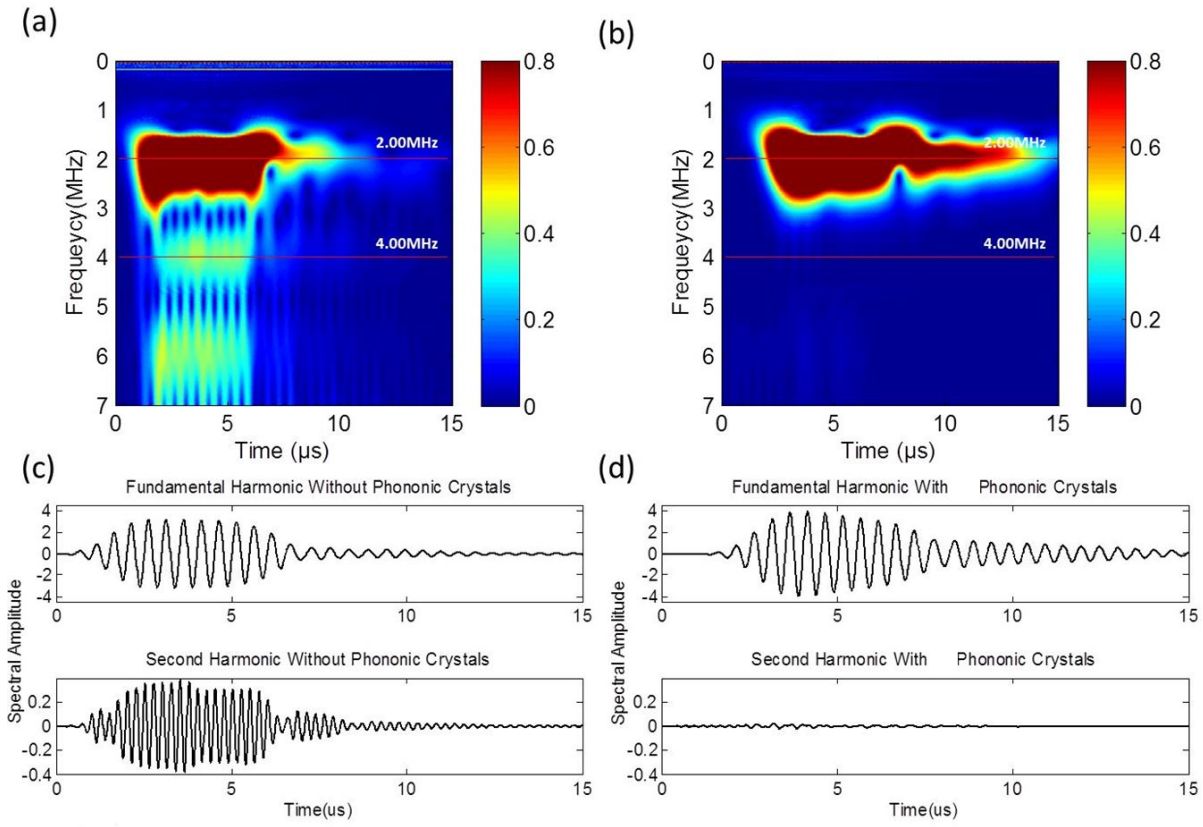

Figure 32. Contact NLUT, (a) and (b) the spectrograms of the received signals for the cases without and with the presence of SLs, respectively, (c) and (d) the harmonic waveforms extracted using WT, respectively.

that the SLs with a band gap tuned to the second harmonic frequency, and a pass band that includes the fundamental frequency make the immersion NLUT as an alternative to measure the micro-structural changes in materials with minimizing the coupling effect and allowing volumetric scanning of structures. Moreover, no correlation was observed between the plastic strain level and the third order acoustic non-linearity parameter γ using the immersion NLUT with the SLs.

To remove the instrument originated non-linearity in the contact mode NLUT, solid-solid SLs are designed. Numerical studies show that the periodic layers of 254 (μm) thick steel and 200 (μm) thick glass can pass 2 MHz frequency and block 4 MHz frequency. The SLs structure is experimentally tested and shown that the band gap formation agrees with the numerical results. More experimental studies are required to demonstrate the improvement of defect detection by applying the SLs to the contact NLUT. Additive manufacturing method will be utilized to achieve a more accurate geometry and acceptable bonding between the periodic layers.

CHAPTER 5

ASSESSING CREEP DAMAGE OF STAINLESS STEEL 410 USING NLUT AND WAVELET TRANSFORMATION

This chapter will be partially submitted to a journal with the title of "Assessing Creep Damage in 410 Stainless Steel using Acoustic Micro Imaging" in collaboration with Niloofar Tehrani, Negar Kamali, and Professors Didem Ozevin, Sheng-Wei Chi, J. Ernesto Indacochea.

5.1 Introduction

This chapter presents the measurement of creep damage using the contact NLUT with the second harmonic and the wavelet-based harmonic decomposition method presented in Chapter 3. Two sets of stainless steel 410 specimens are exposed to different levels of creep and thermal aging. The chapter begins by a brief introduction of creep damage. The materials preparation and NLUT experimental setup are discussed. The contact NLUT results in relation to creep strains are presented.

5.2 Creep Damage

Creep is defined as the time dependant deformation of material exposed to both mechanical stress and high temperature. This phonomena is one of the mostly reported damages responsible for the failure of structural materials operating at elevated temperatures such as the components in the power generation industry [130]. Considering the change in strain with creep time, three stages of creep can be identified in creep-induced damage process [27]. The primary stage starts with a sudden increase in strain because of initial loading, followed by a decrease in the strain rate. The secondary stage shows

constant plastic flow and usually the longest part of the creep life. During the tertiary stage, the strain rate starts to increase exponentially until the failure of the component [130]. Creep deformation is associated with several mechanisms such as precipitation of carbides, strain hardening, recovery, etc [130]; however, the most notable mechanism responsible for the creep failure in the engineering applications is the nucleation and coalescence of micro-voids [25]. Micro-voids are created because of the dislocation or wedge cracks attributable to the grain boundary sliding [131]. The applied stress gravitates the nucleated micro-voids orthogonally to the direction of the stress. This will lead to coalescence of micro-voids into the micro cracks which may grow quickly to macro-cracks and eventually lead to failure [130; 131]. It is important to detect flaws before they reach to critical stage by NDE methods.

In literature, different types of NDE methods such as eddy current, acoustic emmision, ultrasonic attenuation and velocity, and infrared thermography are applied to assess creep damage [132]. Ultrasonics velocity meaurement is one of the means to monitor creep damage nucleation in the materials. However, the linear UT is only sensitive to defects greater than the ultrasonic wavelength and are not able to detect the microstructural changes that exhibit in the early stages of creep [8; 25; 133; 134]. Instead, as discussed above, NLUT can detect the micro-structural features in the order of magnitude smaller than the wavelength of ultrasonic signal [8; 35].

5.3 Experimental Procedure

5.3.1 Materials Preparation

The material used in this investigation is stainless steel 410. Two sets of stainless steel 410 specimens are studied in this chapter, (i) dog-bone specimens exposed to different levels of creep damage, and (ii) rectangular specimens exposed to thermal aging. Six dog-bone specimens are machined from a

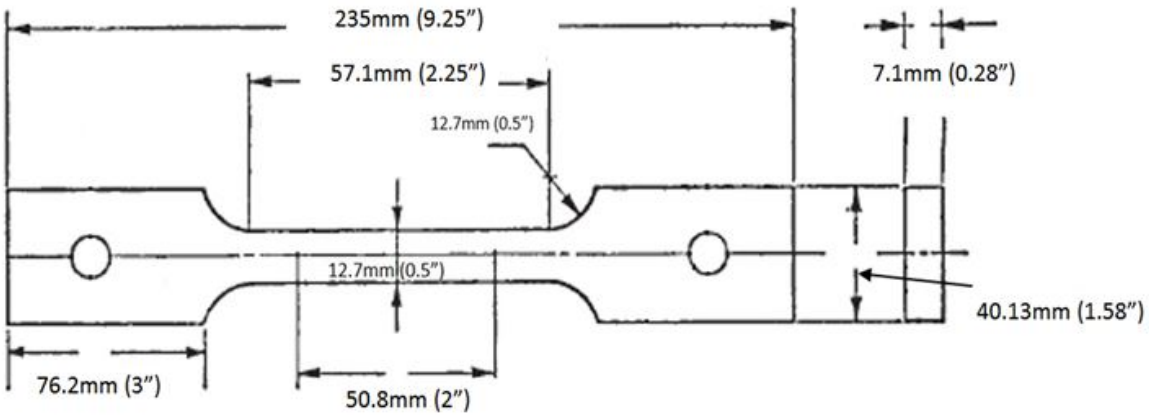

Figure 33. Tensile test sample dimensions (All dimensions are in mm.)

single plate with the thickness of 7.1 mm (0.28") with the dimensions according to the ASTM E139 standard as shown in Figure 33 and six rectangular specimens are machined out of the same plate with the dimensions of $76.2 \times 12.7 \times 7.1\ mm^3$. Before applying creep loading, all the specimens are austenitized for 30 minutes at 980°C temperatures followed by air cooling. The air cooled samples are subsequently tempered at 650°C for two hours. The dog-bone specimens are subjected to creep loading of 150 MPa and 620°C for different duration of 290 hr, 335 hr, 437 hr, 451 hr and 590 hr that results in 0.85%, 2.1%, 3.7%, 3.2%, 2% creep strains, respectively. Six thermal aged specimens with the same thermal condition as the creep specimens without tensile loading are prepared.

5.3.2 Contact Nonlinear Ultrasonic Testing (NLUT)

The NLUT experimental setup is illustrated in Figure 34(a) and (b). Through transmission ultrasonic testing is applied to perform the contact NLUT. The same transducers and experimental setup as

Chapters 3 are utilized (as presented in Figure 34(c)). Stainless steel specimens with different levels of creep and thermal aging damage are placed between transmitter and receiver. Light lubrication oil is used to couple the transducers to the specimen. Tablet UT device manufactured by Mistras Group Inc. is used to generate the 10 cycle tone burst input signal at the frequency of 2.25 MHz and amplitude of 100 V. The received time-domain signal is recorded by the same Tablet UT device at the sampling rate of 100 MHz. A band pass filtre of 0.5-20 MHz is applied to the received signal. To improve the signal to noise ratio 200 received signals are averaged, recorded and sent for post processing in MATLAB software. The acoustic non-linearity parameter is calculated using time-dependent wavelet-based approach presented in chapter 3. A typical received time-domain signal for a pristine specimen is shown in Figure 35(a). The Fourier spectrum of the received signal shows that the first harmonic frequency is 2.25 MHz and the second harmonic frequency is 4.5 MHz (Figure 35(b)). WT is achieved by applying complex-Morlet mother wavelet function with the central frequency of 1.5 Hz and bandwidth of 1 Hz (Figure 35(c)). The first and second harmonic frequencies are marked in the wavelet spectrogram using red dashed lines (Figure 35(c)). The first and second harmonic spectral amplitudes over time, extracted from the wavelet spectrogram, are shown in Figure 35(d). Using the time-history signal of the first and second harmonics, the acoustic non-linearity parameter is calculated over time (Figure 35(d)), and β is calculated by averaging the non-linearity in constant plateau (in this research 2.0-2.5 μs).

5.4 NLUT Results

The measured β for the specimens with different levels of creep and thermal aging are shown in Figure 36. For each specimen, the measurement is repeated three times. Each point in Figure 36 represents the mean value, and the corresponding error bar represents the range of variation in three measurements.

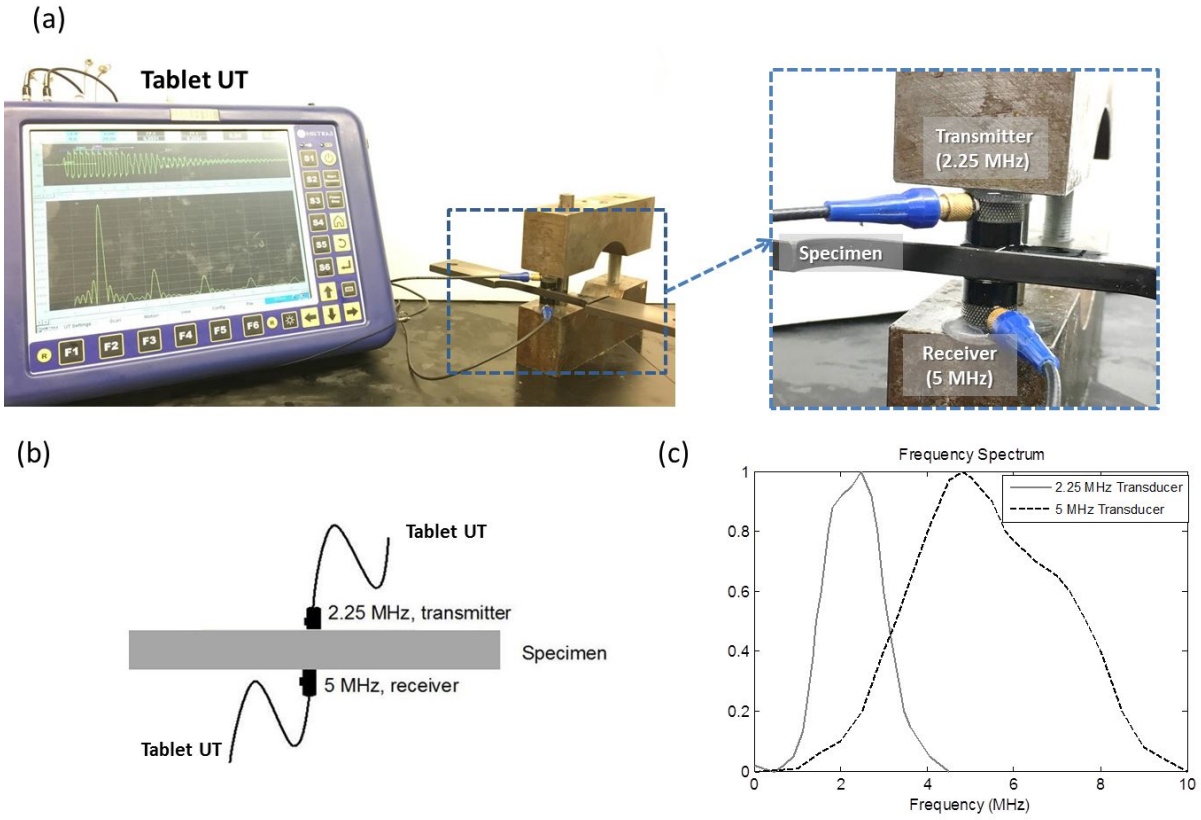

Figure 34. NLUT experiment, (a) experimental setup, (b) schematic of experimental setup, and (c) transducer calibration curves.

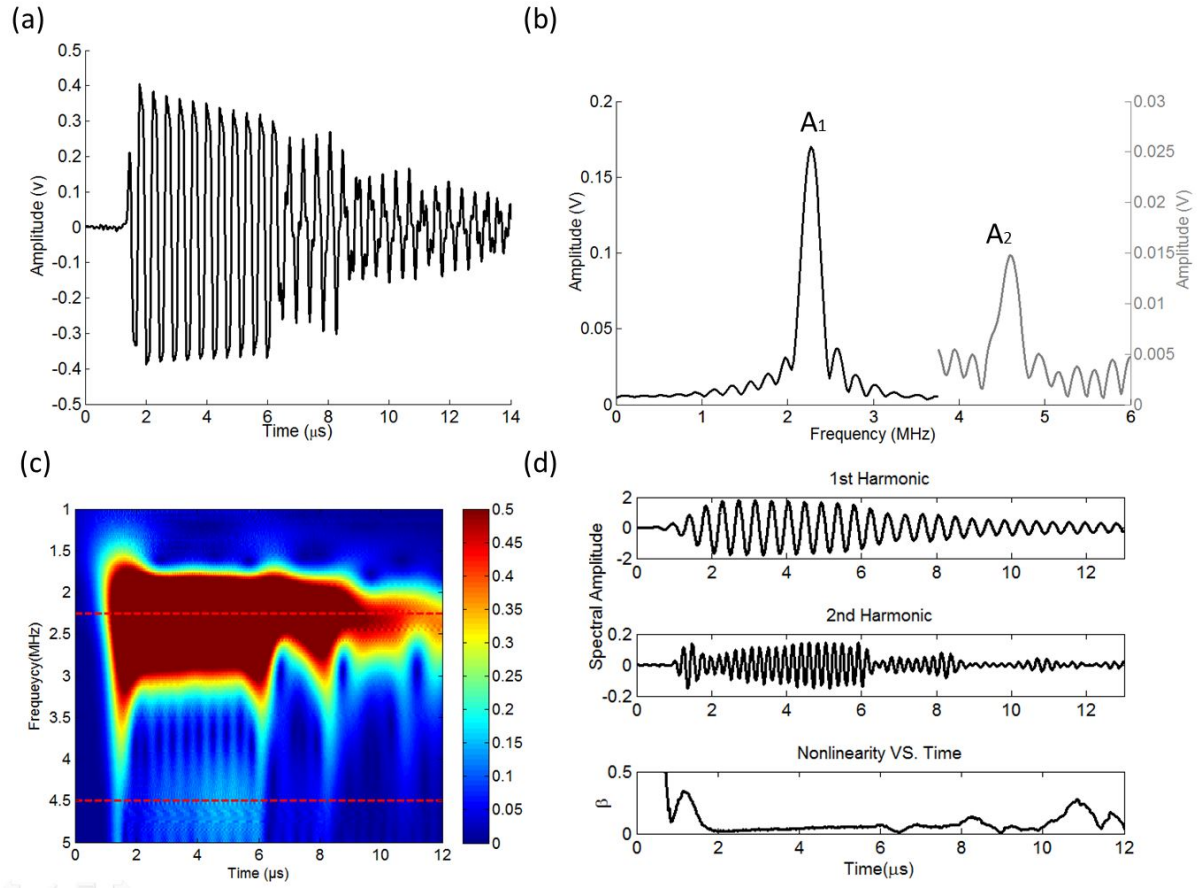

Figure 35. Typical received signal for pristine specimen of stainless steel 410 (a) received time-domain signal, (b) frequency spectra of the received signal, (c) the spectogram of the received signal, and (d) the extracted fundamental and second harmonic waveforms from the wavelet spectrum and the corresponding non-linearity parameter calculated over time.

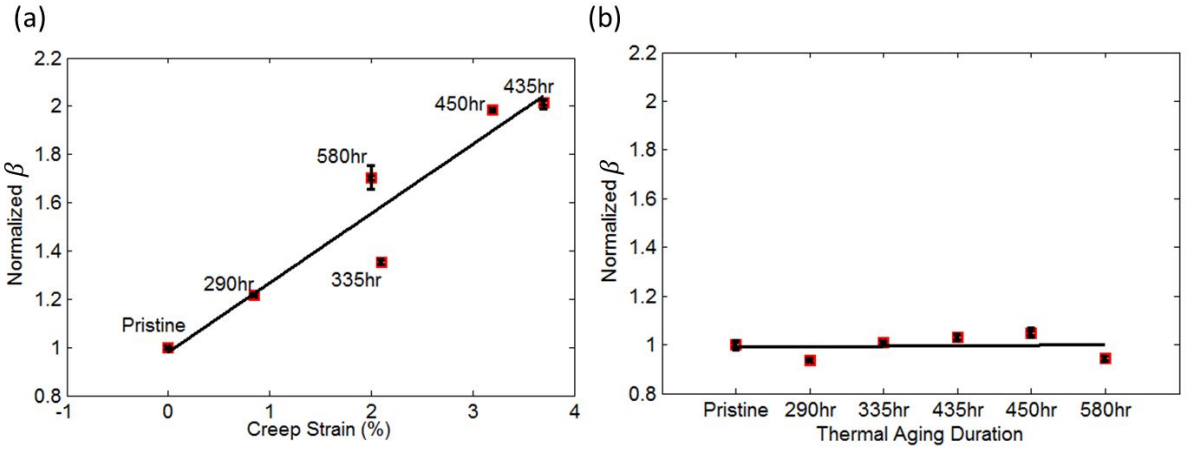

Figure 36. The change in β with, (a) creep damage, and (b) thermal aging.

It is observed that, β increases nearly 100% after 450 hours of creep damage (Figure 36(a)); however, β does not change significantly for the specimens subjected to thermal aging (Figure 36(b)).

5.5 Summary

The SHG method integrated with wavelet-based harmonic decomposition method is employed to detect the creep damage in stainless steel 410. Six specimens with different levels of creep strains are prepared. Moreover, six thermal aged specimens with the same thermal condition as the creep specimens without tensile loading are prepared. It is determined that β increases nearly 100% after 450 hours of creep damage, while β does not change significantly for the specimens subjected to thermal aging.

CHAPTER 6

INTEGRATING SUPERLATTICES AND IMMERSION NLUT TO ASSESS CREEP DAMAGE OF STAINLESS STEEL 410

The content presented in this chapter will be partially submitted to a journal with the title of "Assessing Creep Damage in Stainless Steel 410 using Integrated Immersion Nonlinear Ultrasonic Testing and Acoustic Metamaterials" in collaboration with Minoo Kabir, and Professor Didem Ozevin.

6.1 Introduction

This chapter presents an integrated immersed NLUT and SLs setup to characterize the creep damage in stainless steel 410 using the third harmonic generation method. The specimens used in this investigation are the same as the dog-bone specimens with different levels of creep damage prepared in chapter 5. The chapter begins with an introduction of the technical approach. Then, the experimental setup is discussed. The measured third harmonic coefficient is compared for two cases: (i) without the SLs and (ii) with the SLs.

6.2 Technical Approach

As discussed in chapter 2, the third harmonic signal is more sensitive to creep damage. However, it is also more sensitive to the experimental variables, such as coupling condition and instrumental non-linearities than the second harmonic signal due to smaller wavelength. To remove the undesirable non-linearity generated during the immersion NLUT process, SLs are integrated with the measurement system. Figure 37(a) shows the immersion NLUT setup. The transducers are immersed in the water

tank. The central frequencies of transmitter and receiver are 2.25 and 5 MHz, respectively. The solid medium (stainless steel 410) is placed in the ultrasonic propagation path, and the SLs are placed right before the solid medium facing to the transmitter. In this research, the same SLs as in chapter 4 are implemented. The band gap of SLs includes the third harmonic frequency. Figure 37(b) shows the frequency domain of a typical received signal with the black line, and the designed band gap, presented by a transmission loss, with a blue shade. A_3 is within the band gap frequency range. By blocking the third harmonic generated in water and instruments, it is expected that the calculated non-linearity in the received signal consists of only the non-linearity of micro-structural features in solid. Consequently, the sensitivity of the immersion NLUT using the third harmonics is expected to be improved.

6.3 Experimental Setup

Based on the numerical study in chapter 4, the desired SLs have periodic layers of 100 μm glass and 100 μm water. The SLs geometry of six layers of water and glass is prepared in laboratory, as shown in Figure 38(a). To evaluate the band gap formation, the SLs are tested in the immersion NLUT setup without any specimen between transmitter and receiver. Figure 38(b) and (c) show the experimental setup and schematic diagram of the immersion NLUT. The immersion NLUT setup is the same as the one used in section 4.4; however, 10 cycles of tone burst are utilized. The calibration curves of the employed transducers are presented in Figure 38(d). The sensitivity of the receiving transducer to 4.5 MHz (second harmonic frequency) is nearly the same as its sensitivity to 6.75 MHz (third harmonic frequency). The frequency spectra of the received signal in two cases ((i) without and (ii) with the SLs) are shown in Figure 38(e). It can be seen that 2.25 MHz (fundamental harmonic) completely passes through the SLs, while the 6.75 MHz (third harmonic) is blocked.

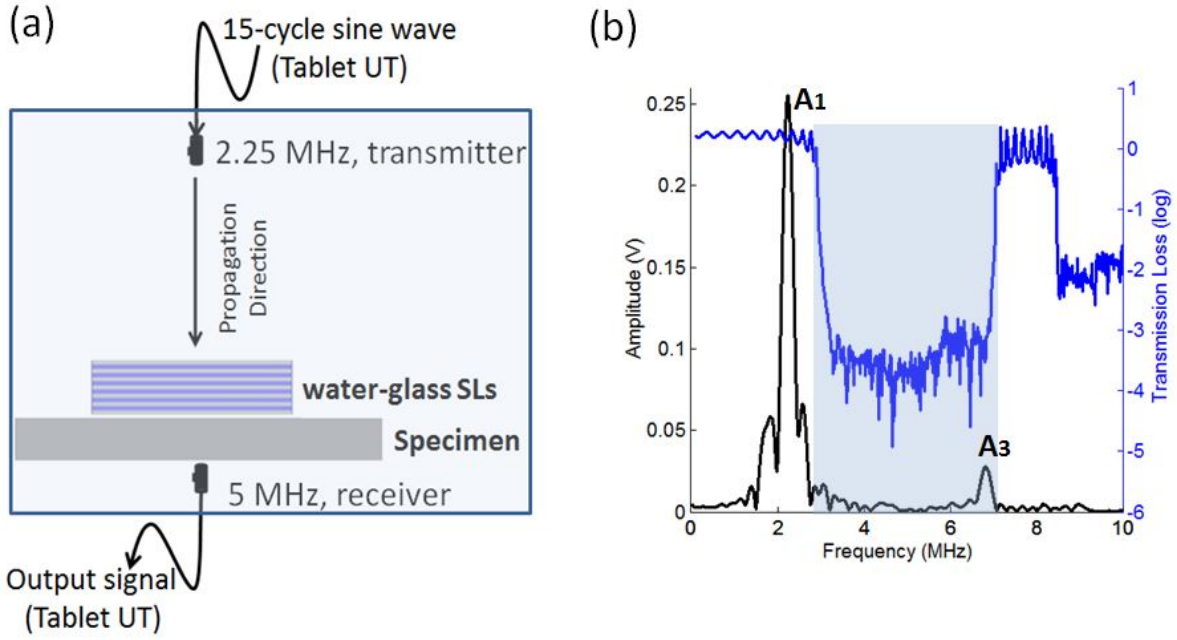

Figure 37. Proposed approach to block the third harmonic signal (a) the immersion NLUT setup with the presence of SLs, (b) the designed band gap tuned to the second and third harmonic frequencies.

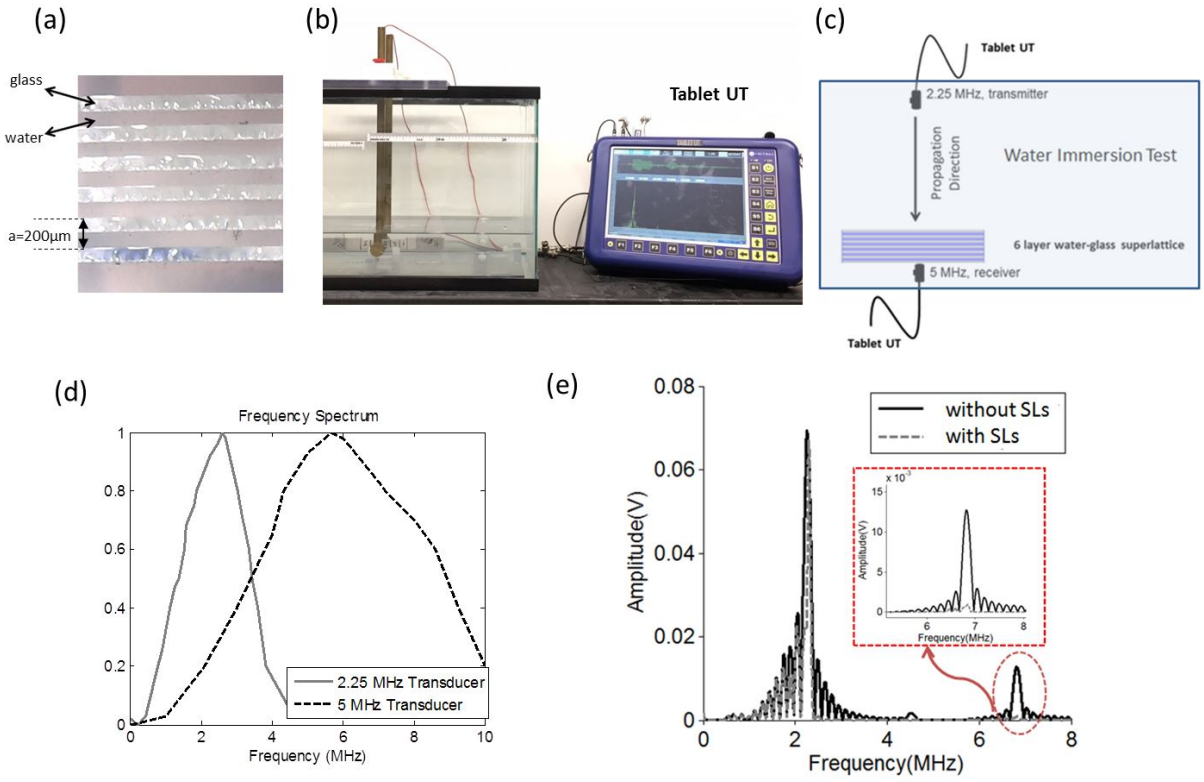

Figure 38. Testing the band gap formation of the designed SLs (a) the fabricated SLs made of glass and water, (b) the immersion NLUT setup, (c) schematic diagram of experimental setup to test the SLs, (d) the calibration curves of ultrasonic transducers, and (e) frequency spectra of ultrasonic signals for two cases as without and with the SLs.

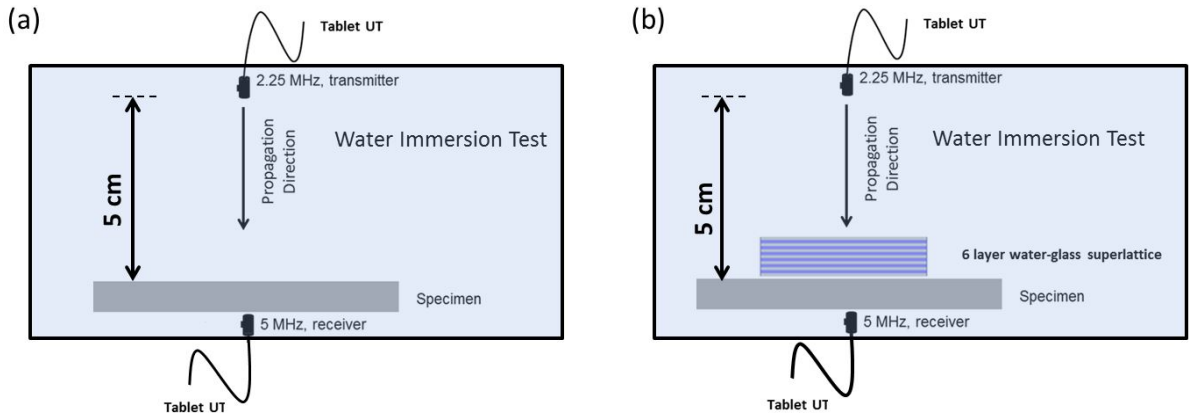

Figure 39. Immersion NLUT setup using stainless steel specimens, (a) schematic diagram of immersion NLUT without the presence of SLs, and (b) schematic diagram of immersion NLUT with the presence of SLs.

Once the formation of band gap at the third harmonic frequency is numerically and experimentally confirmed, stainless steel specimens are placed between SLs and receiving transducer to measure the third non-linearity parameters.

As compared to the experiment above, stainless steel specimens with different levels of creep damage are placed between transmitter and receiver. Because the presence of solid medium in the wave propagation path decreases the transmitted wave energy, the amplitude of input signal is increased to 400 V. The experiments are repeated for two cases: (i) without the SLs and (ii) with the SLs facing the transmitting transducer (Figure 39(a) and (b)).

6.4 Third Harmonic Non-linearity Parameter with the Immersion NLUT and SLs

A typical measured time-domain signal for the pristine specimen without the presence of SLs is presented in Figure 40(a). The first 10-cycle of the signal is selected to calculate the frequency spectrum as shown in Figure 40(b). The fundamental and higher harmonic amplitudes are plotted in two different scales. Figure 41 shows a typical time-domain signal and its frequency spectrum for the pristine specimen with the presence of SLs. It is observed that although the second harmonic (4.5 MHz) is visible in Figure 40(b), it is not detectable in Figure 41(b). Therefore, the third harmonic generation method is utilized to detect the creep damage. The ratio of the third harmonic amplitude to the cubic fundamental harmonic amplitude $(\frac{A_3}{A_1^3})$ results in the acoustic non-linearity parameter γ. The third harmonic amplitude measured for the pristine specimen with the presence of the SLs is 20 times lower than the third harmonic amplitude measured for the same specimen without the presence of SLs as the third harmonic generated in water is blocked by the SLs.

The ultrasonic measurement is performed at the middle point of the specimens, and the measurement is repeated three times. Figure 42 shows the third harmonic non-linearity parameters obtained without and with the SLs. The vertical axis presents the value of measured γ normalized by the average measured γ of the pristine specimen. Each red square represents the mean values of three measurements, and the corresponding error bar represents the range of variation within the measured values. It is observed that for the immersion NLUT without the presence of SLs, the measured γ has no correlation with the creep damage (Figure 42(a)). On the other hand, the results from the immersion NLUT with the presence of SLs show that γ increases almost 200% as the creep strain increases from 0% to 3.8% (Figure 42(b)). This result indicates that the non-linearity generated in water dominates such that it masks the non-

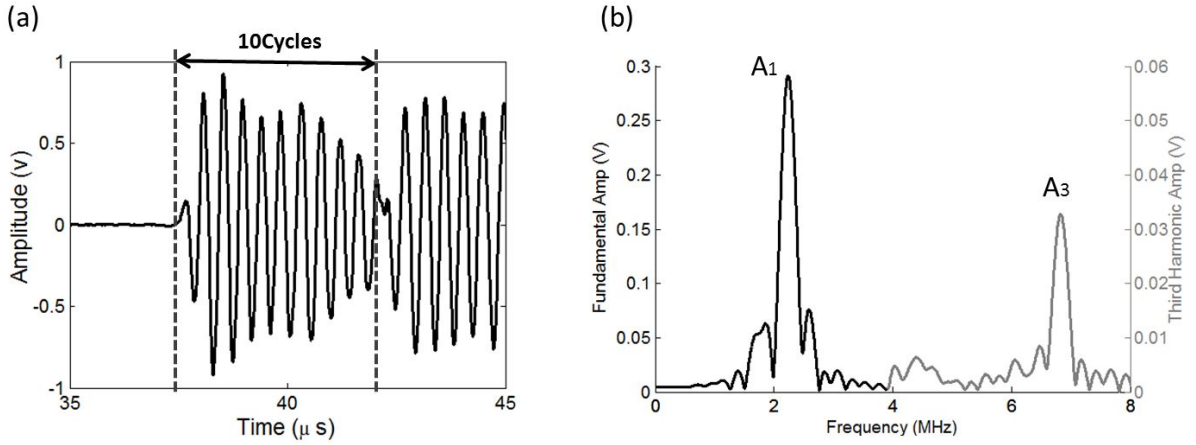

Figure 40. Immersion NLUT without the presence of SLs, (a) time-domain signal, (b) frequency spectrum using the first 10 cycles of time-domain signal.

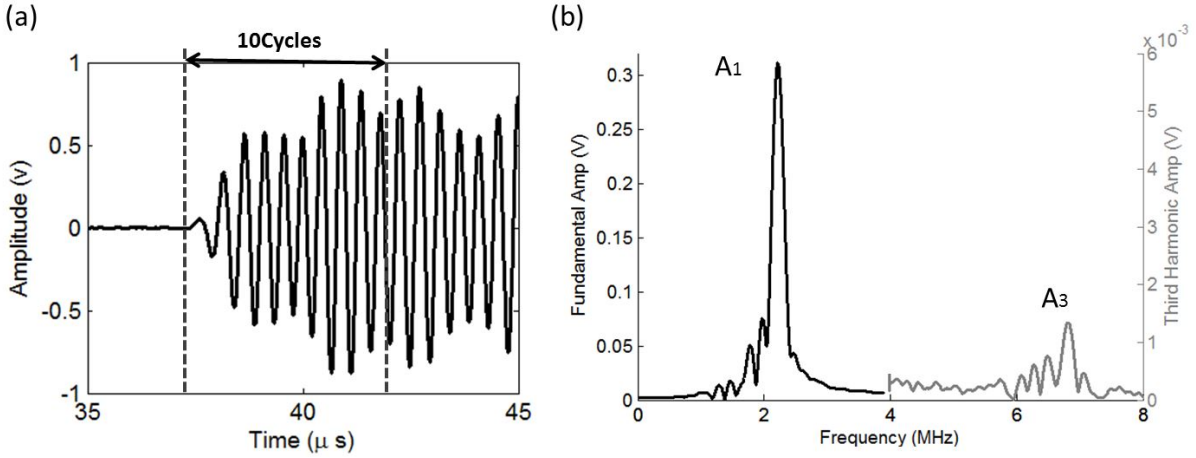

Figure 41. Immersion NLUT with the presence of SLs, (a) time-domain signal, (b) frequency spectrum using the first 10 cycles of time-domain signal.

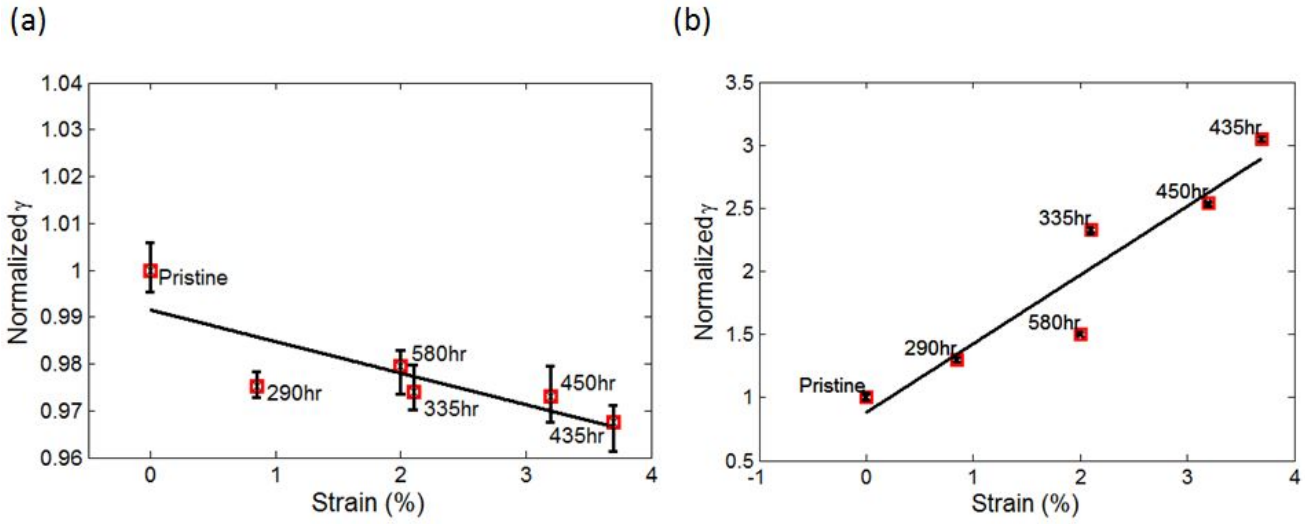

Figure 42. Normalized γ versus creep strain resulted from (a) the immersion NLUT without the presence of SLs, and (b) the immersion NLUT with the presence of SLs.

linearity due to the creep damage. By removing water non-linearity using the SLs, a good correlation between γ and creep damage is obtained.

6.5 Summary

The integration of SLs with the immersion NLUT using the third harmonic nonlinear parameter is applied to assess the creep damage of stainless steel 410 specimens. The SLs are applied to block the strong non-linearity generated in water through designing its band gap at the third harmonic frequency. The numerical results show that the SLs consisting of periodic layers of 100 μm thick water and 100 μm thick glass can block 6.75 MHz (third harmonic frequency) while it allows 2.25 MHz (fundamental frequency) to pass. It is experimentally observed that the immersion NLUT without the presence of

SLs is not sensitive to the creep damage due to dominant non-linearity in water, while the experimental setup with the immersion NLUT and the SLs shows an increase of 200% in γ due to the change in creep strain from 0% to 3.8%. The presence of SLs between transmitter and specimen reduces the influence of strong non-linearity generated in water. The results reveal that the SLs with a band gap tuned to the third harmonic frequency, and a pass band that includes the fundamental harmonic frequency considerably enhance the creep damage detection using the immersion NLUT. Comparing the results of γ calculated in this chapter with the non-linearity parameters calculated for aluminum 1100 in chapter 4, it is concluded that γ shows a good correlation with the creep damage in stainless steel 410, while it is not sensitive to the plastic strain in aluminum 1100 specimens. On the other hand, β shows strong correlation with plastic strain in aluminum 1100 specimens, while the second harmonic is not observed for the stainless steel 410 creep specimens using the integrated immersion NLUT with SLs.

CHAPTER 7

CONCLUSIONS AND FUTURE WORK

7.1 Conclusions

Nonlinear ultrasonic testing based on measuring fundamental and higher harmonics generated within materials is highly sensitive to the micro-structural changes in materials, hence there is significant potential for this method to be applied for the early state damage detection in energy, transportation, and aviation industries. However, weak non-linearity due to micro defects is highly influenced by the post-signal processing to decompose the ultrasonic signal into its harmonics and the coupling condition of transducers. The objective of this research is to enhance the NLUT method by introducing wavelet-based signal processing method to minimize the error due to post-processing signal decomposition and superlattice design to block non-linearity in coupling medium and electronics. The major conclusions of this study are as follows.

- **Enhance the post-signal processing using the wavelet-based harmonic decomposition method**

  The wavelet-based algorithms were introduced to obtain the acoustic non-linearity parameter β. The FFT-based and wavelet-based signal decomposition methods were applied to aluminum 1100 specimens strained up to different levels of plastic deformations. The calculated β resulted from the FFT-based signal decomposition exhibit strong dependence on the waveform window selection. Two wavelet-based algorithms were introduced to analyze the waveform in nonlinear

ultrasonic testing: time-dependent and time-invariant. The error of harmonic decomposition of nonlinear wave signal due to plastic deformation was reduced. Consequently, a good correlation between the increase of the acoustic non-linearity parameter β and the increase in plastic deformation was obtained.

- **Implementing immersion NLUT to remove the influence of inconsistent coupling condition**

  Another challenge introduced by the contact NLUT method is coupling condition. The materials used as couplant and the force applied to provide good contact between transducers and specimen introduce error in ultrasonic amplitude measurements. To provide a consistent coupling condition, water is proposed as a suitable couplant with comparatively low acoustic attenuation. The immersion NLUT provides a coupling condition which does not depend on coupling force and thickness, and it facilitates the movement of the transducers to perform a complete volume scan of materials. When a period of finite amplitude sinusoidal wave propagates in water, high pressure zone (the crests of the wave) travels faster than low pressure zone (the troughs of the wave). This phenomenon leads to wave distortion and transfer of energy to higher harmonics. The non-linearity in water adversely affects the sensitivity of immersion NLUT and masks the weak non-linearity in solids.

- **The integration of superlattices with immersion NLUT to address coupling issues and electronic non-linearity**

  Superlattices (SLs) are one-dimensional phononic crystals that provide unnatural features to manipulate propagation of elastic wave. The dispersion behavior of SLs can be tuned to exhibit band gaps that restrict the propagation of particular frequency and wave mode through the path

of PCs. The SLs structure was integrated with the immersion NLUT to remove the non-linearity generated in water and instruments. The SLs structure consisting of periodic layers of 100 μm thick water and 100 μm thick glass was designed to block higher harmonics while they passing the fundamental frequency. The non-linearity experiments of plastically strained aluminum 1100 specimens were repeated using the immersion NLUT, and the SLs structure was placed in the path of transmitter and solid surface. The results revealed that the sensitivity of NLUT was improved by an order of magnitude as compared to the contact NLUT method. The approach eliminated the errors introduced by coupling condition and instruments and increased the minimum detectable micro-structural changes in solids.

- **Apply the developed methods to detect creep damage in 410 stainless steel specimens**

  Six dog-bone specimens subjected to different creep strains were prepared to apply the wavelet-based signal decomposition using the contact NLUT and then the immersion NLUT with the SLs structure. The contact NLUT showed 100% increase in acoustic non-linearity parameter β as the creep strain increased from 0% to 3.8%.

  The same specimens were tested using the immersion NLUT integrated with the SLs. It was observed that the second harmonics were very weak, and did not exhibit any correlation with the creep strain. The NLUT method based on the third harmonic amplitude, γ, was applied.

  The results revealed an increase of about 200% in γ as the creep strain increased from 0% to 3.8%, while the immersion NLUT without the presence of SLs was not sensitive to detect the creep damage in the specimens due to strong non-linearity effect in water masking weak non-linearity in solid.

7.2 Future Work

Further research is required to exploit the full potentials of NLUT. The followings are the directions that the research will be expanded.

- The implementation of solid-solid SLs to remove the non-linearity generated in contact NLUT will be studied. Solid-solid SLs provide a narrower band gap compared to the solid-fluid SLs. This requires a very precise manufacturing technique. The multi-layer additive manufacturing method will be applied to achieve precise layer geometries and good bonding between the layers.
- The analytical and numerical models will be built in order to study the acoustic metamaterials that can remove the non-linearity generated in experiments for different wave modes (such as Rayleigh waves, shear waves). The structure will be a two dimensional PCs made of periodically arranged pillars as both transmitter and receiver will be placed on the same side for conditions such that access to both sides of structure is not possible.
- The NLUT method will be expanded to the cases where the linear UT method fails. One example is to detect porosity in welded samples. The contact NLUT with the SLs and the wavelet-based signal decomposition will be applied to porosity detection in welded specimens.

APPENDICES

Appendix A

COPYRIGHT PERMISSION

The paper titled "Wavelet based harmonics decomposition of ultrasonic signal in assessment of plastic strain in aluminum" published in the Journal of the International Measurement Confederation (IMEKO).

The paper titled "The integration of superlattices and immersion nonlinear ultrasonics to enhance damage detection threshold" published at Applied Physics Letters (APL).

The paper titled "The application of water coupled nonlinear ultrasonics to quantify the dislocation density in aluminum 1100" published at AIP Conference Proceedings.

The permission to reuse the of Figure 3 and Figure 4 from the work done by Bjorno [41].

Appendix (Continued)

Appendix (Continued)

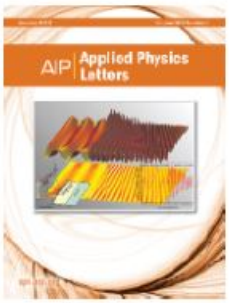

Title:	The integration of superlattices and immersion nonlinear ultrasonics to enhance damage detection threshold
Author:	Amir Mostavi, Minoo Kabir, Didem Ozevin
Publication:	Applied Physics Letters
Volume/Issue	111/20
Publisher:	AIP Publishing
Date:	Nov 13, 2017
Page Count:	5

Order Completed

Thank you for your order.

This Agreement between Amir Mostavi ("You") and AIP Publishing ("AIP Publishing") consists of your license details and the terms and conditions provided by AIP Publishing and Copyright Clearance Center.

Your confirmation email will contain your order number for future reference.

printable details

License Number	4334881319677
License date	Apr 23, 2018
Licensed Content Publisher	AIP Publishing
Licensed Content Publication	Applied Physics Letters
Licensed Content Title	The integration of superlattices and immersion nonlinear ultrasonics to enhance damage detection threshold
Licensed Content Author	Amir Mostavi, Minoo Kabir, Didem Ozevin
Licensed Content Date	Nov 13, 2017
Licensed Content Volume	111
Licensed Content Issue	20
Requestor type	Author (original article)
Format	Print and electronic
Portion	Excerpt (> 800 words)
Attachment	
Requestor Location	Amir Mostavi 1155 W Roosevelt Rd Apt # 311 Chicago, IL 60608 United States Attn:
Billing Type	Invoice
Billing address	Amir Mostavi 1155 W Roosevelt Rd Apt # 311 Chicago, IL 60608 United States Attn: Amir Mostavi
Total	0.00 USD

Appendix (Continued)

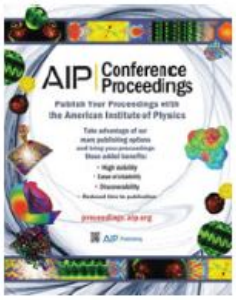

Title:	The application of water coupled nonlinear ultrasonics to quantify the dislocation density in aluminum 1100
Author:	Amir Mostavi, N. Tehrani, N. Kamali, et al
Publication:	AIP Conference Proceedings
Volume/Issue	1806/1
Publisher:	AIP Publishing
Date:	Feb 16, 2017
Page Count:	7

Order Completed

Thank you for your order.

This Agreement between Amir Mostavi ("You") and AIP Publishing ("AIP Publishing") consists of your license details and the terms and conditions provided by AIP Publishing and Copyright Clearance Center.

Your confirmation email will contain your order number for future reference.

printable details

License Number	4334890016103
License date	Apr 23, 2018
Licensed Content Publisher	AIP Publishing
Licensed Content Publication	AIP Conference Proceedings
Licensed Content Title	The application of water coupled nonlinear ultrasonics to quantify the dislocation density in aluminum 1100
Licensed Content Author	Amir Mostavi, N. Tehrani, N. Kamali, et al
Licensed Content Date	Feb 16, 2017
Licensed Content Volume	1806
Licensed Content Issue	1
Requestor type	Author (original article)
Format	Print and electronic
Portion	Excerpt (> 800 words)
Attachment	
Requestor Location	Amir Mostavi 1155 W Roosevelt Rd Apt # 311 Chicago, IL 60608 United States Attn:
Billing Type	Invoice
Billing address	Amir Mostavi 1155 W Roosevelt Rd Apt # 311 Chicago, IL 60608 United States Attn: Amir Mostavi

Appendix (Continued)

Copyright Clearance Center RightsLink®

Home | Account Info | Help

Title: Introduction to nonlinear acoustics
Author: Leif Bjørnø
Publication: Physics Procedia
Publisher: Elsevier
Date: 1 January 2010
Copyright © 2010 Published by Elsevier B.V.

Logged in as:
Amir Mostavi
Account #:
3001277287
LOGOUT

Order Completed

Thank you for your order.

This Agreement between Amir Mostavi ("You") and Elsevier ("Elsevier") consists of your license details and the terms and conditions provided by Elsevier and Copyright Clearance Center.

Your confirmation email will contain your order number for future reference.

printable details

License Number	4334870063239
License date	Apr 23, 2018
Licensed Content Publisher	Elsevier
Licensed Content Publication	Physics Procedia
Licensed Content Title	Introduction to nonlinear acoustics
Licensed Content Author	Leif Bjørnø
Licensed Content Date	Jan 1, 2010
Licensed Content Volume	3
Licensed Content Issue	1
Licensed Content Pages	12
Type of Use	reuse in a thesis/dissertation
Portion	figures/tables/illustrations
Number of figures/tables/illustrations	2
Format	both print and electronic
Are you the author of this Elsevier article?	No
Will you be translating?	No
Original figure numbers	Fig.1, Fig.2
Title of your thesis/dissertation	The Enhancement of Nonlinear Ultrasonic Testing to Detect Micro-structural Defects in Metals
Expected completion date	May 2018
Estimated size (number of pages)	130
Attachment	
Requestor Location	Amir Mostavi 1155 W Roosevelt Rd Apt # 311 Chicago, IL 60608 United States Attn:
Publisher Tax ID	98-0397604

CITED LITERATURE

1. Mostavi, A., Kamali, N., Tehrani, N., Chi, S.-W., Ozevin, D., and Indacochea, J. E.: Wavelet based harmonics decomposition of ultrasonic signal in assessment of plastic strain in aluminum. Measurement, 106:66–78, 2017.

2. Mostavi, A., Kabir, M., and Ozevin, D.: The integration of superlattices and immersion nonlinear ultrasonics to enhance damage detection threshold. Applied Physics Letters, 111(20):201905, 2017.

3. MOSTAVI, A., KABIR, M., and OZEVIN, D.: Enhancing the robustness of nonlinear ultrasonic testing by implementing 1d phononic crystals. Structural Health Monitoring 2017, pages 2228–2235, 2017.

4. Mostavi, A., Tehrani, N., Kamali, N., Ozevin, D., Chi, S., and Indacochea, J.: The application of water coupled nonlinear ultrasonics to quantify the dislocation density in aluminum 1100. In AIP Conference Proceedings, volume 1806, page 060003. AIP Publishing, 2017.

5. Chassignole, B., El Guerjouma, R., Ploix, M.-A., and Fouquet, T.: Ultrasonic and structural characterization of anisotropic austenitic stainless steel welds: Towards a higher reliability in ultrasonic non-destructive testing. NDT & E International, 43(4):273–282, 2010.

6. Hirsekorn, S., Van Andel, P., and Netzelmann, U.: Ultrasonic methods to detect and evaluate damage in steel. Nondestructive Testing and Evaluation, 15(6):373–393, 1998.

7. Ebrahimkhanlou, A., Dubuc, B., and Salamone, S.: Damage localization in metallic plate structures using edge-reflected lamb waves. Smart Materials and Structures, 25(8):085035, 2016.

8. Nagy, P. B.: Fatigue damage assessment by nonlinear ultrasonic materials characterization. Ultrasonics, 36(1-5):375–381, 1998.

9. Sagar, S. P., Das, S., Parida, N., and Bhattacharya, D.: Non-linear ultrasonic technique to assess fatigue damage in structural steel. Scripta materialia, 55(2):199–202, 2006.

10. Cantrell, J. H. and Yost, W. T.: Nonlinear ultrasonic characterization of fatigue microstructures. International Journal of fatigue, 23:487–490, 2001.

11. Kumar, A., Torbet, C. J., Jones, J. W., and Pollock, T. M.: Nonlinear ultrasonics for in situ damage detection during high frequency fatigue. Journal of Applied Physics, 106(2):024904, 2009.

12. Dowell, E., Gorman, G., and Smith, D.: Acoustoelasticity: general theory, acoustic natural modes and forced response to sinusoidal excitation, including comparisons with experiment. Journal of Sound and vibration, 52(4):519–542, 1977.

13. Buenos, A. A., Pereira, P., Mei, P. R., and dos Santos, A. A.: Influence of grain size on the propagation of l _\mathrm {CR} cr waves in low carbon steel. Journal of Nondestructive Evaluation, 33(4):562–570, 2014.

14. Abiza, Z., Destrade, M., and Ogden, R. W.: Large acoustoelastic effect. Wave Motion, 49(2):364–374, 2012.

15. Gedroits, A. and Krasilnikov, V.: Finite-amplitude elastic waves in solids and deviations from hooke's law. Soviet Phys. JETP, 16:1122–1126, 1963.

16. Breazeale, M. and Ford, J.: Ultrasonic studies of the nonlinear behavior of solids. Journal of Applied Physics, 36(11):3486–3490, 1965.

17. Jhang, K.-Y.: Nonlinear ultrasonic techniques for nondestructive assessment of micro damage in material: a review. International journal of precision engineering and manufacturing, 10(1):123–135, 2009.

18. Matlack, K. H., Bradley, H. A., Thiele, S., Kim, J.-Y., Wall, J. J., Jung, H. J., Qu, J., and Jacobs, L. J.: Nonlinear ultrasonic characterization of precipitation in 17-4ph stainless steel. NDT & E International, 71:8–15, 2015.

19. Matlack, K., Kim, J.-Y., Jacobs, L., and Qu, J.: Review of second harmonic generation measurement techniques for material state determination in metals. Journal of Nondestructive Evaluation, 34(1):1–23, 2015.

20. Walker, S. V., Kim, J.-Y., Qu, J., and Jacobs, L. J.: Fatigue damage evaluation in a36 steel using nonlinear rayleigh surface waves. NDT & E International, 48:10–15, 2012.

21. Lim, H. J., Song, B., Park, B., and Sohn, H.: Noncontact fatigue crack visualization using nonlinear ultrasonic modulation. Ndt & E International, 73:8–14, 2015.

22. Pruell, C., Kim, J.-Y., Qu, J., and Jacobs, L. J.: Evaluation of fatigue damage using nonlinear guided waves. Smart Materials and Structures, 18(3):035003, 2009.

23. Rao, V. J., Kannan, E., Prakash, R. V., and Balasubramaniam, K.: Observation of two stage dislocation dynamics from nonlinear ultrasonic response during the plastic deformation of aa7175-t7351 aluminum alloy. Materials Science and Engineering: A, 512(1):92–99, 2009.

24. Zhang, J., Li, S., Xuan, F.-Z., and Yang, F.: Effect of plastic deformation on nonlinear ultrasonic response of austenitic stainless steel. Materials Science and Engineering: A, 622:146–152, 2015.

25. Baby, S., Kowmudi, B. N., Omprakash, C., Satyanarayana, D., Balasubramaniam, K., and Kumar, V.: Creep damage assessment in titanium alloy using a nonlinear ultrasonic technique. Scripta Materialia, 59(8):818–821, 2008.

26. Balasubramaniam, K., Valluri, J. S., and Prakash, R. V.: Creep damage characterization using a low amplitude nonlinear ultrasonic technique. Materials Characterization, 62(3):275–286, 2011.

27. Xiang, Y., Zhu, W., Liu, C.-J., Xuan, F.-Z., Wang, Y.-N., and Kuang, W.-C.: Creep degradation characterization of titanium alloy using nonlinear ultrasonic technique. NDT & E International, 72:41–49, 2015.

28. Ruiz, A., Ortiz, N., Medina, A., Kim, J.-Y., and Jacobs, L.: Application of ultrasonic methods for early detection of thermal damage in 2205 duplex stainless steel. NDT & E International, 54:19–26, 2013.

29. Nucera, C. and di Scalea, F. L.: Nonlinear wave propagation in constrained solids subjected to thermal loads. Journal of Sound and Vibration, 333(2):541–554, 2014.

30. Viswanath, A., Rao, B. P. C., Mahadevan, S., Parameswaran, P., Jayakumar, T., and Raj, B.: Nondestructive assessment of tensile properties of cold worked aisi type 304 stainless steel using nonlinear ultrasonic technique. Journal of materials processing technology, 211(3):538–544, 2011.

31. Shui, G., Wang, Y.-S., and Gong, F.: Evaluation of plastic damage for metallic materials under tensile load using nonlinear longitudinal waves. NDT & E International, 55:1–8, 2013.

32. Kim, J.-Y., Jacobs, L. J., Qu, J., and Littles, J. W.: Experimental characterization of fatigue damage in a nickel-base superalloy using nonlinear ultrasonic waves. The Journal of the Acoustical Society of America, 120(3):1266–1273, 2006.

33. Walker, S. V., Kim, J.-Y., Qu, J., and Jacobs, L. J.: Fatigue damage evaluation in a36 steel using nonlinear rayleigh surface waves. Ndt & E International, 48:10–15, 2012.

34. Zeitvogel, D. T., Matlack, K. H., Kim, J.-Y., Jacobs, L. J., Singh, P. M., and Qu, J.: Characterization of stress corrosion cracking in carbon steel using nonlinear rayleigh surface waves. Ndt & E International, 62:144–152, 2014.

35. Matlack, K., Kim, J.-Y., Jacobs, L., and Qu, J.: Review of second harmonic generation measurement techniques for material state determination in metals. Journal of Nondestructive Evaluation, 34(1):273, 2015.

36. Liu, S., Croxford, A. J., Neild, S. A., and Zhou, Z.: Effects of experimental variables on the nonlinear harmonic generation technique. IEEE transactions on ultrasonics, ferroelectrics, and frequency control, 58(7):1442–1451, 2011.

37. Kim, Y. Y. and Kim, E.-H.: Effectiveness of the continuous wavelet transform in the analysis of some dispersive elastic waves. The Journal of the Acoustical Society of America, 110(1):86–94, 2001.

38. Thiele, S., Kim, J.-Y., Qu, J., and Jacobs, L. J.: Air-coupled detection of nonlinear rayleigh surface waves to assess material nonlinearity. Ultrasonics, 54(6):1470–1475, 2014.

39. Duck, F. A.: Nonlinear acoustics in diagnostic ultrasound. Ultrasound in medicine & biology, 28(1):1–18, 2002.

40. Ohara, Y. and Kawashima, K.: Detection of internal micro defects by nonlinear resonant ultrasonic method using water immersion. Japanese journal of applied physics, 43(5S):3119, 2004.

41. Bjørnø, L.: Introduction to nonlinear acoustics. Physics Procedia, 3(1):5–16, 2010.

42. Humphrey, V. F.: Nonlinear propagation in ultrasonic fields: measurements, modelling and harmonic imaging. Ultrasonics, 38(1):267–272, 2000.

43. Solovchuk, M., Sheu, T. W., and Thiriet, M.: Simulation of nonlinear westervelt equation for the investigation of acoustic streaming and nonlinear propagation effects. The Journal of the Acoustical Society of America, 134(5):3931–3942, 2013.

44. Landsberger, B. and Hamilton, M.: Second-harmonic generation in sound beams reflected from, and transmitted through, immersed elastic solids. The Journal of the Acoustical Society of America, 109(2):488–500, 2001.

45. Croxford, A. J., Wilcox, P. D., Drinkwater, B. W., and Nagy, P. B.: The use of non-collinear mixing for nonlinear ultrasonic detection of plasticity and fatigue. The Journal of the Acoustical Society of America, 126(5):EL117–EL122, 2009.

46. Hasanian, M. and Lissenden, C. J.: Second order harmonic guided wave mutual interactions in plate: Vector analysis, numerical simulation, and experimental results. Journal of Applied Physics, 122(8):084901, 2017.

47. Zhu, R., Ma, C., Zheng, B., Musa, M. Y., Jing, L., Yang, Y., Wang, H., Dehdashti, S., Fang, N. X., and Chen, H.: Bifunctional acoustic metamaterial lens designed with coordinate transformation. Applied Physics Letters, 110(11):113503, 2017.

48. D'Alessandro, L., Belloni, E., Ardito, R., Corigliano, A., and Braghin, F.: Modeling and experimental verification of an ultra-wide bandgap in 3d phononic crystal. Applied Physics Letters, 109(22):221907, 2016.

49. Kushwaha, M. S., Halevi, P., Martinez, G., Dobrzynski, L., and Djafari-Rouhani, B.: Theory of acoustic band structure of periodic elastic composites. Physical Review B, 49(4):2313, 1994.

50. Deymier, P. A.: Acoustic metamaterials and phononic crystals, volume 173. Springer Science & Business Media, 2013.

51. Gorishnyy, T., Maldovan, M., Ullal, C., and Thomas, E.: Sound ideas. Physics World, 18(12):24, 2005.

52. Benchabane, S., Gaiffe, O., Salut, R., Ulliac, G., Laude, V., and Kokkonen, K.: Guidance of surface waves in a micron-scale phononic crystal line-defect waveguide. Applied Physics Letters, 106(8):081903, 2015.

53. Martinezsala, R., Sancho, J., Sánchez, J. V., Gómez, V., Llinares, J., Meseguer, F., et al.: Sound-attenuation by sculpture. nature, 378(6554):241–241, 1995.

54. Liang, B., Guo, X., Tu, J., Zhang, D., and Cheng, J.: An acoustic rectifier. Nature materials, 9(12):989–992, 2010.

55. El Hassouani, Y., El Boudouti, E., Djafari-Rouhani, B., and Aynaou, H.: Sagittal acoustic waves in finite solid-fluid superlattices: Band-gap structure, surface and confined modes, and omnidirectional reflection and selective transmission. Physical Review B, 78(17):174306, 2008.

56. Zhang, S., Zhang, Y., Guo, Y., Leng, Y., Feng, W., and Cao, W.: Realization of subwavelength asymmetric acoustic transmission based on low-frequency forbidden transmission. Physical Review Applied, 5(3):034006, 2016.

57. Ebrahimkhanlou, A. and Salamone, S.: Acoustic emission source localization in thin metallic plates: A single-sensor approach based on multimodal edge reflections. Ultrasonics, 78:134–145, 2017.

58. Nazarian, E., Ansari, F., and Azari, H.: Recursive optimization method for monitoring of tension loss in cables of cable-stayed bridges. Journal of Intelligent Material Systems and Structures, 27(15):2091–2101, 2016.

59. Babanajad, S. K. and Ansari, F.: Mechanistic quantification of microcracks from dynamic distributed sensing of strains. Journal of Engineering Mechanics, 143(8):04017041, 2017.

60. Zhang, L., Ozevin, D., Hardman, W., and Timmons, A.: Acoustic emission signatures of fatigue damage in idealized bevel gear spline for localized sensing. Metals, 7(7):242, 2017.

61. Dubuc, B., Ebrahimkhanlou, A., and Salamone, S.: Effect of pressurization on helical guided wave energy velocity in fluid-filled pipes. Ultrasonics, 75:145–154, 2017.

62. Fierro, G. P. M. and Meo, M.: Nonlinear imaging (nim) of flaws in a complex composite stiffened panel using a constructive nonlinear array (cna) technique. Ultrasonics, 74:30–47, 2017.

63. Rose, J. L.: Ultrasonic guided waves in solid media. Cambridge University Press, 2014.

64. Zhang, L., Luo, W., Rose, J. L., Thompson, D. O., and Chimenti, D. E.: Ultrasonic guided wave focusing beyond welds in a pipeline. In AIP Conference Proceedings, volume 820, pages 877–884. AIP, 2006.

65. Cantrell, J. H.: Fundamentals and applications of nonlinear ultrasonic nondestructive evaluation. In Ultrasonic nondestructive evaluation, pages 377–448. CRC Press, 2003.

66. Guyer, R. A. and Johnson, P. A.: Nonlinear mesoscopic elasticity: Evidence for a new class of materials. Physics today, 52:30–36, 1999.

67. Payan, C., Garnier, V., Moysan, J., and Johnson, P.: Applying nonlinear resonant ultrasound spectroscopy to improving thermal damage assessment in concrete. The Journal of the Acoustical Society of America, 121(4):EL125–EL130, 2007.

68. Van Den Abeele, K.-A., Johnson, P. A., and Sutin, A.: Nonlinear elastic wave spectroscopy (news) techniques to discern material damage, part i: nonlinear wave modulation spectroscopy (nwms). Journal of Research in Nondestructive Evaluation, 12(1):17–30, 2000.

69. Ballad, E., Vezirov, S. Y., Pfleiderer, K., Solodov, I. Y., and Busse, G.: Nonlinear modulation technique for nde with air-coupled ultrasound. Ultrasonics, 42(1-9):1031–1036, 2004.

70. Larmat, C. S., Guyer, R. A., and Johnson, P. A.: Time-reversal methods in geophysics. Phys. Today, 63(8):31–35, 2010.

71. Breazeale, M. and Thompson, D.: Finite-amplitude ultrasonic waves in aluminum. Applied Physics Letters, 3(5):77–78, 1963.

72. Doerr, C., Kim, J.-Y., Singh, P., Wall, J. J., and Jacobs, L. J.: Evaluation of sensitization in stainless steel 304 and 304l using nonlinear rayleigh waves. NDT & E International, 88:17–23, 2017.

73. Zarembo, L. and Krasil'Nikov, V.: Nonlinear phenomena in the propagation of elastic waves in solids. Soviet Physics Uspekhi, 13(6):778, 1971.

74. Herrmann, J., Kim, J.-Y., Jacobs, L. J., Qu, J., Littles, J. W., and Savage, M. F.: Assessment of material damage in a nickel-base superalloy using nonlinear rayleigh surface waves. Journal of Applied Physics, 99(12):124913, 2006.

75. Chillara, V. K. and Lissenden, C. J.: Constitutive model for third harmonic generation in elastic solids. International Journal of Non-Linear Mechanics, 82:69–74, 2016.

76. Lissenden, C., Liu, Y., Choi, G., and Yao, X.: Effect of localized microstructure evolution on higher harmonic generation of guided waves. Journal of Nondestructive Evaluation, 33(2):178–186, 2014.

77. Narayana, V., Balasubramaniam, K., and Prakash, R.: Detection and prediction of creep-damage of copper using nonlinear acoustic techniques. In AIP Conference Proceedings, volume 1211, pages 1410–1417. AIP, 2010.

78. Shah, A. and Ribakov, Y.: Non-linear ultrasonic evaluation of damaged concrete based on higher order harmonic generation. Materials & Design, 30(10):4095–4102, 2009.

79. Liu, S., Croxford, A. J., Neild, S. A., and Zhou, Z.: Effects of experimental variables on the nonlinear harmonic generation technique. IEEE transactions on ultrasonics, ferroelectrics, and frequency control, 58(7), 2011.

80. Scott, K., Kim, J.-Y., and Jacobs, L. J.: Signal processing methods for second harmonic generation in thin specimens. NDT & E International, 95:57–64, 2018.

81. Mallat, S.: A wavelet tour of signal processing: the sparse way. Academic press, 2008.

82. Olbrycht, R., Więcek, B., Gralewicz, G., Świątczak, T., and Owczarek, G.: Comparison of fourier and wavelet analyses for defect detection in lock-in and pulse phase thermography. Quantitative InfraRed Thermography Journal, 4(2):219–232, 2007.

83. Golmohamadi, M., Badri, H., and Ebrahimi, A.: Damage diagnosis in bridges using wavelet. In IACSIT Coimbatore Conferences, IPCSIT, volume 28, pages 202–207, 2012.

84. Bayissa, W., Haritos, N., and Thelandersson, S.: Vibration-based structural damage identification using wavelet transform. Mechanical Systems and Signal Processing, 22(5):1194–1215, 2008.

85. Gabor, D.: Theory of communication. part 1: The analysis of information. Journal of the Institution of Electrical Engineers-Part III: Radio and Communication Engineering, 93(26):429–441, 1946.

86. Gao, R. X. and Yan, R.: Wavelets: Theory and applications for manufacturing. Springer Science & Business Media, 2010.

87. Aydin, N. and Markus, H. S.: Optimization of processing parameters for the analysis and detection of embolic signals. European Journal of ultrasound, 12(1):69–79, 2000.

88. Cohen, L.: Time-frequency distributions-a review. Proceedings of the IEEE, 77(7):941–981, 1989.

89. Li, C. J. and Ma, J.: Wavelet decomposition of vibrations for detection of bearing-localized defects. Ndt & E International, 30(3):143–149, 1997.

90. Goedecker, S. and Ivanov, O.: Frequency localization properties of the density matrix and its resulting hypersparsity in a wavelet representation. Physical Review B, 59(11):7270, 1999.

91. Liner, C.: An overview of wavelet transform concepts and applications. University of Houston, pages 1–17, 2010.

92. Basu, B. and Gupta, V. K.: Non-stationary seismic response of mdof systems by wavelet transform. Earthquake engineering & structural dynamics, 26(12):1243–1258, 1997.

93. Basu, B.: Identification of stiffness degradation in structures using wavelet analysis. Construction and building materials, 19(9):713–721, 2005.

94. Gaul, L. and Hurlebaus, S.: Identification of the impact location on a plate using wavelets. Mechanical systems and signal processing, 12(6):783–795, 1998.

95. Ykhlef, F., Arezki, M., Guessoum, A., and Berkani, D.: A wavelet denoising method to improve detection with ultrasonic signal. In Industrial Technology, 2004. IEEE ICIT'04. 2004 IEEE International Conference on, volume 3, pages 1422–1425. IEEE, 2004.

96. Lin, J. and Qu, L.: Feature extraction based on morlet wavelet and its application for mechanical fault diagnosis. Journal of sound and vibration, 234(1):135–148, 2000.

97. Debnath, L. and Shah, F. A.: Wavelet transforms and their applications. Springer, 2002.

98. Joo, D. J.: Damage detection and system identification using a wavelet energy based approach. 2012.

99. Silva, M., Gouyon, R., and Lepoutre, F.: Hidden corrosion detection in aircraft aluminum structures using laser ultrasonics and wavelet transform signal analysis. Ultrasonics, 41(4):301–305, 2003.

100. Taplidou, S. A. and Hadjileontiadis, L. J.: Nonlinear analysis of wheezes using wavelet bicoherence. Computers in biology and medicine, 37(4):563–570, 2007.

101. Teolis, A. and Benedetto, J. J.: Computational signal processing with wavelets, volume 182. Springer, 1998.

102. Enflo, B. O. and Hedberg, C. M.: Theory of nonlinear acoustics in fluids, volume 67. Springer Science & Business Media, 2006.

103. Breazeale, M.: Physics and engineering principles of nonlinear acoustics. Japanese Journal of Applied Physics, 27(S1):12, 1988.

104. Walsh, T. and Torres, M.: Finite element methods for nonlinear acoustics in fluids. Journal of Computational Acoustics, 15(03):353–375, 2007.

105. Simon, S. H.: The Oxford solid state basics. Oxford University Press, 2013.

106. Perkowitz, S.: Phonons. http://www.britannica.com/science/phonon, 2016. Accessed: 2016-03-16.

107. Craster, R. V. and Guenneau, S.: Acoustic metamaterials: Negative refraction, imaging, lensing and cloaking, volume 166. Springer Science & Business Media, 2012.

108. Pai, P. F.: Metamaterial-based broadband elastic wave absorber. Journal of Intelligent Material Systems and Structures, 21(5):517–528, 2010.

109. Matlack, K. H., Bauhofer, A., Krödel, S., Palermo, A., and Daraio, C.: Composite 3d-printed metastructures for low-frequency and broadband vibration absorption. Proceedings of the National Academy of Sciences, page 201600171, 2016.

110. Hou, Z., Wu, F., and Liu, Y.: Phononic crystals containing piezoelectric material. Solid State Communications, 130(11):745–749, 2004.

111. Charles, C., Bonello, B., and Ganot, F.: Propagation of guided elastic waves in 2d phononic crystals. Ultrasonics, 44:e1209–e1213, 2006.

112. Tol, S., Degertekin, F., and Erturk, A.: Phononic crystal luneburg lens for omnidirectional elastic wave focusing and energy harvesting. Applied Physics Letters, 111(1):013503, 2017.

113. Kabir, M., Allen, M. G., and Ozevin, D.: 3d printed metamaterial design to focus wave energy in thin plates. In SPIE Smart Structures and Materials+ Nondestructive Evaluation and Health Monitoring, pages 101691I–101691I. International Society for Optics and Photonics, 2017.

114. Tol, S., Degertekin, F., and Erturk, A.: Gradient-index phononic crystal lens-based enhancement of elastic wave energy harvesting. Applied Physics Letters, 109(6):063902, 2016.

115. Kabir, M. and Ozevin, D.: Integration of periodic structure and highly narrowband mems sensor to enhance crack detection ability in steel structures. In SPIE Nanoscience+ Engineering, pages 99181N–99181N. International Society for Optics and Photonics, 2016.

116. Zanjani, M. B., Davoyan, A. R., Mahmoud, A. M., Engheta, N., and Lukes, J. R.: One-way phonon isolation in acoustic waveguides. Applied Physics Letters, 104(8):081905, 2014.

117. Carta, G. and Brun, M.: Bloch–floquet waves in flexural systems with continuous and discrete elements. Mechanics of Materials, 87:11–26, 2015.

118. Brûlé, S., Javelaud, E., Enoch, S., and Guenneau, S.: Experiments on seismic metamaterials: Molding surface waves. Physical review letters, 112(13):133901, 2014.

119. Colombi, A., Colquitt, D., Roux, P., Guenneau, S., and Craster, R. V.: A seismic metamaterial: The resonant metawedge. Scientific reports, 6:27717, 2016.

120. Peng, H. and Pai, P. F.: Acoustic metamaterial plates for elastic wave absorption and structural vibration suppression. International Journal of Mechanical Sciences, 89:350–361, 2014.

121. Li, S., Chen, T., Wang, X., Li, Y., and Chen, W.: Expansion of lower-frequency locally resonant band gaps using a double-sided stubbed composite phononic crystals plate with composite stubs. Physics Letters A, 380(25):2167–2172, 2016.

122. Zhang, D., Zhao, J., Bonello, B., Zhang, F., Yuan, W., Pan, Y., and Zhong, Z.: Investigation of surface acoustic wave propagation in composite pillar based phononic crystals within both local resonance and bragg scattering mechanism regimes. Journal of Physics D: Applied Physics, 50(43):435602, 2017.

123. Hussein, M. I., Leamy, M. J., and Ruzzene, M.: Dynamics of phononic materials and structures: Historical origins, recent progress, and future outlook. Applied Mechanics Reviews, 66(4):040802, 2014.

124. Romeo, F. and Ruzzene, M.: Wave propagation in linear and nonlinear periodic media: analysis and applications, volume 540. Springer Science & Business Media, 2013.

125. Wan, X., Peter, W. T., Chen, J., Xu, G., and Zhang, Q.: Second harmonic reflection and transmission from primary s0 mode lamb wave interacting with a localized microscale damage in a plate: A numerical perspective. Ultrasonics, 2017.

126. Aleshin, V., Delrue, S., Trifonov, A., Matar, O. B., and Van Den Abeele, K.: Two dimensional modeling of elastic wave propagation in solids containing cracks with rough surfaces and friction-part i: Theoretical background. Ultrasonics, 2017.

127. Singh, A. K., Chen, B.-Y., Tan, V. B., Tay, T.-E., and Lee, H.-P.: Finite element modeling of nonlinear acoustics/ultrasonics for the detection of closed delaminations in composites. Ultrasonics, 74:89–98, 2017.

128. Huang, S., Wang, S., Li, W., and Wang, Q.: Electromagnetic ultrasonic guided waves. Springer, 2016.

129. Agarwal, R. P. and Wong, P. J.: Error inequalities in polynomial interpolation and their applications, volume 262. Springer Science & Business Media, 2012.

130. Sposito, G., Ward, C., Cawley, P., Nagy, P., and Scruby, C.: A review of non-destructive techniques for the detection of creep damage in power plant steels. Ndt & E International, 43(7):555–567, 2010.

131. Lin, J., Liu, Y., and Dean, T.: A review on damage mechanisms, models and calibration methods under various deformation conditions. International Journal of damage mechanics, 14(4):299–319, 2005.

132. Raj, B., Moorthy, V., Jayakumar, T., and Rao, K. B. S.: Assessment of microstructures and mechanical behaviour of metallic materials through non-destructive characterisation. International Materials Reviews, 48(5):273–325, 2003.

133. Hafezi, M. H., Alebrahim, R., and Kundu, T.: Peri-ultrasound for modeling linear and nonlinear ultrasonic response. Ultrasonics, 80:47–57, 2017.

134. Wang, Y., Guan, R., and Lu, Y.: Nonlinear lamb waves for fatigue damage identification in frp-reinforced steel plates. Ultrasonics, 80:87–95, 2017.

Amir Mostavi, *Ph.D., E.I.T., LEED GA,*

Chicago, Illinois, Phone: (646) 342-0620 |Email: amirmostavi@gmail.com

SUMMARY STATEMENT

Accomplished and talented structural engineer with extensive skills and experience in civil engineering, structural systems, structural dynamics, nondestructive testing of structures, and project management. A versatile team player who has demonstrated success in research and technically proficient in ETABS, SAP, SAFE, MS project, AutoCAD, MATLAB, ANSYS, Revit and Microsoft Office. With four years of Ph.D. level research experience focused on the nondestructive testing of structures and materials, and three years of construction management experience. It is also planned to take Professional Engineering (PE) in October 2018.

EDUCATION

University of Illinois at Chicago, Ph.D. candidate — Aug. 2014-May 2018
Civil and Materials Engineering with focus on Structural Engineering — GPA: 4/4
Courses in: Theory of Elasticity, Structural Dynamics, Fracture Mechanics I and II, Finite Elements, Nondestructive Testing and Evaluation, Written Communication, Nondestructive Testing of Concrete.

Texas A&M University — Jan. 2014-Aug. 2014
Courses in: Risk Management, Project Estimation, Contract Management.

Sharif University of Technology – Iran — Sept. 2010-Sept. 2012
Master of Science – Civil Engineering, Construction Management — GPA: 3.8/4
Courses in: Construction Scheduling and Planning, Construction Methods, Managing Construction Equipment, Operation Research, Contract Management.

Sharif University of Technology – Iran — Sept. 2005-Sept. 2010
Bachelor of Science – Civil Engineering

CERTIFICATIONS/SKILS

Engineer-In-Training (EIT) - (February 2018)
LEED Green Associate - (February 2018)
(Planned to take Professional Engineering (PE) - Expected October 2018**)**
Engineering Software: COMSOL, ANSYS, ETABS, SAP, SAFE, MS project, AutoCAD, Revit
Computer Programming\General Software: MATLAB, Pascal, LaTex, Microsoft Office

PROFESSIONAL EXPERIENCE

Technical Project Manager — June 2011- Dec 2013
Amitis Tall Building Construction Co., Tehran, Iran
(Construction Management Group)

- Project scheduling, monitoring workflow and make timeline adjustments;
- Worked as a part of an interdisciplinary team to achieve project milestones;
- Developed status reports, cost estimates, and resource plan;
- Participated procurement management, manage the contract with suppliers and equipment providers;
- Human resource allocation, management, and optimization according to the project schedules.

Project Contracts Manager — May 2010- May 2011
Intern, Boland Payeh Construction Co., Tehran, Iran
(Construction Management Group)

- EPC/BOT contract document management and preparation and cost estimation;
- Worked as a part of an interdisciplinary team to achieve Bid documents;
- Reviewed invoices to ensure compliance with contract terms and budget;
- New mass building technology research and development;
- Participated in weekly subcontract meetings.

HONORS

- Achieved the 5th rank of Iran Ph.D. studies entrance exam
- Achieved the 10th rank in Iran national civil engineering Olympiad in 2011

- Achieved the 15th rank in national exam for graduate studies of Iran in 2010
- Achieved the 206th rank (the top 0.1% of all applicants) in national entrance exam of Iran universities in 2005.

RESEARCH EXPERIENCE

Graduate Research Assistant, Fall 2014-Present
University of Illinois at Chicago, IL, USA
The Enhancement of Nonlinear Ultrasonic Testing (NLUT) to Predict Micro-structural Defects in Metals
My research focuses on enhancing nonlinear ultrasonic testing through improved signal processing and integration with acoustic metamaterials. Funded by National Science Foundation (NSF) the research includes the following:

- Nonlinear ultrasonic testing to detect plastic deformation in metals
- Post-signal processing by implementing the Wavelet based harmonic decomposition
- Linear and nonlinear ultrasonic testing to detect creep damage in stainless steel 410
- Numerical and experimental studies of band-gap formation in acoustic metamaterials
- Integrated metamaterial and nonlinear ultrasonic testing to detect fatigue damage in metal bridges
- Noise isolation through phononic crystals to detect active cracks in steel bridges; (The Idea is submitted to the **Unites States Patent and Trademark Office (USPTO)**)
- Pipeline leak detection by means of acoustic emission method

Graduate Research Assistant, Fall 2010-Spring 2012
Sharif University of Technology, Tehran, Iran
Identifying and Ranking the Factors that Affect Concrete Construction Productivity
The most important factors that affect the construction productivity in concrete tall building were studied through questionnaires. Questionnaires were submitted to the major parties involved in this type of construction.

TEACHING EXPERIENCE

Teaching Assistant Spring 2015-Spring 2018
Courses: Statics, Strength Of Materials, Civil Engineering Systems Design, Undergrad Thesis I, Foundation Design, Statics, Behavior and Design of Metal Structures.

- Assisted students with the final project, graded homework and quizzes, conducted weekly office hours, occasional guest lecturer.

PUBLICATIONS

Journal Manuscripts

1. **A. Mostavi**, N. Kamali, N. Tehrani, S.-W. Chi, D. Ozevin, and J. E. Indacochea, "Wavelet based harmonics decomposition of ultrasonic signal in assessment of plastic strain in aluminum," Measurement, vol. 106, 2017.
2. **A. Mostavi**, M. Kabir, and D. Ozevin, "The integration of superlattices and immersion nonlinear ultrasonics to enhance damage detection threshold," Appl. Phys. Lett., vol. 111, p. 201905, 2017.
3. M. Kabir, **A. Mostavi**, D. Ozevin, "Noise Isolation with Phononic Crystals to Enhance Fatigue Crack Growth Detection Capability of Acoustic Emission in Steel Structures", *Journal of Civil Structural Health Monitoring, (Under Review).*
4. M. Kabir, **A. Mostavi,** D. Ozevin, "Integrating Phononic Crystals and Acoustic Emission to Enhance Crack Growth Detection Capability in CFRP Structures", *(In preparation).*
5. N. Kamali, N. Tehrani, **A. Mostavi**, S.W. Chi, D. Ozevin, J.E. Indacochea, "Numerical Studies on How Plastic Deformation Affects Higher Harmonics", *(In preparation).*
6. N. Tehrani, **A. Mostavi**, N. Kamali, S.W. Chi, D. Ozevin, J.E. Indacochea, "Assessing Creep Damage of Stainless Steel 410 Using Linear and Nonlinear Ultrasonic Testing", *(In preparation).*

REFERENCES

Dr. Didem Ozevin
Associate Professor

Dr. Ernesto Indacochea
Professor
Civil and Material Engineering
University of Illinois at Chicago
Chicago, Illinois.
Email: jeindaco@uic.edu

Dr. Sheng-Wei Chi
Assistant Professor
Civil and Material Engineering
University of Illinois at Chicago
Chicago, Illinois.
Email: swchi@uic.edu

Civil and Material Engineering
University of Illinois at Chicago
Chicago, Illinois.
Email: dozevin@uic.edu